Technische Universität München

Institut für organische Chemie und Biochemie

Lehrstuhl für Biotechnologie

Characterization of bacterial defense systems against oxidative stress

Bastian Groitl

Vollständiger Abdruck der von der Fakultät für Chemie der Technischen Universität München zur Erlangung des akademischen Grades eines

Doktors der Naturwissenschaften (Dr. rer. nat.)

genehmigten Dissertation.

Vorsitzender:		Prof. Dr. Aymelt Itzen
Prüfer der Dissertation:	1.	Prof. Dr. Johannes Buchner
	2.	Prof. Dr. Ursula Jakob

Die Dissertation wurde am 12.05.2017 bei der Technischen Universität München eingereicht und durch die Fakultät für Chemie am 01.06.2017 angenommen.

To my family and friends without whose support I would not be here

Table of Contents

Index of Figures

Index of Tables

Abbreviations

2D	two-dimensional
A_{600}	optical density at 600 nm
aa	amino acid
ADP	adenosine diphosphate
Arg	arginine
Asn	asparagine
ATP	adenosine triphosphate
°C	degree Celsius
C-terminal	carboxyl-terminal
Cys	cysteine
DNA	deoxyribonucleic acid
DTT	dithiothreitol
E. coli	*Escherichia coli*
x g	gravity
g	gram
Gdn-HCl	guanidine hydrochloride
Gln	glutamine
Grx	glutaredoxin
GSH	reduced glutathione (L-γ-glutamyl-L-cysteineglycine)
GSSG	oxidized glutathione
h	hour
HAP	hydroxyapatite
His	histidine
Hsp	heat shock protein
HOCl	hypochloride acid
HOBr	hypobromous acid
HOSCN	hypothiocyanous acid
HOX	(pseudo)hypohalous acid
H_2O_2	hydrogen peroxide
IAM-TEMPO	iodoacetamide tetramethyl-1-piperidinyloxy
IPTG	isopropyl β-D-1-thiogalactopyranoside
kDa	kilo Dalton

l	liter
Lys	lysine
m	milli
M	molar
Met	methionine
min	minute
µ	micro
n	nano
N-terminal	amino-terminal
NADPH	nicotinamide adenine dinucleotide phosphate
NPY	neuropeptide Y
O_2^-	superoxide
O_2	oxygen
ox	oxidized
P. aeruginosa	*Pseudomonas aeruginoa*
red	reduced
RNA	ribonucleic acid
ROS	reactive oxygen species
RCS	reactive chlorine species
RT	room temperature
SDS	sodium dodecyl sulfate
TCA	Trichloroacetic acid
Trp	tryptophan
Trx	thioredoxin
Tyr	tyrosine
v/v	volume per volume
w/v	weight per volume

Declaration

I, Bastian Groitl, hereby declare that this thesis was prepared by me independently and using only the references and resources stated. This work has not been submitted to any other audit commission. Parts of this work have been published in scientific journals.

Erklärung

Hiermit erkläre ich, Bastian Groitl, dass ich die vorliegende Arbeit selbständig verfasst und keine anderen als die angegebenen Quellen und Hilfsmittel verwendet habe. Die Arbeit wurde bisher keiner Prüfungskommission vorgelegt. Teile dieser Arbeit wurden in wissenschaftlichen Journalen veröffentlicht.

_____

Bastian Groitl

Ann Arbor, 01. Mai 2017

1 Summary

Specialized cells of the innate immune system (e.g. neutrophils) phagocytize pathogens and kill them by releasing toxic concentrations of antimicrobial oxidants, including hypochlorous acid (HOCl), hypobromous acid (HOBr), and hypothiocyanous acid (HOSCN). Bacteria have developed dedicated systems to sense and react to oxidative stress but little is known whether bacteria utilize the same or individual stress systems to counteract these oxidants. To investigate their molecular effects and reveal the respective response mechanisms they elicit in bacteria, we tested them on the bacterial pathogen *Pseudomonas aeruginosa* strain PA14. We discovered that HOCl and HOBr both cause substantial killing in dormant cells and trigger similar gene responses, including the upregulation of heat shock genes. HOSCN, however, primarily targets actively metabolizing PA14 cells, and impacts membrane associated proteins as identified by gene expression analysis. We identified that all three oxidants trigger protein unfolding and aggregation. Our data suggest that the chemical chaperone polyphosphate acts as a universal response to all three oxidants, protecting cells against protein unfolding. The redox regulated chaperone Hsp33 only becomes activated by HOCl and HOBr, suggesting that the extremely quick activation of Hsp33 provides additional protection against these harsher and faster acting oxidants compared to HOSCN. Attenuation of polyP generation by the anti-inflammatory drug mesalamine effectively rendered PA14 more susceptible to all three oxidants, opening a potential avenue for future treatment regimens against *P. aeruginosa* infections. To investigate how Hsp33 uses redox-mediated conformational changes to recognize and bind client proteins, I used a strategy combining incorporation of unnatural amino acids at amber stop codon sites with fluorine-19 NMR and *in vivo* crosslinking studies. The results revealed that Hsp33 uses its conditionally disordered regions, which emerge as Hsp33 is oxidatively activated, in binding unfolding client proteins. These data directly link partial protein unfolding in stress-induced chaperones to a client binding mechanism. Conceivably, structural similarities found both in client proteins and in Hsp33's own linker region are the common feature that facilitates Hsp33's switch from self-recognition to high-affinity client binding.

Zusammenfassung

Spezielle Zellen des angeborenen Immunsystems, wie beispielsweis Neutrophile, phagozytisieren Pathogene und töten sie durch Freisetzung toxischer Konzentrationen an antimikrobieller Oxidationsmittel, einschließlich hypochloriger Säure (HOCl), hypobromer Säure (HOBr) und Hypothiocyanat-Säure (HOSCN). Bakterien haben spezialisierte Systeme entwickelt, um oxidativen Stress wahrzunehmen und darauf zu reagieren, aber es ist nur wenig darüber bekannt, ob Bakterien ein universales oder jeweils spezialisierte Stresssysteme verwenden, um diesen Oxidantien entgegenzuwirken. Um die molekularen Effekte der drei Oxidationsmittel zu untersuchen und die entsprechenden Reaktionsmechanismen, die sie in Bakterien hervorrufen, haben wir sie auf an dem pathogen Bakterienstamm *Pseudomonas aeruginosa* PA14 getestet. Wir stellten fest, dass HOCl und HOBr v.a. in ruhenden Zellen tötlich wirken und ähnliche Genantworten auslösen, so z.B. die Hochregulierung von Hitzeschockgenen. HOSCN zielt jedoch primär auf aktiv metabolisierende PA14-Zellen ab und beeinflusst membranassoziierte Proteine, was ebenfalls durch die Genexpressionsanalyse ersichtlich wurde. Wir identifizierten alle drei Oxidationsmittel als Auslöser für die Proteinentfaltung und Aggregation. Unsere Daten deuten darauf hin, dass das chemische Chaperon Polyphosphat als universelle Antwort auf alle drei Oxidationsmittel wirkt und Zellen vor Proteinentfaltung schützt. Das redoxregulierte Chaperon Hsp33 wird nur durch HOCl und HOBr aktiviert, was darauf hindeutet, dass die extrem schnelle Aktivierung von Hsp33 einen zusätzlichen Schutz gegen diese härteren und schnell wirkenden Oxidationsmittel im Vergleich zu HOSCN bietet. Eine verminderte PolyP-Erzeugung durch das entzündungshemmende Arzneimittel Mesalamin zeigte sich darin wirksam PA14 anfälliger für alle drei Oxidationsmittel zu machen und eröffnet so einen möglichen Weg für zukünftige Behandlungspläne gegen *P. aeruginosa*-Infektionen. Um zu untersuchen, wie Hsp33 redoxvermittelte Konformationsänderungen zur Erkennung und Bindung von Clientproteinen verwendet, habe ich eine Strategie verwendet, die den Einbau von unnatürlichen Aminosäuren an Amber-Stop-Codonstellen mit Fluor-19-NMR

und *In vivo*-Vernetzungsstudien kombiniert. Die Ergebnisse dieser Studien zeigten, dass Hsp33 seine bedingt ungeordneten Regionen verwendet, die entstehen, wenn Hsp33 oxidativ aktiviert wird, um mit den Substratproteinen zu interagieren und diese zu binden. Diese Daten verknüpfen die partielle Protein-Entfaltung in stressinduzierten Chaperonen direkt mit einem Substrat-Bindungsmechanismus. Es ist denkbar, dass strukturelle Ähnlichkeiten sowohl in den Substratproteinen als auch in der Hsp33-eigenen Linkerregion das gemeinsame Merkmal darstellen, welches den Wechsel von Hsp33 von der Selbsterkennung hin zur hochaffinen Substratbindung ermöglicht.

2 Introduction

2.1 Life in an aerobic environment

About 2.5 billion years ago, oxygen producing cyanobacteria laid the foundation for the evolution of aerobic respiration and ultimately for the development of multi-cellular organisms (Nisbet and Sleep 2001, Lesser 2006). First discovered and described in the 1950s by Gerschman et al., life in an aerobic environment inevitably comes with the production of toxic oxygen-derived compounds called reactive oxygen species (ROS) (Gerschman, Gilbert et al. 1954). These ROS include superoxide, hydrogen peroxide (H_2O_2), hydroxyl radicals (OH●), and (pseudo)hypohalous acids like hypochlorous acid (HOCl, bleach), hypobromous acid (HOBr) and hypothiocyanous acid (HOSCN). Exogenous contributors to the generation of ROS include ultraviolet light, ionization irradiation, environmental toxins, and a variety of chemicals such as chemotherapeutics (Imlay 2008).

Intracellular and extracellular oxygen concentrations are equal due to the free permeation in and out of the cells (Ligeza, Tikhonov et al. 1998, Imlay 2008). Superoxide, which arises from the transfer of an electron to molecular oxygen, is enzymatically decomposed by superoxide dismutase to molecular oxygen and hydrogen peroxide. The fates of H_2O_2 differ depending on the respective cellular conditions. For instance, catalases and peroxidases detoxify hydrogen peroxide leading to the formation of a water molecule and oxygen. In the presence of redox-active metals, such as copper or iron, however, H_2O_2 is rapidly converted into highly reactive hydroxyl radicals, which damage DNA, lipids and proteins (Lemire, Harrison et al. 2013). Alternatively, haloperoxidases, such as myeloperoxidase (MPO), lactoperoxidase (LPO) or eosinoperoxidas (EPO), turn hydrogen peroxide and chloride (Cl^-), bromide (Br^-) or thiocyanate (SCN^-) into the highly reactive (pseudo)hypohalous acids HOCl, HOBr and HOSCN, respectively (Das, De et al. 1995, Wang and Slungaard 2006, Ashby 2008, Davies 2011, Winterbourn, Kettle et al. 2016). Typically, a network of proteins is in charge of maintaining redox homeostasis and keeping correct level of ROS. In times of an imbalance in the concentrations of ROS, such as by an excess production of ROS or a decreased detoxification, however, cells encounter what it known as

oxidative stress, a condition that is employed by the innate immune system when dealing with pathogens.

2.2 Oxidative burst as part of the innate immune response

HOCl, the active component in household bleach, is used in domestic and clinical settings as a potent antimicrobial agent (Rutala and Weber 1997). Mammalian hosts also employ HOCl as part of their host defense system against invading pathogens, specifically upon engulfment of bacteria by phagocytic cells. During the subsequent oxidative burst, activated NADPH-oxidases in the phagosome membrane, generate superoxide, which is decomposed to hydrogen peroxide. The enzyme myeloperoxidase (MPO) together with its oxidants HOCl, HOBr, and HOSCN, (van Dalen, Whitehouse et al. 1997) are released into the phagosome where they exert their toxic effects on the engulfed pathogen (Weiss and LoBuglio 1982, McKenna and Davies 1988, Hampton, Kettle et al. 1998, Klebanoff 1999). Targets of HOCl and HOBr include amino acids (e.g. cysteine, methionine), DNA, lipids, cholesterol and NADH (Carr, van den Berg et al. 1996, Prutz 1996, Winterbourn and Brennan 1997, Klebanoff 2005, Davies, Hawkins et al. 2008). HOSCN is more specific in its reactivity and appears to primarily attacks thiol groups (e.g. glutathione; protein cysteines) and selenogroups (Skaff, Pattison et al. 2009, Skaff, Pattison et al. 2012). A minor role in the antimicrobial defense is attributed to $O_2^{\bullet}$ and H_2O_2, although much higher concentrations and exposure times are necessary to yield sufficient killing (Klebanoff 1980). A similar strategy is used by the dual oxidase (DuOx), a two-domain enzyme consisting of an NAPH oxidase domain and a peroxidase, to limit bacterial colonization of mucosal barrier epithelia of the airway and intestine (Bae, Choi et al. 2010). Bacteria, on the other hand, employ specialized systems to combat the effects of oxidative stress, including i) expression of transcription factors and genes involved in detoxification and reduction of side chain modifications (Gebendorfer, Drazic et al. 2012, Gray, Wholey et al. 2013, Parker, Schwessinger et al. 2013), ii) posttranslational activation of stress specific molecular chaperones (e.g. Hsp33 and RidA) (Winter, Ilbert et al. 2008, Muller, Langklotz et al. 2014), and iii)

conversion of ATP into inorganic polyphosphate, a chemical chaperone effective in stabilizing protein structures (Gray, Wholey et al. 2014, Gray and Jakob 2015). HOCl is not only famous for its antimicrobial effects but has also been associated with damage to cellular compartments of the host itself, where excess HOCl production by activated neutrophils has been found to elicit a variety of human diseases, such as chronic inflammation and atherosclerosis (Weitzman and Gordon 1990, Winterbourn and Kettle 2000, Lau and Baldus 2006, Wu and Yotnda 2011). Despite good knowledge about the generation of HOCl, HOBr, and HOSCN, very little is known how efficient these three oxidants are in their bacterial killing, about their mode of action, or if bacteria employ the same response systems for all three stressors or display individualized defense strategies.

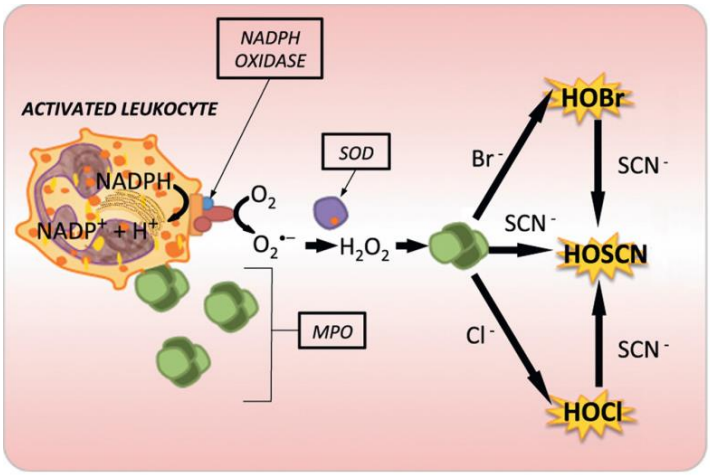

Figure 2.1: Oxidative burst and (pseudo)hypohalous acid production

During oxidative burst activated leukocytes release myeloperoxidase (MPO) and generate superoxide with the help of NADPH oxidase. Subsequent degradation of superoxide by superoxide dismutase (SOD) produces hydrogen peroxide, which MPO consumes to generate HOCl, HOBr, and HOSCN from the respective (pseudo)halide. In a non-enzymatic reaction SCN^- is able to scavenge HOCl and HOBr to yield HOSCN. Adapted from (Love, Barrett et al. 2016)

2.3 Generation of Haloperoxides

Several dedicated haloperoxidases generate hypohalous acids (HOX) involved in host defense. These include (i) myeloperoxidases (MPO) in activated neutrophils and macrophages during inflammation (Davies 2011); (ii) lactoperoxidases (LPO)

and salivary peroxidases in saliva and mucosal glands to inhibit bacterial growth in the oral cavity (Ashby 2008); (iii) eosinophil peroxidases in eosinophil granulocytes (EPO) (Wang and Slungaard 2006); and (iv) gastric peroxidases (GPO) in the stomach (Das, De et al. 1995). All of these haloperoxidases share their abilty to generate hypohalous acid from peroxide (H_2O_2) and the respective halides (e.g., Cl^-, Br^-) and/or pseudohalides (e.g., SCN^-). However, MPO is the only enzyme capable of synthesizing HOCl (Davies 2011, Winterbourn, Kettle et al. 2016) while the others prefer to generate HOBr and HOSCN. Additionally, the outcome of oxidants depends on the competing concentrations of the respective anions in the plasma (Cl^-: 100-140 mM, Br^-: 20-100 µM, SCN^-: 50-100 µM) as well as the substrate specificity of MPO for those halides (van Dalen, Whitehouse et al. 1997). MPO been shown to exert a more than 700-fold higher selectivity for SCN^- compared to Cl^-, resulting in 45% of all hydrogen peroxide consumed by MPO to generate HOCl, 5% HOBr and 50% HOSCN (van Dalen, Whitehouse et al. 1997). EPO is able to oxidize both SCN^- and Br^-, whereas LPO and GPO are limited to SCN^-.

2.4 (Pseudo)hypohalous acids (HOX) and their antimicrobial actions

A summary of relevant biochemical specifications of HOX is shown in Table 1.

2.4.1 Hypochlorous acid

The disinfecting power of HOCl was first reported by the French chemist Antoine-Germain Labarraque in 1828, when he discovered that chlorinated lime and soda solutions prevent infection and are able to treat putrefying and septic wounds (Scott 1828). HOCl is a strong oxidizing agent generated by the neutrophil-derived enzyme myeloperoxidase, which is the sole producer of HOCl due to its high redox potential under physiological conditions (Zuurbier, Bakkenist et al. 1990, Furtmuller, Zederbauer et al. 2006). Plasma concentrations for halides vary widely, ranging from millimolar concentrations for chloride (Cl^-: 100-140 mM) to micromolar concentrations for bromide (Br^-: 20-100 µM) and the pseudohalide thiocyanate (SCN^-: 50-100 µM) (van Dalen, Whitehouse et al. 1997). HOCl is one of the major players in antimicrobial host defense. The main targets of HOCl are

proteins, largely due to their abundance and the fast kinetic reactions with which HOCl reacts with certain side chains. This oxidation can lead to protein unfolding and aggregation (Winter, Ilbert et al. 2008). HOCl interacts with a plethora of amino acids, with cysteine and methionine residues reacting the fastest. At a physiological pH of 7.4, HOCl reacts with amino acid side chains in the following order: Met > Cys >> Cystine ~ His ~ α-amino > Trp > Lys >> Tyr ~ Arg > Gln ~ Asn (Pattison and Davies 2001). Cysteine and to a minor degree methionine modifications can serve as functional redox-switches in proteins, and serve at the forefront of redox sensing, catalysis in enzymes, and conferring structural rigidity by forming disulfide bonds. Changes in the redox environment and cellular oxidant levels are easily sensed through reversible modifications of the thiol group in cysteines of redox-sensitive proteins (Cook and Hogg 2013, Groitl and Jakob 2014). One specific trait of redox-sensitive cysteine residues is their lower than usual pK_a value (Roos, Foloppe et al. 2013), rendering them reactive to modifications by oxidants such as HOCl. The first intermediate in the oxidation of cysteine thiols is sulfenic acid, which is generally considered to be a very short-lived modification due to its high reactivity (Poole, Karplus et al. 2004, Kettenhofen and Wood 2010, Lo Conte and Carroll 2013). Sulfenic acids quickly attack other thiols in proteins to form intra- or intermolecular disulfide bonds. Alternatively, they form mixed disulfide bonds with small redox compounds such as glutathione (GSH) (i.e., S-glutathionylation), or react with amino groups to form cyclic sulfenamides (Groitl and Jakob 2014). Subsequent oxidation of sulfenic acid or sulfonamides results in the formation of sulfinic and sulfonic acids, a typically irreversible process. Peroxiredoxin, whose functions will be explained in more detail in chapter 2.5.3.1, is an exception, as its overoxidation product is reduced by sulfiredoxin, a specialized ATP-dependent sulfinic acid reductase (Rhee, Jeong et al. 2007, Moon, Kim et al. 2013). Reversible oxidative thiol modifications are reduced by members of the thioredoxin or glutaredoxin systems (Berndt, Lillig et al. 2007, Lu and Holmgren 2014) as explained in chapter 2.5.2.3.

2.4.2 Hypobromous acid

Hypobromous acid (HOBr), the major product of the oxidation of Br^- and H_2O_2 by eosinoperoxidase (EPO) is much less well characterized (Winterbourn, Kettle et al. 2016). HOBr has been associated with the defense against metazoan pathogens such as helminthic parasites (Klion and Nutman 2004). Although no significant correlation between lung function and levels of HOBr has been found, a crosstalk between elevated EPO levels and asthma has been reported (Sanz, Parra et al. 1997). Like HOCl, HOBr will react indiscriminately with both pathogens and the host organism, eliciting damage such as protein and lipid oxidation as well as DNA oxidation (i.e, bromination of nucleobases) (Asahi, Nakamura et al. 2015). Similarly to HOCl, the primary targets of HOBr are proteins, with cysteine, methionine and tryptophan being the most reactive (Choe, Richards et al. 2015). Studies in a sepsis model in mice showed that 3-bromotyrosine, a biomarker for HOBr protein modification, showed elevated level in wild-type mice but decreased levels in MPO-deficient mice, emphasizing the role of MPO in HOBr mediated protein oxidation (Gaut, Yeh et al. 2001). Despite its destructive character, recent studies also revealed an involvement in a more anabolic role of HOBr in tissue biogenesis, where peroxidasin-generated HOBr aids in the sulfilimine bond formation between the methionine sulfur and hydroxylysine nitrogen to stabilize the collagen IV network in epithelia and endothelia (Bhave, Cummings et al. 2012).

2.4.3 Hypothiocyanous acid

Natural sources for the pseudohalide SCN^-, derived from cyanide and cyanogenic compounds, include edible plants in the *Brassicacae* family such as cauliflower, broccoli and cabbage (Bliss and Oconnell 1984). Present in human bodily fluids such as tear, saliva and milk in millimolar concentrations, it exists in the micromolar range in plasma (Scherer 2006). Its chemical nature and reactivity during the reaction with haloperoxidases resembles that of halides, hence the name ‘pseudohalide’. One major factor influencing organismal SCN^- levels is smoking, since hydrogen cyanide (HCN) is one of the products released

during tobacco consumption. Smoking has been shown to increase cyanide and subsequently thiocyanate levels in the blood from ~40 ± 24 µM to ~130 ± 31 µM (Morgan, Pattison et al. 2011). Other SCN^- sources include drug exposure (e.g., sodium nitroprusside) and the metabolism of organic solvents such as acetonitrile (Vesey and Cole 1985). MPO preferentially reacts with SCN^- with a specificity constant of 1:60:730 for Cl^-, Br^- and SCN^-, respectively. Additionally to the enzymatic production of HOSCN, SCN^- can react in a non-enzymatic manner with HOCl and HOBr, thus scavenging these oxidants and decreasing their detrimental effects on the host. Patients suffering from the hereditary disease cystic fibrosis experience an imbalance in the concentrations of hypohalous acids in the lung, with an increase of HOCl and a decrease in HOSCN due to a defect in the cystic fibrosis transmembrane conductance regulator (CFTR), which also regulates the transport SCN^- and the cellular reducing agent glutathione (Kogan, Ramjeesingh et al. 2003, Lorentzen, Durairaj et al. 2011). These patients experience frequent and reoccurring lower respiratory tract infections (e.g. *P. aeruginosa*), chronic inflammation and progressive tissue damage in the lungs (Rao and Grigg 2006). Treatment of mice, infected with *P. aeruginosa* in their lungs with nebulized SCN^- has been shown to improve the respiratory function and decrease the bacterial load (Chandler, Min et al. 2013). Due to its pK_a of 5.3, the main form of HOSCN at neutral pH is hypothiocyanate (^-OSCN). It is considered to be highly specific to reactions with thiols (e.g. GSH; protein cysteines) and selenogroups (Skaff, Pattison et al. 2009, Barrett, Pattison et al. 2012), leading to a number of reversible oxidation products, including sulfenyl thiocyanates, sulfenic acids or disulfides (Barrett, Pattison et al. 2012). It has also been demonstrated that HOSCN targets numerous enzymes with catalytically active cysteines residues, thus rendering them inactive. Examples include thiol-containing proteins involved in metabolism and glycolysis such as fructose bisphosphate aldolase, triosephosphate isomerase, glyceraldehyde-3-phosphate dehydrogenase (GAPDH), and creatine kinase (Love, Barrett et al. 2016).

Oxidant	Description
Hypochlorous acid (**HOCl**) Hypobromous acid (**HOBr**)	• Strong two-electron oxidants with wide substrate variety • pK_a (HOCl) = 7.4; pK_a (HOBr) = 8.6 • Fastest reaction with cysteine and methionine • Ionized (low pK_a) thiols are more reactive • Thiol oxidation products include disulfides and high oxidation products • Minor reactions include chlorination and bromination of tyrosines (3-Cl-Tyr, 3-Br-Tyr) and nucleotides, as well as lipid peroxidation
Hypothiocyanous acid **(HOSCN)**	• Predominantly as $^-$OSCN at neutral pH • pK_a (HOSCN) = 5.3 • biological reactions predominantly with cysteines to give disulfides • Ionized (low pK_a) thiols are more reactive • Inert with methionine

Table 1: Characterization of (pseudo)hypohalous acids. Adapted from (Winterbourn, Kettle et al. 2016)

2.5 Oxidative stress defenses in bacteria

Various bacterial systems are known that protect microbes against the detrimental effect of ROS. Transcription factors are the first line of response to oxidative stress (chapter 2.5.1), regulating the gene expression of dedicated detoxifying systems such as catalase and peroxidases (chapter 2.5.2). In parallel, bacteria utilize posttranslational activation of stress-activated chaperone holdases to prevent proteins from aggregation and support their refolding once stress conditions are over (chapter 2.5.3).

2.5.1 Transcriptional regulation

2.5.1.1 The transcriptional regulator OxyR

The LysR family protein OxyR is a homotretrameric transcription factor found in redox-sensitive gram-negative bacteria, such as *E. coli* or *P. aeruginosa* (Kullik, Stevens et al. 1995, Imlay 2008, Vazquez-Torres 2012). Activation of OxyR is induced by H_2O_2 or HOCl mediated oxidation of a conserved cysteine concomitant with structural changes resulting in the cooperative binding of RNA polymerase (Tao, Fujita et al. 1993, Zheng, Aslund et al. 1998, Choi, Kim et al. 2001). Upregulated transcripts comprise genes involved in bacterial stress

response, including catalases, peroxidases like the alkyl hydroperoxide reductase (AhpC), and disulfide reductases such as *gorA* (glutathione reductase), *grxA* (glutaredoxin), *trxA* (thioredoxin) and *trxB* (thioredoxin reductase) (Christman, Morgan et al. 1985, Gonzalez-Flecha and Demple 1997). Further upregulated genes are *dps*, a DNA-iron binding protein, *fur,* an iron-binding repressor of iron transport, and *dsbG*, a periplasmic disulfide (Imlay 2008, Chiang and Schellhorn 2012). Additionally, OxyR is responsible for the generation of OxyS, a small non-coding RNA, which regulates the translation efficiency and/or mRNA stability of approximately 30 genes (Altuvia, WeinsteinFischer et al. 1997). One of the targets, whose transcription is negatively regukated by OxyS is RpoS, a major regulator of the general stress response regulon in bacteria. Presumably this negative regulation allows for a more specific response to stress condition by upregulating oxidative stress-specific genes and by downregulating more general stress repair pathways (Zhang, Altuvia et al. 1998). Reduction of OxyR is executed by the glutaredoxin and thioredoxin system, explaining the partial constitutive activation of OxyR when genes of the thioredoxin and glutaredoxin pathway (*gorA trxA* or *gshA trxA*) are deleted (Hausladen, Privalle et al. 1996, Zheng, Aslund et al. 1998, Aslund, Zheng et al. 1999).

2.5.1.2 The SoxRS regulon

Superoxide is the activating factor of the SoxRS regulon. In its activated state, SoxR induces the transcription of SoxS, which, once activated itself, regulates genes involved in the superoxide stress response (Wu and Weiss 1991) (Nunoshiba, Hidalgo et al. 1992). Superoxide is the predominant activator of SoxR, but other oxidants such as nitric oxide (NO), HOCl or elevated levels of H_2O_2 have been reported to active SoxR as well (Tsaneva and Weiss 1990, Nunoshiba, deRojas-Walker et al. 1993, Wang, Deng et al. 2009). Activation of SoxR, a member of the MerR family of transcriptional regulators, involves oxidation of the two 2Fe-2S clusters, causing significant structural rearrangements in SoxR and the subsequent transcription of *soxS* (Hidalgo and

Demple 1994, Hidalgo, Bollinger et al. 1995, Ha 2005). In this context, only the induction of the *soxS* gene transcription is redox dependent, whereas binding of SoxR to the *soxS* gene itself is not (Hidalgo and Demple 1994). The AraC family protein SoxS regulates the expression of more than 100 genes, many of which are important in the response to oxidative stress conditions (Blanchard, Wholey et al. 2007). One of the major SoxR/S regulated genes is manganese superoxide dismutase (*sodA*), which is responsible for the dismutation of superoxide to hydrogen peroxide. Another target is the repressor protein Fur (*fur*), whose increased expression will decrease the cellular iron uptake, which, in turn, decreases the Fenton reaction (Zheng, Doan et al. 1999). Further gene targets affect the cell membrane, such as *tolC* (outer membrane protein), *acrAB* (drug efflux pump) as well as *micF*, a small SoxR-regulated antisense RNA that represses OmpF translation (Dukan, Dadon et al. 1996, Storz and Imlay 1999). Once stress conditions are lifted, SoxR appears to be reduced by the gene products of *rsxBC* and *rseC* (Koo, Lee et al. 2003), whereas SoxS becomes quickly degraded (Griffith, Shah et al. 2004).

2.5.1.3 NemR

The TetR family protein NemR is a redox-regulated transcriptional repressor initially discovered to be sensitive to cysteine-modifying electrophiles (Umezawa, Shimada et al. 2008). *E.coli* NemR was recently found to respond to be reactive to chlorine species such as HOCl and N-chlorotaurine by the reversible modification of a redox-sensitive cysteine residue both *in vivo* and *in vitro* (Gray, Wholey et al. 2013). Once oxidized, NemR loses its repressing function leading to the upregulation of two genes, whose products are required for the detoxification of methylglyoxal (i.e., glyoxalase 1) and other reactive electrophiles (i.e. *N*-ethylmaleimide reductase). Enzymes involved in the detoxification of reactive chlorine species (RCS) stress triggered electrophiles have been studied in a plethora of gram-positive and gram-negative organisms, such as *E. coli*, *B. subtilis*, and *P. aeruginosa* (Small, Chang et al. 2007, Wang, Deng et al. 2009, Chi, Gronau et al. 2011, Gebendorfer, Drazic et al. 2012). Interestingly, the

crystal structure of *E. coli* NemR revealed a close proximity between the crucial cysteine residue (Cys106) and a conserved lysine residue (Lys175). These form a reversible cysteine-lysine sulfenamide bond upon oxidation, a thiol switch novel and unprecedented in other proteins (Gray, Li et al. 2015).

2.5.1.4 OhrR

The MarA family protein OhrR is a conserved transcriptional repressor present in both Gram-negative and Gram-positive bacteria. OhrR has been extensively studied in *B. subtilis*, where it contributes to the stress response to peroxide stress (e.g. organic hydroperoxides) along with other regulators such as PerR and sigma(B) (Fuangthong, Atichartpongkul et al. 2001, Vazquez-Torres 2012). The exposure to organic hydroperoxides mediates the oxidation of a critical cysteine and triggers a structural rearrangement leading to transcriptional de-repression of OhrR, which controls its own transcription as well as the organic hydroperoxide reductase OhrA (Fuangthong, Atichartpongkul et al. 2001, Cussiol, Alves et al. 2003). In *P. aeruginosa*, it has been shown that the organic hydroperoxide sensing regulator OspR, which controls the transcription of *gpx* (glutathione peroxidase), is connected to *ohrR* and can functionally complement an *ohrR* mutant (Atichartpongkul, Vattanaviboon et al. 2016). HOCl mediated RCS stress either directly or indirectly through organic hydroperoxides leads to the induction of the expression of the *ohr* gene in a variety of gram-positive and gram-negative organisms (Ceragioli, Mols et al. 2010, Peeters, Sass et al. 2010). *In vivo* studies in *B. subtillis* revealed that *ohrR* and *ohrA* mutants are more susceptible to HOCl stress in comparison to the respective wild-type strain (Chi, Gronau et al. 2011).

2.5.1.5 HypT

Recent studies using a genomic expression library unraveled a novel transcription factor in *E. coli* sensitive to the activation by RCS called HypT (hypochlorite-responsive transcription factor), a LysR family protein conserved in various gram-negative bacteria (Gebendorfer, Drazic et al. 2012). *In vitro*, HypT

exists as a dodecameric ring structure that changes its oligomerization state to a dimeric and tetrametric form upon HOCl stress to become activated. Expression changes elicited by HypT include an upregulation of cysteine, methionine and sulfur metabolism genes, and a downregulation of iron uptake genes, which, in consequence, leads to a decreased production of ROS by the Fenton reaction (Gebendorfer, Drazic et al. 2012). *In vivo* assays confirmed HypT's high specificity for HOCl, whereas other RCS and ROS species, such as monochloramine, hydroxyl radicals, or methionine sulfoxide, failed to activate the transcriptional regulator. Mutational studies, where select or numerous of the five cysteines in *E. coli* HypT were mutated, showed the existence of a stability conferring (Cys150) and an oligomerization critical (Cys4) cysteine residue (Drazic, Tsoutsoulopoulos et al. 2013). Methionine oxidation to methionine sulfoxide, however, was discovered to activate HypT, a mechanisms that was generally thought to inactivate cellular proteins. Methionine sulfoxide reductases A/B (*msrA* and *msrB)* trigger the subsequent inactivation of HypT once stress conditions are relieved (Drazic, Miura et al. 2013). In *E. coli*, *msrB* itself was found not be under the control of HypT upon HOCl induction whereas a *hypT* deletion mutant in *P. aeruginosa* PAO1 showed no discernable difference in the expression levels of *msrB* upon HOCl treatment (Romsang, Atichartpongkul et al. 2013).

2.5.2 Enzymatic detoxification systems

2.5.2.1 Catalases and peroxidases

Hydrogen peroxide is degraded by two systems, catalases and peroxidases, which decompose H_2O_2 to water and molecular oxygen. Catalases are adapted to scavenging high H_2O_2-concentrations, whereas peroxidases only fulfill their H_2O_2 decomposing function at low concentrations of peroxide. Surprisingly, strains lacking catalase in a variety of organisms such as *E. coli*, *P. aeruginosa* and *B. subtilis* are not only sensitive towards H_2O_2 treatment but also towards reactive chlorine species. Moreover, the gene expression for catalase is upregulated in response to RO/CS (Small, Chang et al. 2007, Wang, Deng et al.

2009, Chi, Gronau et al. 2011). These results suggest an involvement of catalases in the stress response to reactive H_2O_2 and reactive chlorine species. Studies on peroxidases as well as organic hydroperoxide reductases, such as OhrA, show an involvement in the detoxification of organic peroxides, which might stem from RCS, thus linking peroxidases to the defense against HOCl as well (Cussiol, Alves et al. 2003). Organic hydroperoxide reductases and peroxidases are also upregulated in a number of bacteria, including *E. coli*, *P. aeruginosa*, *B. cereus*, in response to HOCl, and mutants lacking OhrA (e.g. in *B. subtilis*) show increased HOCl sensitivity (Small, Chang et al. 2007, Wang, Deng et al. 2009, Ceragioli, Mols et al. 2010, Chi, Gronau et al. 2011).

2.5.2.2 Methionine sulfoxide reductase

In all three kingdoms of life, HOCl and other reactive oxygen species have been associated with the oxidation of methionine residues (Met) to methionine sulfoxide (MetO) (Boschi-Muller, Gand et al. 2008). MetO exists in two enantiomeric forms (*S* and *R*). Oxidative stress triggers the upregulation of the gene encoding the enzyme methionine sulfoxide reductase (Msr) in a variety of bacteria. Msr reduces methionine sulfoxide to methionine in concert with thioredoxin (Trx), thioredoxin reductase (Trr), and NADPH (Moskovitz, Weissbach et al. 1996). MsrA and MsrB reduce *S*-MetO and *R*-MetO, respectively (Moskovitz, Poston et al. 2000, Grimaud, Ezraty et al. 2001, Singh, Moskovitz et al. 2001, Lowther, Weissbach et al. 2002), thereby preventing the accumulation of oxidized and inactive proteins *(Moskovitz, Rahman et al. 1995, Singh, Moskovitz et al. 2001). In vivo* experiments in *E. coli* found that overexpression of Msr increases HOCl tolerance, whereas the respective deletion strain showed increased sensitivity (Rosen, Klebanoff et al. 2009). In *H. pylori* and *E. coli,* Msr has been shown to reduce oxidized catalase and repair the inactivation of the molecular chaperone GroEL, respectively thus conferring resistance to oxidative stress (Khor, Fisher et al. 2004, Mahawar, Tran et al. 2011).

2.5.2.3 The glutaredoxin and thioredoxin system

Bacteria such as *E. coli* utilize a range of enzymes to directly scavenge ROS and RCS. In addition, *E. coli* employs two dedicated systems to reverse oxidation events and restore the reducing environment in the cell, the thioredoxin (Trx) and the glutaredoxin (Grx) system. These systems share structural and functional similarity and are equally dependent on NADPH as ultimate electron source (Dyson, Holmgren et al. 1989, Xia, Bushweller et al. 1992, Martin 1995). Members of the thioredoxin system include two thioredoxins (*trxA/C*) and one thioredoxin reductase (*trxB*). The glutaredoxin system is composed of three glutaredoxins (*grxA/B/C*), one glutathione oxidoreductase (*gorA*), and glutathione (GSH, L-γ-glutamyl-L-cysteineglycine). The underlying mechanism for client reduction by thioredoxin and glutaredoxin is a thiol-disulfide exchange reaction, involving the two critical active site cysteine residues C-X-X-C motif (Mossner, Huber-Wunderlich et al. 1999). The client proteins of the thioredoxin and glutaredoxin systems included primarily cytosolic proteins, whose cysteines were oxidized to sulfenic acids or disulfide bonds, or were modified by nitrosylatation or S-glutathionylation (Holmgren 1989). Although the two pathways have some degree of specificity, the thioredoxin and glutathione systems operate in parallel to reduce oxidized cysteines. One specific reaction for the glutaredoxin system is the reduction of protein glutathionylations, whereas the thioredoxin system appears to be specifically necessary to transfer reducing equivalents from the cytoplasm to periplasm (Rietsch, Bessette et al. 1997). *In vivo* studies revealed a functional redundancy of both systems, and deletion of both systems results in lethality (Toledano, Kumar et al. 2007).

Two critical steps comprise the reduction of client proteins by Trx and Grx: (i) The N-termimal cysteine in the C-X-X-C motif forms an intermolecular disulfide bond with the client protein, thereby freeing one thiol from the intramolecular disulfide bond in the client; (ii) in a subsequent step, the C-terminal cysteine nucleophilically attacks the intermolecular disulfide bond resulting in a disulfide bonded Trx/Grx and a fully reduced client protein (Brandes, Larimer et al. 1993). Oxidized Trx is reduced in an enzymatic reaction by thioredoxin reductase.

Disulfide bonded Grx is reduced by two thiol exchange events with the tripeptide GSH, where Grx-GSH is an intermediate that is further reduced by a second GSH molecule to form oxidized glutathione (GSSG) and reduced Grx (Williams 1995). The FAD-containing thiol enzyme glutathione reductase (*gorA*) restores the GSH pool. The reducing power for both systems is fueled by NADPH generated in the pentose phosphate pathway (Holmgren 1988).

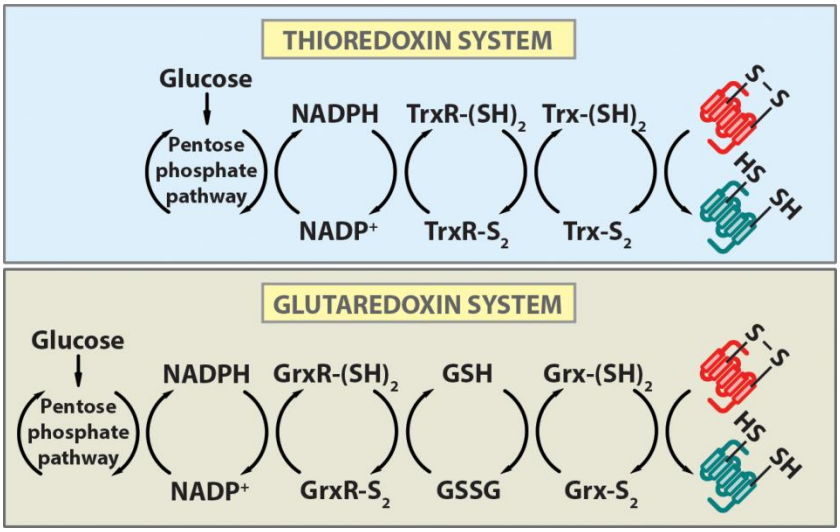

Figure 2.2: The thioredoxin and glutaredoxin system

Both the thioredoxin and glutaredoxin system function through protein disulfide oxidoreductases, and reduce the disulfide bond on an oxidized protein (red) to thiol groups (green). Thioredoxin (Trx) system: Central to Trx's activity is a -Cys-Gly-Pro-Cys- motif, which reduce disulfide bonds. Reduced Trx-$(SH)_2$ becomes oxidized to Trx-S_2 upon electron transfer to the oxidized client protein. Oxidized thioredoxin, in turn, becomes then reduced again by thioredoxin reductase (TrxR), which receives its reducing equivalents from the NADPH formed in pentose cycle. Glutaredoxin (Grx) system: In Grx a -Cys-Pro-Tyr-Cys- motif forms the active site for the oxidoreduction reaction. Glutaredoxin fulfills two functions. As a dithiol–disulfide oxidoreductase it reduces the client protein. When it acts as a GSH–disulphide oxidoreductase.it facilitates the reversal of mixed protein disulfides between proteins and GSH. To reduce Grx-S_2 or Grx-SSG back to Grx-$(SH)_2$ it interacts with GSH, which in turn is kept in its reduced state by glutathione reductase (GrxR). Like the thioredoxin system the reducing power is ultimately derived from NADPH. Adapted from (Berridge 2014)

2.5.3 Oxidative stress-induced chaperones

2.5.3.1 Hsp33 – A redox-regulated chaperone holdase

The heat shock protein 33 (Hsp33) is a highly conserved cytosolic chaperone in a variety of different bacteria as well as in select eukaryotes, including *Leishmania* and *Trypanosoma*, as well as certain algae and several higher plant species (Jakob, Muse et al. 1999). Hsp33 has previously been shown to specifically protect cytosolic proteins from oxidative stress mediated protein aggregation, caused by hydrogen peroxide in conjunction with elevated temperatures or by reactive chlorine species (e.g. HOCl) (Jakob, Muse et al. 1999, Winter, Linke et al. 2005, Ilbert, Horst et al. 2007, Winter, Ilbert et al. 2008). Bacteria encounter these stress conditions during inflammation (Jacquier-Sarlin, Fuller et al. 1994), and other host-mediated defense situations (Ryu, Ha et al. 2010). Activation of Hsp33 is one of the means by which bacteria significantly increase their resistance and survival towards these stress conditions.

Oxidative stress conditions result in a drop in cellular ATP levels as well as stress-mediated inactivation of some of the ATP-dependent chaperones (Tamarit, Cabiscol et al. 1998, Khor, Fisher et al. 2004). Examples include the eukaryotic homologue of DnaJ, Hdj2, which is inactivated by the hydrogen peroxide triggered oxidation of its zinc-binding domain (Choi, Lee et al. 2006), and GrpE, which has previously been found to unfold upon exposure to HOCl *in vitro* (Winter, Ilbert et al. 2008). Under these stress conditions, ATP-dependent bacterial chaperones such as DnaK or the GroEL-system are no longer able to facilitate in maintaining proteostasis. In turn, ATP-independent chaperones, such as the posttranslationally activated chaperone holdase Hsp33 take over to prevent protein aggregation (Winter, Linke et al. 2005, Winter, Ilbert et al. 2008).

Interestingly, Hsp33 is activated under the very same conditions that trigger the oxidative unfolding of a plethora of other proteins, including various crucial chaperones for proteostasis. Chaperone-inactive Hsp33 is compactly folded under non-stress condition and coordinates a zinc ion via four absolutely conserved cysteines in the C-X-C-X_n-C-X-X-C motif of Hsp33's C-terminal redox switch domain (Jakob, Eser et al. 2000). In the reduced and inactive state, the

flexible linker between the N- and C-terminal domains of Hsp33 is compactly folded (Vijayalakshmi, Mukhergee et al. 2001, Janda, Devedjiev et al. 2004). Intramolecular disulfide bond formation occurs upon exposure of Hsp33 to oxidizing conditions, linking the next neighbor cysteines (Barbirz, Jakob et al. 2000, Leichert, Gehrke et al. 2008). This oxidation causes zinc release, which, destabilizes the C-terminal redox switch domain and unfolds the adjacent linker region (Graf, Martinez-Yamout et al. 2004, Ilbert, Horst et al. 2007). Subsequently, dimerization between two conditionally unfolded monomers takes place to form the chaperone active dimer (Graf, Martinez-Yamout et al. 2004). Intriguingly, the normally stabilizing and structure shaping disulfide bonds turn Hsp33 into a natively unfolded protein (Graf, Martinez-Yamout et al. 2004, Reichmann, Xu et al. 2012). In its partially unfolded state, Hsp33 exposes binding sites responsible for client interaction both in the linker region and the adjacent N-terminus, but the exact sites and residues involved are unknown (Cremers, Reichmann et al. 2010, Reichmann, Xu et al. 2012). After the restoration of non-stress conditions, the disulfide bonds are reduced and zinc is re-coordinated (Hoffmann, Linke et al. 2004). For client transfer and shuttling to other molecular chaperones, such as the DnaK/DnaJ/GrpE system, cellular ATP-levels need to be replenished to release the client proteins from Hsp33, return Hsp33 to the chaperone-inactive state and support the client refolding to their native state (Hoffmann, Linke et al. 2004, Reichmann, Xu et al. 2012).

In recent years, several chaperones have been studied which use their stress-induced protein unfolding as a mechanism for posttranslational activation of their chaperone function. The pH-activated *E. coli* chaperones HdeA and HdeB, quickly lose structure upon low pH and aid in the prevention of low pH-mediated aggregation (Tapley, Korner et al. 2009, Tapley, Franzmann et al. 2010, Foit, George et al. 2013, Dahl, Koldewey et al. 2015). Other examples include members of the small heat shock protein family, whose chaperone funtions are activated by heat-induced structural rearrangements (Haslbeck, Ignatiou et al. 2004, Peschek, Braun et al. 2013). Employing these activation mechanisms abrogates the need for elaborate and time-consuming transcription and

translation processes, and provides instantaneous protection against fast acting protein unfolding stresses, including HOCl exposure or acid treatment (Bardwell and Jakob 2012).

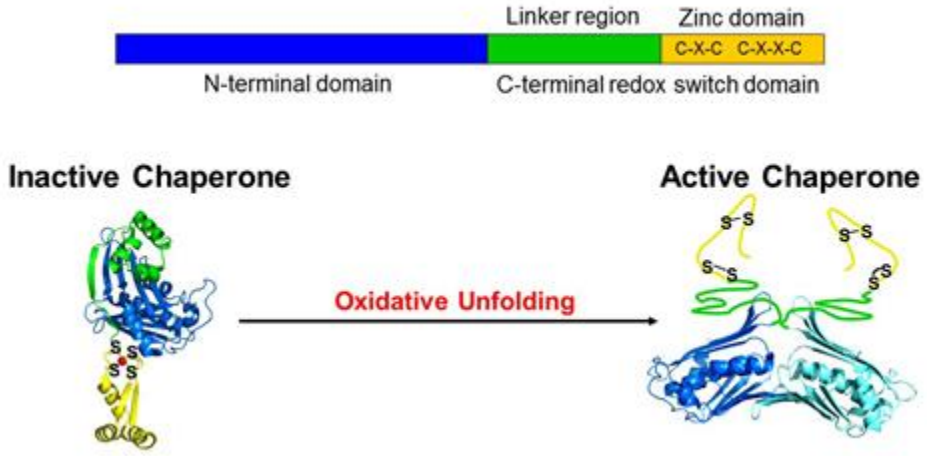

Fig. 2.3: Domain structure and activation of Hsp33

Hsp33 is a two domain protein, consisting of an N-terminal domain (blue) and a C-terminal domain based of the flexible linker region (green) and the redox switch domain (yellow). In its reduced and inactive form Hsp33 is compactly folded monomer, and four cysteines coordinate a zinc ion (red sphere) in a tetrahedral conformation. Exposure to oxidative stress conditions leads to a zinc release form the redox switch domain upon oxidation of the two distal cysteines (Cys265/Cys268) and to unfolding of this domain. The linker region is in equilibrium between the folded and unfolded state. Only after disulfide bond formation of the proximal cysteines the linker region is shifted to its unfolded state, enabling dimerization and the chaperone activation of Hsp33. This crucial disulfide bond formation is facilitated by fast acting oxidants, such as HOCl. Adapted from (Cremers, Reichmann et al. 2010).

2.5.3.1.1 Client binding sites in Intrinsically Disordered Chaperones

So far, little information is available as to what exact regions and residues in conditionally unfolded chaperones, such as Hsp33, are involved in the interaction with unfolding client proteins. To date, there are only limited structural data on client-chaperone complexes available to give an answer to this question. Chen et al. 2013 were able to trap the transient interaction between GroEL/ES and RuBisCO, and visualize substrate binding by cryo-electron microscopy (Chen, Madan et al. 2013). Moreover, Zhang et al. 2011 employed unnatural amino acids incorporation in combination with crosslinking to identify residues of HdeA that are involved in client binding (Zhang, Lin et al. 2011). Recently Horowitz et

al. 2016 used a novel structural biology approach based on X-ray crystallography, termed residual electron and anomalous density (READ), to identify the substrate binding site of Spy and determined that substrate folding of Spy's client protein, immunity protein 7 (Im7), occurs while bound to Spy (Horowitz, Salmon et al. 2016).

Intrinsically unfolded regions have long been postulated to be crucial for chaperone function and substrate binding (Tompa and Csermely 2004). One example is the flexible N-terminal domain in the small heat shock protein PsHsp18-1, which was proposed to be involved in client binding (Jaya, Garcia et al. 2009). Transient chaperone-client interactions using the disordered C-terminus of DnaK have been shown to contribute extensively to DnaK's chaperone function (Smock, Blackburn et al. 2011). It has previously been proposed that the loss of structure in Hsp33 during the activation process (Graf 2004, Ilbert, Horst et al. 2007, Winter, Ilbert et al. 2008, Reichmann, Xu et al. 2012) could potentially be involved in client protein binding. In this work we set out to ultimately solve the puzzle of the substrate binding site in Hsp33 and give answers to how conditionally disordered proteins work.

2.5.3.2 Peroxiredoxin

Peroxiredoxins are one of the essential players in the protection against oxidative stress conditions, the maintenance of redox homeostasis and controlling H_2O_2-sensitive signaling cascades (Wood, Poole et al. 2003, Rhee, Chae et al. 2005). They are found in all domains of life (Hofmann, Hecht et al. 2002), where they efficiently detoxify H_2O_2, organic hydrogen peroxides and peroxynitrite (Rhee, Chae et al. 2005). Deletion of peroxiredoxin-encoding genes causes severe phenotypes and premature aging in several model organisms (Lee, Kim et al. 2003, Neumann, Krause et al. 2003, Kumsta, Thamsen et al. 2011).

Members of the peroxiredoxin family all share an active site cysteine (i.e., peroxidatic cysteine) responsible for the detoxification of peroxides. During the catalytic cycle, this cysteine residue becomes oxidized and forms a sulfenic acid intermediate (Poole 2007, Hall, Nelson et al. 2011). The mechanism by which

this thiol groupd is re-reduced defines the specific classes of peroxiredoxins (Poynton and Hampton 2014). The sulfenic acid in 1-Cys peroxiredoxins (e.g. Prx-6), is regenerated by reducing agents such as ascorbate or low molecular weight thiols *in vitro*. However, the underlying mechanism for its *in vivo* reduction still remains elusive. In the second class of peroxiredoxins, so-called 2-Cys peroxiredoxins, a conserved second cysteine (i.e. resolving cysteine) attacks the peroxidatic sulfenic acid group and forms either an intra- or an intermolecular disulfide bond (Knoops, Loumaye et al. 2007). In a cascade of reduction events employing thioredoxin, thioredoxin-reductase and NADPH, the disulfide bond is reduced (Du, Zhang et al. 2013). Select 2-Cys peroxiredoxins use a thiol-exchange mechanism interacting with redox-sensitive cysteines in other proteins to ensure their own re-reduction.

Due to the spatial distance between the peroxidative and the resolving cysteine, substantial conformational changes and a local unfolding event in the active site are necessary to ensure disulfide bond formation (Schroder, Littlechild et al. 2000). In some 2-Cys peroxredoxins, this unfolding process is kinetically impaired by a C-terminal extension, leading to the overoxidation of the peroxidatic sulfenic acid to sulfinic acid (Wood, Poole et al. 2003). This seemingly evolutionarily illogical phenomenon in peroxiredoxins could be explained after two separate discoveries; i) overoxidized, peroxidase-inactive peroxiredoxins exert a second function as molecular chaperones; ii) specialized enzymes (i.e., sulfiredoxins) exist, which specifically to re-reduce overoxidized peroxiredoxins and, thus, reverse the transient inactivation of these enzymes (Biteau, Labarre et al. 2003). Overoxidation of peroxiredoxin has been found to exert beneficial effects during high oxidative stress conditions. In mammalian cells, overoxidation of peroxiredoxin is thought to regulate signal cascades by providing an optimal amount of the second messenger H_2O_2 (Wood, Poole et al. 2003). In *Schizosaccharomyces pombe* the inactivation of peroxiredoxin leads to liberation of the thioredoxin pool enabling the reduction of oxidized and aggregation-prone protein (Day, Brown et al. 2012).

In recent studies in yeast and other organisms, inactivation of peroxiredoxin has been associated with the formation of oligomeric structures, including decamers. This process turns peroxiredoxin into an ATP-independent chaperone, whose mode of action is comparable to other redox-regulated chaperones such as Hsp33 (Jang, Lee et al. 2004). In the protozoan parasite *Leishmania infantum*, mitochondrial peroxiredoxin (Prx) is able to prevent the aggregation of a plethora of proteins during heat stress both *in vitro* and *in vivo* (Teixeira, Castro et al. 2015). Upon oligomerization, aggregation-prone client proteins are tightly bound in the center of the decameric ring, they are kept in refolding-competent conformation state. When stress conditions subsided, client proteins are transferred to the ATP-dependent refolding machinery.

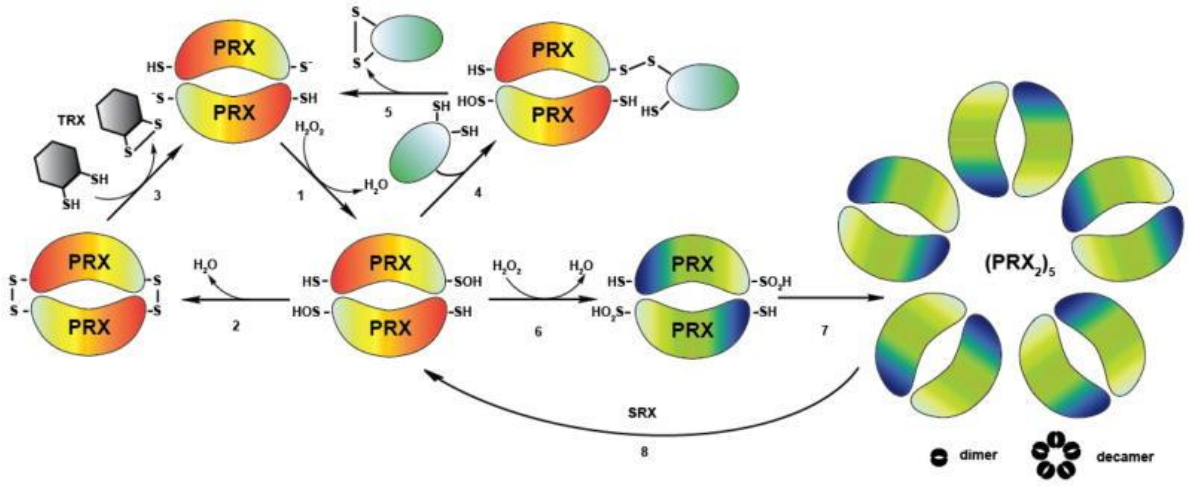

Figure 2.4: Peroxiredoxin – peroxidatic and chaperone function

1) Peroxiredoxins (orange) degrade hydrogen peroxide, and their peroxidatic cysteines form sulfenic acids. (2) Subsequently, the resolving cysteine in Prx forms a disulfide bond with the sulfenic acid. (3) The thioredoxin systems reduces this disulfide bond in Prx. (4) Oxidized peroxiredoxin can also react with the thiol group of a reduced client protein (e.g. Yap1p) and thus generates an intermolecular disulfide bond. (5) By thiol-disulfide exchange this disulfide bond is broken again, resulting in reduced Prx and a disulfide bond in the client protein. (6) In case of severe oxidative stress, high levels of peroxide accumulate. H_2O_2 then causes the overoxidation to sulfinic acid at the active site cysteine and inactivates the peroxidase function. (7) Subsequently, higher oligomers form, which prevent protein aggregation *in vitro*. (8) Peroxiredoxin is reversed to its reduced state by the ATP-dependent enzyme sulfiredoxin (SRX). Adapted from (Groitl and Jakob 2014)

2.5.3.3 RidA – Chaperone activation by N-chlorination

The *E. coli* protein RidA, an enamine/imine deaminase (Lambrecht, Flynn et al. 2012), is member of a conserved, functionally diverse YjgF/YER057c/UK114 family. In a recent study, HOCl treated RidA from *E. coli* has been found to rapidly activate as a potent chaperone holdase *in vitro*, and rescue client proteins from HOCl-stress induced unfolding (Muller, Langklotz et al. 2014). Increased susceptibility to oxidative stress in *E. coli* strains lacking *ridA* underlined RidA's relevance as a bacterial defense system against bleach. Unlike other redox-regulated chaperones, such as Hsp33 or 2-Cys peroxiredoxins (Kumsta and Jakob 2009), the activation of RidA is not cysteine mediated.

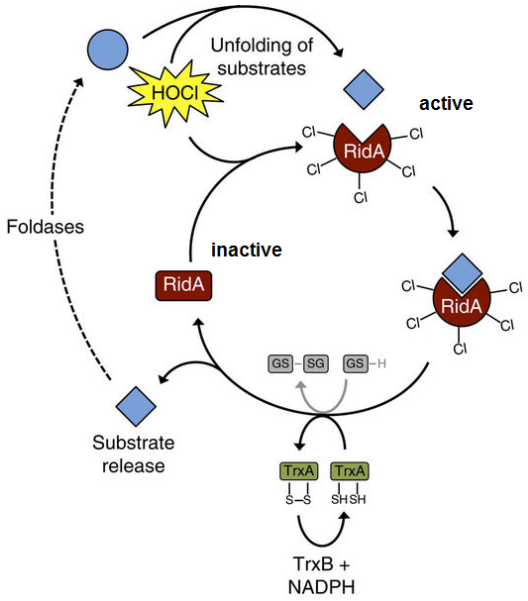

Figure 2.5: RidA – a chaperone activated by *N*-chlorination

HOCl trigger proteins unfolding in cellular proteins. *N*-chlorination of RidA leads to its activation, preventing the aggregation of a plethora of unfolding client proteins. Thioredoxin and GSH reduce RidA, resulting in the release of the client, which can then be refolded by the foldase machinery. Adapted from (Muller, Langklotz et al. 2014)

Instead, *N*-chlorination of lysine and arginine residues as well as of the N-terminus activates RidA's chaperone function, a modification that is usually associated with protein damage, unfolding and aggregation (Hawkins and Davies 1998, Winter, Ilbert et al. 2008, Muller, Langklotz et al. 2014). This novel activation mechanism is fully reversible *in vitro* by the addition of reducing agents

(e.g. DTT), transferring RidA back into its inactive form. *In vivo*, glutathione and to a minor degree the NADPH dependent thioredoxin system facilitate in the inactivation. *N*-chlorination of proteins adds a new regulatory layer to the toolbox of post-translational activation mechanisms of chaperone foldases, and it is conceivable that other stressors, such as HOBr, similarly activate RidA's chaperone function (Muller, Langklotz et al. 2014).

2.5.3.4 Polyphosphate as a molecular chaperone

Polyphosphate (polyP), a polymer found in all realms of life, is composed of up to 1,000 orthophosphate groups linked via phosphoanhydride bonds (Rao, Gomez-Garcia et al. 2009). In eukaryotes it has been associated with apoptosis (Hernandez-Ruiz, Gonzalez-Garcia et al. 2006), stimulation of mTOR-activity (Wang, Fraley et al. 2003), blood clotting (Morrissey, Choi et al. 2012), and inflammation (Dinarvand, Hassanian et al. 2014). A variety of different functions has been reported in prokaryotes ranging from metal chelating and phosphate storage functions (Weiss, Bental et al. 1991), to biofilm formation (Shi, Rao et al. 2004) to regulatory roles in growth, development and survival (Kornberg, Rao et al. 1999). The Nobel Prize laureate Arthur Kornberg, who spent the last ten years of his life working on polyphosphate, discovered that the deletion of the gene encoding for the polyphosphate generating enzyme polyphosphate kinase (PPK) makes bacteria susceptible to stressors, such as heat and oxidation. During the exposure to ROS, especially HOCl, cellular ATP levels drop, and ATP is converted and reversibly stored in the form of polyphosphate, a reaction executed by PPK (Gray, Wholey et al. 2014). Exopolyphosphatase (PPX) is the enzyme responsible for the degradation of polyP.

A recently discovered polyphosphate mediated defense mechanism against extremely potent oxidizing agents, such as HOCl, is its function as an efficient molecular chaperone (Gray, Wholey et al. 2014). HOCl, and presumably HOBr, elicit protein aggregation by modifying and reacting with several amino acids side chains, as mentioned earlier. Exposure of *E. coli* to sublethal doses of bleach cause significant accumulation of polyphosphate, in part triggered by the

oxidation-mediated inhibition of PPX (Gray, Wholey et al. 2014). Both *in vivo* and *in vitro*, polyP was found to be able to protect a wide range of cellular and model proteins from unfolding and aggregation, with longer chains of polyP being more effective in keeping proteins soluble during stress conditions than shorter ones. Interestingly, *in vitro* aggregation studies, for example using the model protein firefly luciferase, showed that polyP converts thermolabile, predominantly α-helical proteins into thermostable, β-sheet rich intermediates, keeping them soluble even under extreme heat stress conditions (Gray, Wholey et al. 2014)(Gray et al). Polyphosphate exerts its general chaperone function by holding proteins in a refolding competent state. Once oxidative stress conditions are relieved and ATP levels restored, clients are handed over to the ATP-dependent DnaK/DnaJ/GrpE system for refolding. Unlike many other chaperones, polyP is inert to the reaction with reactive oxygen species (e.g. HOCl), and can exert its ATP-independent chaperone function instantaneously, abrogating the need for lengthy transcription and translation events. It still remains to be determined how polyP exactly interacts with proteins to prevent aggregation, what common features of client proteins are, and how PolyP aids in combating other oxidation related stresses such as the exposure to HOBr or HOSCN.

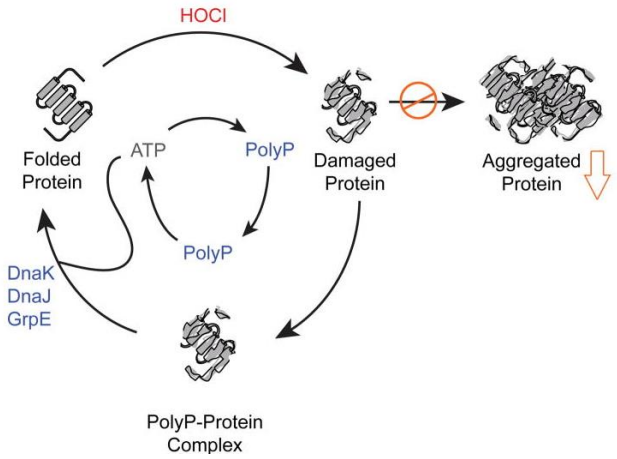

Figure 2.6: Polyphosphate prevents protein aggregation

HOCl leads to oxidation mediated protein unfolding. Under oxidative stress polyP is formed from ATP, which keeps client proteins soluble and refolding competent. ATP-dependent chaperones (*e.g.* DnaK, DnaJ, and GrpE) refold the client protein and polyP is turned back into ATP. Adapted from (Gray and Jakob 2015)

2.6 Outline

Defense systems against oxidative stress are essential for bacteria to rapidly adapt to reactive oxygen and chlorine species released by the innate immune system of the host and ultimately ensure survival. In this thesis, we first determined how posttranslational activation of a redox-sensitive chaperone aids to prevent oxidation-induced unfolding and aggregation. In the second part of the thesis, we sought to obtain deeper understanding as to how bacteria react generally to hypohalous acids as stressors, and which bacterial systems apart from Hsp33 are employed to protect bacteria against these oxidants. Data obtained in this study led us to conclude that the underlying molecular mechanism for the antimicrobial action of all three oxidants involve oxidative protein unfolding and aggregation, and that polyphosphate is the universal defense system to prevent oxidative unfolding mediated killing.

3 Experimental Procedures

Chemicals used for buffer preparation are obtained from Sigma Aldrich, Fisher Scientific, or Molecular Probes. Vendors for all other probes are marked in the text. Use of equipment is universally described or stated within the text.

3.1 Strains and plasmids

	Marker	Relevant genotype	Reference
Strains			
E. coli BL21(DE3) *hslO::kan*	Kan^R	F^- *ompT gal dcm lon hsdSB* (*rB*$^-$ *mB*$^-$)λ (DE3 (*lacI lacUV5-T7 gene 1 ind1 sam7 nin5*)) *hslO*::kan	(Cremers, Reichmann et al. 2010)
E. coli NEB10β		*Δ(ara-leu) 7697 araD139 fhuA ΔlacX74 galK16 galE15 e14- ϕ80dlacZΔM15 recA1 relA1 endA1 nupG rpsL* (Str^R) *rph spoT1 Δ(mrr-hsdRMS-mcrBC)*	New England Biolabs
E. coli MC4100		F- *[araD139]$_{B/r}$ Δ(argF-lac)169* &lambda$^-$ e14- flhD5301 Δ(fruK-yeiR)725 (fruA25)‡ relA1 rpsL150(strR) rbsR22 Δ(fimB-fimE) 632(::IS1)deoC1*	(Cremers, Reichmann et al. 2010)
E. coli S17.1		TpR SmR recA, thi, pro, hsdR-M+RP4: 2-Tc:Mu: Km Tn7 λpir	D. Nyugen, McGill University, Canada
P. aeruginosa PA14		Wild-type PA14	B. Boles, University of Iowa, USA
P. aeruginosa PA14 *hslO*$^-$		PA14 Δ*hslO*	This work
P. aeruginosa PA14 *ppk*$^-$		PA14 Δ*ppk*	This work
P. aeruginosa PA14 *hslO*$^-$ *ppk*$^-$		PA14 Δ*hslO* Δ*ppk*	This work
Plasmids			
pEVOL	Cm^R	Plasmid used for incorporation of BPA	(Young, Ahmad et al. 2010)
pDULE2-pCNF	$Spec^R$	Plasmid used for incorporation of tFPA	(Peeler and Mehl 2012)
pET11a	Amp^R	IPTG inducible expression vector	(Cremers, Reichmann et al. 2010)
pET21b	Amp^R	IPTG inducible expression vector (C-terminal His_6 tag)	Novagen

pET11a *hslO*	Amp^R	Plasmid expressing wild-type Hsp33 (*hslO*)	(Cremers, Reichmann et al. 2010)
pET11a PA14 hslO	Amp^R	Plasmid expressing wild-type *P.aeruginosa* PA14 Hsp33	This work
pET11a *hslO* M172S	Amp^R	Plasmid expressing Hsp33 M172S	(Cremers, Reichmann et al. 2010)
pET21b *hslO* M172S	Amp^R	*hslO M172S* cloned into NdeI/HindIII of pET21b	This work
pBG31	Amp^R	$Y12^{UAG}$ mutation in pET11a *hslO* M172S	This work
pBG32	Amp^R	$F14^{UAG}$ mutation in pET11a *hslO* M172S	This work
pBG33	Amp^R	$Y39^{UAG}$ mutation in pET11a *hslO* M172S	This work
pBG34	Amp^R	$M77^{UAG}$ mutation in pET11a *hslO* M172S	This work
pBG35	Amp^R	$Y127^{UAG}$ mutation in pET11a *hslO* M172S	This work
pBG36	Amp^R	$L142^{UAG}$ mutation in pET11a *hslO* M172S	This work
pBG37	Amp^R	$Y145^{UAG}$ mutation in pET11a *hslO* M172S	This work
pBG38	Amp^R	$F146^{UAG}$ mutation in pET11a *hslO* M172S	This work
pBG39	Amp^R	$F157^{UAG}$ mutation in pET11a *hslO* M172S	This work
pBG40	Amp^R	$M172^{UAG}$ mutation in pET11a *hslO* M172S	This work
pBG41	Amp^R	$F187^{UAG}$ mutation in pET11a *hslO* M172S	This work
pBG42	Amp^R	$L202^{UAG}$ mutation in pET11a *hslO* M172S	This work
pBG43	Amp^R	$L203^{UAG}$ mutation in pET11a *hslO* M172S	This work
pBG44	Amp^R	$W212^{UAG}$ mutation in pET11a *hslO* M172S	This work
pBG45	Amp^R	$Y223^{UAG}$ mutation in pET11a *hslO* M172S	This work
pBG46	Amp^R	$Y267^{UAG}$ mutation in pET11a *hslO* M172S	This work
pBG47	Amp^R	$Y272^{UAG}$ mutation in pET11a *hslO* M172S	This work
pBG48	Amp^R	$F274^{UAG}$ mutation in pET11a *hslO* M172S	This work
pBG49	Amp^R	*hslO M172S* $Y12^{UAG}$ cloned into NdeI/HindIII of pET21b	This work
pBG50	Amp^R	*hslO M172S* $F14^{UAG}$ cloned into NdeI/HindIII of pET21b	This work
pBG51	Amp^R	*hslO M172S* $Y39^{UAG}$ cloned into NdeI/HindIII of pET21b	This work
pBG52	Amp^R	*hslO M172S* $M77^{UAG}$ cloned into NdeI/HindIII of pET21b	This work
pBG53	Amp^R	*hslO M172S* $Y122^{UAG}$ cloned into NdeI/HindIII of pET21b	This work
pBG54	Amp^R	*hslO M172S* $L142^{UAG}$ cloned into NdeI/HindIII of pET21b	This work
pBG55	Amp^R	*hslO M172S* $Y145^{UAG}$ cloned into NdeI/HindIII of pET21b	This work
pBG56	Amp^R	*hslO M172S* $F146^{UAG}$ cloned into NdeI/HindIII of pET21b	This work
pBG57	Amp^R	*hslO M172S* $F157^{UAG}$ cloned into NdeI/HindIII of pET21b	This work

pBG58	Amp^R	*hslO M172*^{UAG} cloned into NdeI/HindIII of pET21b	This work
pBG59	Amp^R	*hslO M172S F187*^{UAG} cloned into NdeI/HindIII of pET21b	This work
pBG60	Amp^R	*hslO M172S L202*^{UAG} cloned into NdeI/HindIII of pET21b	This work
pBG61	Amp^R	*hslO M172S L203*^{UAG} cloned into NdeI/HindIII of pET21b	This work
pBG62	Amp^R	*hslO M172S W212*^{UAG} cloned into NdeI/HindIII ofpET21b	This work
pBG63	Amp^R	*hslO M172S Y223*^{UAG} cloned into NdeI/HindIII of pET21b	This work
pBG64	Amp^R	*hslO M172S Y267*^{UAG} cloned into NdeI/HindIII of pET21b	This work
pBG65	Amp^R	*hslO M172S Y272*^{UAG} cloned into NdeI/HindIII of pET21b	This work
pBG66	Amp^R	*hslO M172S F274*^{UAG} cloned into NdeI/HindIII of pET21b	This work
pEXGm18	Gm^R	Plasmid for the deletion of genes by homologous recombination in PA14	D. Nyugen, McGill University, Canada
pEX18Gm hslOupdownSOE	Gm^R	Plasmid used for deletion of *hslO* in PA14	This work
pEX18Gm hslOupdownSOE	Gm^R	Plasmid used for deletion of *ppk* in PA14	This work

3.2 Generation of Hsp33 mutants

The Hsp33-M172S stop codon (UAG) mutants were generated by introducing single site mutations into the Hsp33 mutant gene M172S (*hslO*) using pUJ30 (pET11a-*hslO* M172S) (Jakob 2000) as a template. For mutagenesis a single a single primer QuikChange mutagenesis was used. In brief, a mutagenic PCR reaction was set up with the following specifications:

5x GC Buffer	10 µl	10mM dNTPs	1 µl
mutagenic primer	125 ng (0.5 ul)	plasmid template	~ 40 ng (1.0 ul)
Phusion polymerase	0.5 µl	dH2O	to a total of 50 µl

Program:

1) 1 min @ 98°C
2) 0 sec @ 98°C
3) 1 min @ 60°C
4) 5 min @ 72°C (x 30 cycles)
5) 1 min 10 sec per 1kB @ 72°C
6) 4°C

After DpnI treatment of the PCR products for 2 h at 37°C, cloning and subsequent transformation by a heat shock method into BL21 *hslO::kan* the isolated plasmids were sent for sequencing. Clones carrying verified plasmids were stored at -80°C.

3.3 Generation of *P.aeruginosa* PA14 mutant strains

A clean deletion of *hslO*, *ppK* or *hslO/ppK* in *P. aeruginosa* strain PA14 was generated as previously described (Hmelo, Borlee et al. 2015). In brief, a 500 bp upstream and a 500 bp downstream region of the PA14 *hslO* and *ppk* gene were amplified by PCR. Sowing overlap extension PCR was used to amplify the constructs *hslO*updwSOE and *ppk*updwSOE. The plasmids pEX18GmhslOupdwSOE and pEX18GmppkupdwSOE were generated by integrating the constructs into the multiple cloning site (MCS) of the allelic exchange vector pEX18Gm using *BamH*I and *Hind*III restriction sites. Plasmids were verified by PCR using MCS specific primers M13F-21 and M13R. For subsequent puddle mating with the respective PA14 strain, the plasmid constructs were transformed into the donor strain *E. coli* S17.1 (λ pir^+) using standard chemical transformation. Transformed *E. coli* cells were plated onto LB agar plates supplemented with 10 µg ml^{-1} gentamicin and grown overnight at 37°C. The same day, an overnight culture of the recipient strain PA14 was prepared. The following day, an equal volume of fresh LB was added to the PA14 overnight culture, and the PA14 strain was incubated at 42°C for 3 h and until the *E. coli* donor strain had reached A_{600} = 0.5-0.6. 1.5 ml of the *E. coli* donor strain and 0.5 ml of the PA14 recipient strain were mixed and centrifuged for 5 min at 10,000 x *g* at room temperature. Cells were pelleted, resuspended in 50 µl LB medium and transferred onto a LB agar plate for overnight incubation at 30°C. The bacterial lawn was scraped from the plate and resuspended in 1 ml of sterile PBS. Then 10 µl, 100 µl and 500 µl aliquots of the resuspension were plated onto Vogel-Bonner Minimal Medium (VBMM) plates supplemented with 60 µg ml^{-1} gentamicin and the plates were incubated for 48 h at 37°C. For the counter-selection, an isolated colony from the VBMM plate was picked, streaked onto no-salt LB-plates supplemented with 15% (w/v) sucrose, and incubated for 36-48 h

at 30°C. Colonies were PCR verified to confirm the deletion of the PA14 *hslO* and *ppk* genes using the respective sequencing primers.

3.4 Protein purification

Purification of proteins in this work was done manually by employing a P1- pump (Pharmacia LKB) or with an Äkta-FPLC system (GE Healthcare).

3.4.1 Purification of wild-type and Hsp33 mutant proteins

Unlabeled wild-type Hsp33 from *E.coli* was expressed in the *E. coli* expression strain BL21 *hslO::kan* and purified as described (Graumann, Lilie et al. 2001). In brief, Hsp33-expressing cells (BL21 hslO::kan, pET11a *E.coli hslO* or pET11a *P. aeruginosa hslO*) were grown at 37°C in the presence of 1 mM $ZnCl_2$ and harvested 6 hr after induction with 1 mM IPTG. Cells were resuspended in buffer A (40 mM HEPES-KOH, 0.2 M KCl [pH 7.5], 1 tablet Roche complete protease inhibitor mix, 2 mM PMSF) and lysed (French Press, three cycles, 14,000 psi). The cleared supernatant was applied onto a Q-Sepharose column (Pharmacia) and eluted with a KCl gradient between 450 and 600 mM KCl in buffer A. The Hsp33-containing fractions were dialyzed against 10 mM potassium phosphate (pH 6.8) buffer and applied onto a hydroxylapatite column. Hsp33 eluted between 10 and 70 mM potassium phosphate. The Hsp33-containing fractions were then loaded onto a Superdex 75 (Pharmacia) equilibrated in buffer A. Highly purified Hsp33 fractions from the Superdex column were dialyzed against storage buffer (40 mM potassium phosphate buffer [pH 7.5]). ^{15}N-labelled wild-type Hsp33 and Hsp33-Y12E were expressed in M9 minimal medium supplemented with 0.1% (w/v) ^{15}N-labelled ammonium chloride and purified as before. pET11a *P. aeruginosa* PA14 *hslO* was created by cloning the *hslO* gene from genomic *P. aeruginosa* PA14 into pET11a using BamHI and HindIII restriction sites. PA14 Hsp33 was expressed and purified as described for *E. coli* Hsp33.

3.4.2 Purification of Hsp33 M172S amber stop codon mutants for ^{19}F-NMR

A cotransformation of pET21b plasmids containing a His-tagged version of the respective Hsp33^{M172S}-amber variants and pDule2-pCNF (plasmid encoding an orthogonal aminoacyl-tRNA synthetase/tRNA pair) (Peeler and Mehl 2012) into BL21 *hslO::kan* was performed. After overnight growth of transformants on LB plates, supplemented with 200 mg ml^{-1} ampicillin and 100 mg ml^{-1} spectinomycin, transformed cells were scraped off the plates and used to inoculate 1 l of protein expression medium (12 g l^{-1} tryptone, 24 g l^{-1} yeast extract, 4% glycerol (v/v), 2.1 g l^{-1} potassium phosphate (monobasic) and 12.5 g l^{-1} potassium phosphate dibasic), supplemented with 1 mM $ZnCl_2$, 1 mM 4-trifluoromethoxy-phenylalanine (tFPA) (JRD Fluorochemicals), 200 mg ml^{-1} ampicillin and 100 mg ml^{-1} spectinomycin to an A_{600} of 0.4. Following 1 h of incubation at 37 °C with shaking (200 r.p.m.), cells were shifted to 20 °C and protein overexpression was induced with 0.2 mM IPTG and 0.2% (w/v) L-arabinose. The following day harvested cells (4,000*g*, 20 min, 4 °C) were resuspended in 40 mM potassium phosphate (KPi), 200 mM KCl, 10 mM imidazole and pH 7.5 supplemented with one tablet of protease inhibitor (Roche) and 1 mM phenylmethylsulphonyl fluoride (Sigma-Aldrich). Cell lysis was performed using a French press cell (3 × 1,400 p.s.i.). Filtered lysate was loaded onto a nickel-NTA column (GE Healthcare) equilibrated in 40 mM KPi, 200 mM KCl, 10 mM imidazole, pH 7.5 and Hsp33 variants were eluted using a gradient from 10 to 250 mM imidazole in the same buffer. Additional purification of the His-tagged Hsp33 variants was performed employing anion-exchange chromatography (Q-sepharose HP, GE Healthcare). The column was equilibrated with 40 mM KPi, 200 mM KCl and Hsp33 was eluted using a gradient from 200 to 700 mM KCl in 40 mM KPi, pH 7.0. Purified protein fractions were pooled, dialyzed against storage buffer (40 mM KPi, pH 7.5) at 4 °C, concentrated using Amicon Ultra-15 centrifugal tubes (EMD Millipore) and stored at −80 °C.

3.4.3 Purification of wild-type Im7 and Im7 L53A I54A

Immunoprotein 7 (Im7) wild-type and Im7 L53A I54A were purified as described previously, with modifications (Quan, Koldewey et al. 2011, Stull, Koldewey et al. 2016). To summarize, Im7-expressing cells (BL21 (DE3) pET28b his-SUMO Im7 wild-type, or BL21 (DE3) pET28b his-SUMO Im7 L53A I54A) were cultured at 37°C. Protein expression was induced with 0.2 mM IPTG and overnight cultivation at 20°C. Cells were harvested the next day and resuspended in lysis buffer (50 mM potassium phosphate, 400 mM NaCl, 10% (v/v) glycerol, 5 mM imidazole [pH 8.0], 1 tablet Roche complete protease inhibitor mix, 2 mM PMSF) and lysed (French Press, three cycles, 14,000 psi). Soluble protein was fractioned by centrifugation (30 min, 16,000 rpm, 4°C), loaded onto a Ni-HiTrap column (GE Healthcare) and eluted with an imidazole gradient from 5-300 mM. Protein containing fractions were pooled and dialyzed against 50 mM potassium phosphate, 400 mM NaCl, 5% (v/v) glycerol [pH 8.0]. During dialysis Im7 was treated with ULP1 to cleave the His-SUMO tag. Cleaved Im7 was passed through the Ni-HiTrap column again to bind the His-SUMO Tag, and the flow-through was collected and dialyzed against 50 mM potassium phosphate, 0.5 mM EDTA [pH 8.0]. Dialyzed protein was loaded on a HiTrap Q column (GE Healthcare) and eluted with a NaCl gradient from 0-1 M. Fractions containing Im7 wild-type or Im7 L53A I54A were pooled, concentrated, and stored at -80°C in 50 mM potassium phosphate, 400 mM NaCl, 5% (v/v) glycerol [pH 8.0].

3.4.4 Other proteins used during this thesis

Citrate synthase (Sigma Aldrich) was dialyzed against 50 mM Tris, 2 mM NaEDTA, pH 8, aliquoted and stored at -80°C.

3.5 Preparation of HOCl, HOBr and HOSCN

For the preparation of HOCl concentrated NaOCl was diluted in 40 mM KPi, pH 7.5. The concentration of HOCl was monitored by a 1:1000 dilution of NaOCl in 10 mM NaOH ($\varepsilon_{292\,nm}$: 350 M^{-1} cm^{-1}) (Morris 1966). For the generation of HOBr equal volumes of 40 mM HOCl and 45 mM KBr in 40 mM KPi, pH 7.5 were

mixed, and the concentration of HOBr was determined in 10 mM NaOH using $\varepsilon_{329\,nm}$: 332 M^{-1} cm^{-1} (Hawkins, Morgan et al. 2009). For the formation of HOSCN a previously described enzymatic procedure was used (van Dalen, Whitehouse et al. 1997), with modification as follows: 200 units ml^{-1} LPO (Sigma) and 26 mM NaSCN were dissolved in 40 mM KPi, pH 7.5. 10 x 2 mM aliquots of H_2O_2 in 40 mM potassium phosphate buffer, pH 7.5, were added in a stepwise fashion over 5 min. Catalase (500 units ml^{-1}) was used to decompose excess H_2O_2. To separate all enzymes from the solution the sample was centrifuged at 14,000 g for 7.5 min at 4°C in a 10-kDa cutoff filter. A solution of 5-thio-2-nitrobenzoic acid (TNB) was prepared by alkaline hydrolysis of DTNB with 50 mM NaOH. To determine the concentration of HOSCN the loss of signal of the TNB solution at 412 nm ($\varepsilon_{412\,nm}$ 14,150 M^{-1} cm^{-1}) was measured (Chandler, Nichols et al. 2013).

3.6 Protein concentration determination

All protein concentrations were determined spectroscopically using a Jasco spectrophotometer V-550, using the extinction coefficient (ε280) at 280 nm for the respective protein. If concentrations of protein mixtures needed to be calculated the *DC* Protein Assay Kit II (Bio Rad) was used according to the manufactures manual.

3.7 Preparation of Hsp33 and its variants (reduction and oxidation)

Reduced and oxidized Hsp33 from *E. coli* and its variants were prepared as previously reported (Graumann, Lilie et al. 2001, Ilbert, Horst et al. 2007, Winter, Ilbert et al. 2008). Reduced, zinc reconstituted Hsp33 ($Hsp33_{red}$) was generated by incubation with 5 mM DTT (RPI) and 75% $ZnCl_2$ (of Hsp33 molarity) for 2 h at 37°C. Reductant and residual $ZnCl_2$ were removed using a Zeba Spin Column (Thermo Fisher). To prepare oxidized Hsp33, 20µM $Hsp33_{red}$ was incubated with 200 µM HOCl for 2 min at 30°C, or various concentrations of HOCl, HOBr and HOSCN for 2 min at 30°C if otherwise stated. Oxidants were quenched adding a

5x excess of $Na_2S_2O_3$. *E. coli* Hsp33 mutants as well as PA14 Hsp33 were reduced and oxidized as described for wild-type *E. coli* Hsp33.

3.8 Chaperone activity and protein aggregation measurements

Chaperone activity of wild-type Hsp33 and its variants was monitored following a modified protocol from Beissinger et al. (Beissinger and Buchner 1998). The Hsp33 substrate protein citrate synthase (CS) was chemically denatured and diluted into a buffer system not without any denaturant to induce protein aggregation. Thermal aggregation measurements were conducted at temperatures, which induce protein unfolding and aggregation. Light scattering was followed using a Hitachi F4500 fluorimeter equipped with a thermostated cell holder and stirrer. Excitation and emission wavelengths were set at λ_{ex}/ λ_{em} of 360 nm, the excitation and emission slit widths λ_{ex}/ λ_{em} 2.5 nm with an amplification of 700V.

3.8.1 Hsp33 Chaperone activity measurements

CS from porcine heart (Sigma-Aldrich) was denatured to a final concentration of 12 µM in 6.0 M guanidinium-hydrochloride (GdmCl), 40 mM HEPES (pH 7.5) overnight at room temperature. To initiate aggregation of CS and test the chaperone activity of Hsp33 and its variants, the unfolded enzyme was diluted 1:160 into 1,600 µl 40 mM HEPES (pH 7.5) at either 20 or 30 °C in the absence or presence of a 4-fold excess of Hsp33 unless otherwise stated. For the analysis of the effects of Hsp33 on thermally unfolding CS, 0.15 µM CS was incubated in 1,600 µl 40 mM HEPES (pH 7.5) at the indicated temperatures in the absence or presence of Hsp33.

3.8.2 Protein unfolding or aggregation by hypohalous acids

Citrate synthase was diluted to a final concentration of 3 µM in 40 mM KH_2PO_4, pH 7.5 containing 450 µM HOCl, HOBr or HOSCN, respectively, and incubated for 60 min at 30°C. Light scattering was monitored during the incubation.

3.8.3 Neuropeptide Y (NPY) competition studies

Citrate synthase (CS) was diluted to a final concentration of 12 µM in 4.5 M Gdn-HCl, 40 mM Hepes pH 7.5 and denatured over night at room temperature. Aggregation assays were carried out in 40 mM Hepes pH 7.5 at 30°C. The final concentration of CS was 75 nM and a 10fold excess of either NPY or NPY^{D4C} IAM-TEMPO was used and the assay performed as described.

3.9 Preparation of NPY^{D4C} IAM-TEMPO

NPY D4C (GenScript) in 40 mM HEPES, pH 7.5 was incubated with a 10-fold molar excess of tris(2-carboxyethyl)phosphine (TCEP) and incubated for 30 min at 30 °C with shaking (400 r.p.m.) to achieve full reduction of NPY^{D4C}. Then, 4-(2-Iodoacetamido)-2,2,6,6-tetramethyl-1-piperidinyloxy (4–2-(iodoacetamido)-TEMPO or IAM-TEMPO, Sigma-Aldrich) was added stepwise (1/5 of the total volume added every minute) to yield a final molar ratio of peptide to label of 1:10 (Holyoak and Nowak 2001). The peptide solution was subsequently incubated in the dark for 2 h at 30 °C with shaking (400 r.p.m.). A dialysis step against 40 mM KPi, pH 7.5 using a Spectra/Por Micro Float-A-Lyzer device (500 Da–1 kDa) (Spectrum Laboratories) was used to remove residual, non-reacted IAM-TEMPO. The concentration of NPY^{D4C} IAM-TEMPO was determined before use in NMR experiments or competition studies.

3.10 Far-UV circular dichroism (CD) spectroscopy

Far-UV CD spectroscopy measurement monitor the differential absorption of left and right circularly polarized light, which serves as a readout for changes in the secondary structure of proteins.

E.coli Hsp33 wild-type and mutant far-UV CD spectra were recorded in 40 mM KH_2PO_4, pH 7.5 at 25°C using a Jasco-J1500 spectropolarimeter as previously described (Graf, Martinez-Yamout et al. 2004). Briefly, Hsp33 and its variants were diluted to a final concentration of 0.2 mg/ml into 40 mM KH_2PO_4, pH 7.5 and far-UV CD spectra were cumulatively recorded between 260-190 nm, buffer corrected and molar ellipticity was calculated according to the following equation:

$$molar\ ellipticity = \frac{\theta x\ \mathrm{M}}{c\ x\ l\ x\ 10}$$

θ = mdeg

M = relative molecular mass

c = concentration in mg/l

l = path length in $\mathrm{deg} * \mathrm{cm}^2 * \mathrm{dmole}^{-1}$

For measurements of changes in the secondary structure of citrate synthase and Im7 upon exposure to the hypohalous acids HOCl, HOBr, and HOSCN, proteins were diluted to 0.2 mg/ml into 40 mM KH_2PO_4, pH 7.5 in the presence or absence of a 150x excess of HOX for CS, and a 10x excess for Im7. Proteins were incubated at 30°C for 30 min before CD spectra were acquired. The temperature was controlled with a Jasco Peltier device. Spectra were buffer corrected and subsequently analyzed.

3.11 Protein SDS-PAGE gels

For the separation of proteins on 12% SDS-PAGE gels (TGX-gel, BioRad), protein samples were supplemented with 5x Laemmli buffer to a final concentration of 60 mM Tris, 12.5% glycerol, 2% SDS, 0.01% bromphenol blue, +/- 125 mM β-mercaptoethanol. Dissolved samples were then boiled at 95°C for 5 min. Gel electrophoresis was performed by following the manufacturer's specifications (BioRad) in SDS running buffer (25 mM Tris, 192 mM glycine, 0.1% SDS, pH 8.0). Proteins were visualized by Coomassie blue (Wong, Sridhara et al. 2000).

3.12 Western blotting

Proteins separated by SDS-PAGE were then blotted onto a PVDF membrane using semi-dry blotting apparatus following the manufacturer's specifications. Membranes were incubated in 5% (w/v) milk (non-fat milk powder) TBS-T (25 mM Tris, 0.05% (v/v) Tween, 137 mM NaCl, 3 mM KCl, pH 7.4) solution for 30 min at RT, or ON at 4°C to minimize unspecific antibody binding. The primary antibody (Rabbit anti-Hsp33; Jakob lab, Alpha Diagnostic Intl.) was applied for

1 h at RT, unbound antibody was removed by 3 washing steps with TBS-T for 10 min before the secondary antibody (Goat anti-rabbit (peroxidase labeled) (ThermoScientific) was applied for 1 h at RT. Subsequent washing 3x with TBS-T removed unbound antibody before signal detection was achieved with the SuperSignal West Pico Chemiluminescent substrate (ThermoScientific) kit according to the manufacturers specifications.

3.13 Trichloroacetic acid (TCA) precipitation

For TCA precipitation of proteins, a final TCA concentration in the sample of 10% was used. Ice cold TCA was added to the sample, vortexed, and incubated for 15 min on ice. Precipitated proteins were spun down at 16000 x g, 4°C, 30 min. The supernatant was removed and the pellet was washed twice carefully with 400 µl ice cold acetone. Residual acetone was removed by evaporation at 30°C.

3.14 *P. aeruginosa* growth and survival assays

P. aeruginosa PA14 wild-type and mutant strains were grown aerobically at 37°C in lysogenic broth (LB) or potassium morpholinopropanesulf-onate (MOPS) minimal medium (Teknova, Inc.) containing 0.2% glucose, 1.32 mM potassium phosphate and 10 µM thiamine. For experiments assessing the growth and survival after oxidative stress treatment, PA14 wild-type and the respective mutant strains were grown until A_{600} = 0.4-0.5 was reached. Subsequently, the cells were washed with and resuspended in pre-warmed (i) phosphate buffer saline (PBS), pH 7.5, (ii) MOPS-glucose media, or (iii) MOPS media, and treated with the indicated concentrations of HOCl, HOBr, and HOSCN at either 30°C (PBS) or 37°C (MOPS-glucose; MOPS), respectively. Growth was recorded every 30 to 60 min for 10 h by measuring the optical density at 600 nm. To test for cell survival, 0.5 ml of bacteria were harvested at the indicated time points and normalized to their A_{600}. MOPS medium containing 10 mM $Na_2S_2O_3$ was added to quench excess HOX, and the cells were then diluted into 0.85% NaCl and spot-titered onto LB agar using a Precision XS Microplate Sample Processor (Bio-Tek). The LB plates were incubated overnight at 37°C. To test the effects of

mesalamine (Sigma Aldrich) treatment on the oxidative stress resistance of PA14 wild-type and *ppk* deletion strain, 500 μM mesalamine dissolved in MOPS glucose medium was added to the cultures 120 min before the stress treatment. Stress treatment with the respective oxidants and survival analysis was conducted as described above.

3.15 *In vivo* aggregation assay

Preparation of membrane protein-free cellular soluble and insoluble protein fractions was conducted by a slight modification of the method of Tomoyasu et al. (2001) (Tomoyasu, Mogk et al. 2001). *P. aeruginosa* PA14 wild-type and *hslO*$^-$, *ppk*$^-$, and *ppk*$^-$ *hslO*$^-$ mutant strains were grown in MOPS glucose medium to an A_{600} ~0.4, and treated with various concentrations of HOCl, HOBr and HOSCN for 20 min. Cells equivalent to 4 ml of A_{600} = 1 were harvested by centrifugation and resuspended in 40 µl Buffer A (10 mM potassium phosphate, pH 6.5, 1 mM EDTA, 20% [w/v] sucrose, 1 mg/ml lysozyme, 0.2 mg/ml DNase), and then incubated 30 min on ice and frozen at −80°C. After thawing on ice and addition of 360 µl Buffer B (10 mM potassium phosphate, pH 6.5, 1 mM EDTA), ~100 µl 0.5 mm glass beads (BioSpec Products) were added, and the microfuge tubes were shaken for 30 min at 1,400 rpm, 8°C, to lyse the cells completely. 200 µl aliquots were removed and insoluble fractions were separated by centrifugation (20 min at 16,100 *g*, 4°C), washed once with Buffer B, once with Buffer C (Buffer 2 plus 2% Nonidet P-40 (ICN Biomedicals)), and again with Buffer 2. Soluble fractions were TCA precipitated (10% final concentration), separated by centrifugation (20 min at 16,100 *g*, 4°C) and washed twice with ice-cold acetone (-20°C) to remove residual TCA. Both the soluble and insoluble fractions were visualized by SDS-PAGE. Survival of treatment with HOX was monitored by spotting serially diluted and sodium thiosulfate ($Na_2S_2O_3$) quenched cells on LB plates, and growing them overnight growth at 37°C.

3.16 Polyphosphate (polyP) sample extraction and quantification

Changes in intracellular polyP levels upon treatment with HOCl, HOBr, or HOSCN were quantified as previously described (Dahl, Gray et al. 2017) with minor modifications. The PA14 wild-type and PA14 *ppk*$^{-}$ strains were grown aerobically in 50 ml MOPS glucose medium and split into 10 ml cultures in new flasks when the culture reached an optical density A_{600} = 0.4 – 0.5. Then, sublethal doses of HOX (0.5 mM HOCl, 0.15 mM HOBr or 0.25mM HOSCN) were added and after incubation for 2.5 h cells sufficient to yield 200 µg total cellular proteins were harvested by centrifugation. For cell lysis the bacterial strains were incubated for 10 min at 95°C in 0.25 ml GITC Lysis Buffer (4 M guanidine isothiocyanate, 50 mM Tris-HCl, pH 7.0). Protein content of each sample was determined using the Bradford assay (Bio-Rad). PolyP was extracted by sequential addition of 15 µl 10% sodium dodecyl sulfate, 0.5 ml 95% ethanol, and 5 µl glassmilk (0.1 g ml^{-1} acid-washed silicon dioxide in GITC Lysis Buffer). This mixture was applied (1 min @ 3,000 x g) to silica membrane spin columns (Econospin^{TM}, Epoch Life Science, Inc.) and rinsed twice with 0.75 ml NW Buffer (5 mM Tris-HCl, pH 7.5, 50 mM NaCl, 5 mM EDTA, 50% v/v ethanol). After spin-drying, 50 µl 50 mM Tris-HCl, pH 8 was added before incubating for 15 min at room temperature. The polyP sample was then eluted by centrifugation. PolyP extracts were incubated for 1 hour at 37°C with 250 µM highly-pure ADP (Cell Technology), 50 mM HEPES (pH 7.5), 50 mM ammonium sulfate, 5 mM $MgCl_2$ in the presence or absence of 50 nM *E. coli* PPK. The resulting ATP was quantified with QuantiLum® Recombinant Luciferase (Promega). The reactions contained 50 mM Tricine buffer, pH 7.8, 10 mM $MgSO_4$, 0.2 mM EDTA, 0.2 mM sodium azide, 1 mM DTT, 100 µM luciferin, 25 nM luciferase, and measurements were conducted on a FLUOstar Omega microplate reader (BMG Labtech). The difference in the sample luminescence value in the presence and absence of PPK was calculated and normalized to the values obtained for the untreated samples of each strain in order to calculate the fold-change in polyP accumulation in each sample.

3.17 RNA$_{Seq}$ library construction

For the differential gene expression analysis wild-type *P. aeruginosa* PA14 was cultivated in MOPS glucose medium at 37°C to an A_{600} of 0.4, and subsequently treated with sublethal concentrations of HOX (0.5 mM HOCl, 0.15 mM HOBr, or 0.25 mM HOSCN). 1 ml of cells from three biological replicates with an A_{600} of 0.4 was harvested before (control) or 15 min after the treatment. To stop transcription 1 ml of ice-cold methanol (-80°C) was added immediately after the samples were taken. The supernatant was removed from the sample by centrifugation and an Ambion RiboPure-Bacteria Kit (Thermo Fisher Scientific) was used to prepare the total RNA according to the manufacturer's instructions. After DNase I treatment rRNA was depleted from the samples using the Illumina Ribo Zero Kit (Illumina) for Gram-negative bacteria. The University of Michigan DNA Sequencing Core performed 50 base single end sequencing on a Illumina HiSeq 2500.

3.18 RNA$_{Seq}$ data analysis

The *Pseudomonas aeruginosa* UCBPP-PA14 reference genome (Accession number: NC_008463.1) was used for read alignment applying the software packages bwa v. 0.7.8-r455 (Li and Durbin 2009) and samtools (Li, Handsaker et al. 2009). Read count normalization and differential expression analysis was done with the statistical software programs edgeR and limma, respectively (Robinson, McCarthy et al. 2010, Ritchie, Phipson et al. 2015). The multidimensional scaling plot was made with the plotMDS function from the limma package used with default settings. The threshold parameters for differentially expressed genes were chosen to be a false discovery rate (fdr) ≤ 0.005 – the fdrf was determined using the Benjamini-Hochberg procedure (Benjamini and Hochberg 1995) - and a $\log_2$(fold change) ≥ 1.5 for upregulated genes or a $\log_2$(fold change) ≤ 1.5 for downregulated genes.

3.19 Quantitative real-time PCR

Gene expression analysis by RT-PCR was performed on PA14 wild-type and PA14 *ppk*⁻ strains upon HOSCN treatment. Briefly, cells were grown aerobically to mid-log phase in MOPS glucose at 37°C. HOSCN was added to a final concentration of 0.25 mM and incubated for 20 min. RNA was prepared using the NucleoSpin RNA kit (Macherey&Nagel) and DNA-free™ kit (Ambion). For the generation of cDNA the PrimeScript 1st strand cDNA Synthesis Kit (Takara) was used. RT-PCRs were set up with SYBR(R) GreenER™ qRT-PCR mix (Invitrogen) and data were recorded on a Mastercycler(R) realplex2 real-time PCR system (Eppendorf). Expression ratios were calculated comparing the expression of each gene in untreated PA14 and PA14 *ppk* cultures, respectively, by the ΔΔCT method (Pfaffl 2001) and normalized to expression of *rrsD* (encoding 16S rRNA), which did not change under the conditions tested. Primers used for RT-PCR analysis were are listed in Table 2.

Table 2: List of primers used for quantitative real-time PCR

Primer	Sequence	Description
PA14_16SrRNA_fw	TATCAGATGAGCCTAGGTCGGATTA	RT-PCR forward primer *rrsD*
PA14_16SrRNA_rv	TTTACAATCCGAAGACCTTCTTCAC	RT-PCR reverse primer rrsD
PA14_ibpA_fw	TTCCGTCATTCCGTAGG	RT-PCR forward primer *ibpA*
PA14_ibpA_rv	AGGTCTTCTTCCTGG	RT-PCR reverse primer *ibpA*
PA14_rpoH_fw	AACCTGTACATGCCTTGGTTCC	RT-PCR forward primer *rpoH*
PA14_rpoH_rv	ATAACTCTTGGCGATATGAACAACG	RT-PCR reverse primer *rpoH*
PA14_dnaK_fw	GGTAACGTCAAGGTCATCGAGAA	RT-PCR forward primer *dnaK*
PA14_dnaK_rv	GTCTTTCTGTACCACGTTCTCTTCG	RT-PCR reverse primer *dnaK*

3.20 ^{19}F NMR experiments

For ^{19}F NMR experiments Hsp33^{M172S}-tFPA variants (300–700 µM) were incubated in 40 mM KPi, 5 mM DTT, supplemented with 2 mM trifluoracetic

acid for intensity and chemical shift referencing, and 10% (v/v) D_2O. Spectra were recordered on a 500 MHz Varian VNMRS spectrometer (Agilent Technologies), equipped with a 5 mm PFG OneNMR probe, and a single 90° pulse with carbon decoupling was used. Peptide titration spectra of Hsp33 with NPY/NPY^{D4C}-IAM-TEMPO were performed at 30 °C or 35 °C, and temperature-dependent spectra were recorded between 10 °C and 45 °C in steps of 5 °C. iNMR was used to process acquired data.

3.21 $^{1}H–^{15}N$ HSQC protein NMR measurement

For $^{1}H–^{15}N$ HSQC experiments reduced and oxidized Hsp33^{Y12E} (300–700 µM) ± neuropeptide Y were incubated in 40 mM KPi, 5 mM DTT (only for reduced Hsp33^{Y12E}), supplemented with 10% (v/v) D_2O. All $^{1}H–^{15}N$-NMR experiments were performed on an 800 MHz Varian VNMRS spectrometer (Agilent Technologies), equipped with a 5 mm HCN inverse probe with *z*-axis gradient. The NMR operating software was VnmrJ 3.2. iNMR was used to process acquired data.

3.22 *In vivo* crosslinking procedure

For *in vivo* crosslinking experiments Hsp33^{M172S}-amber mutants encoded on pET11a expression vectors were co-transformed with the pEVOL plasmid into BL21 *hslO::kan* (Young, Ahmad et al. 2010). pEVOL contains two copies of *M. jannaschii* aminoacyl-tRNA synthetases and an optimized suppressor tRNA^{CUA} necessary for the incorporation of non-canonical amino acids at amber stop codon sites. Strains were plated on lysogeny broth (LB) plates supplemented with 200 mg ml^{-1} ampicillin and 34 mg ml^{-1} chloramphenicol and grown overnight at 37 °C. Transformants were scraped off the plates the following day and resuspended in LB medium. The cell suspension was used to inoculate 5 ml of LB medium supplemented with 1 mM $ZnCl_2$, 1 mM *p*-benzoyl-L-phenylalanine (BPA) (Bachem Holding AG), 200 mg ml^{-1} ampicillin and 34 mg ml^{-1} chloramphenicol to an A_{600} of 0.4 (Lennon, Ross et al. 2012). Cells were incubated for 1 h of at 37 °C, transferred to 30 °C and then 0.2 mM IPTG

and 0.2% L-arabinose were used to induce protein expression. After 6 h harvested cells were washed twice. 100 µl of phosphate-buffered saline, pH 7.4 per 1 A_{600} unit was used to resuspend the cells. Cells were then incubated at either 30 °C or heat-shock temperature (43 °C) for 5, 10 or 20 minutes, respectively, with shaking (400 r.p.m.). 100 µl cells were transferred into 96-well plates and placed on ice following the incubation. Crosslinking of samples was conducted for 10 min using a 25 W, 365 nm UV lamp (UVGL-58; 115 V, 60 Hz, 0.16 A) by applying UV irradiation from the top at distance of ~2 cm from the 96-well plates. Next, cells were lysed by adding lysozyme (50 mg ml^{-1}), followed by sonication (15%, 15 s) and DNase treatment (1 mg ml^{-1}; (Fu, Shi et al. 2013). Finally, samples were separated by SDS – PAGE and Hsp33 bands were visualized by western blot using a rabbit anti-Hsp33 antibody (Jakob lab, Alpha Diagnostic Intl.; 1:5,000 dilution) (Winter, Ilbert et al. 2008, Bruel, Castanie-Cornet et al. 2012).

3.23 *In vitro* crosslinking procedure

For crosslinking studies 20 µM $Hsp33_{red}$ or $Hsp33_{ox}$ and 40 µM NPY or SNPY were mixed, and reacted with either cyanur-biotin-dimercapto-propionyl-succinimide (CBDPS)-H8/D8 (Creative Molecules) (Petrotchenko, Serpa et al. 2011), ABAS-^{12}C6/^{13}C6 (Creative Molecules) (Brodie, Makepeace et al. 2015) or 1-ethyl-3-(3-dimethylaminopropyl)carbodiimide (EDC) (Sigma-Aldrich). Ammonium bicarbonate (ABC) was used to quench and stop the reaction.

3.23.1 Crosslinking with EDC

An equimolar mixture of ^{14}N- and ^{15}N-metabolically labelled protein of Hsp33 (20 µM) and 40 µM NPY was crosslinked by addition of 60 mM EDC at room temperature for 15 min. 10 mM ABC was used to quench and stop the reaction.

3.23.2 Crosslinking with ABAS

The Hsp33-NPY mixtures were incubated with 1 mM of an equimolar mixture of light and heavy isotopic forms of ABAS-^{12}C6/^{13}C6 (Creative Molecules) (Brodie, Makepeace et al. 2015) dissolved in dimethyl sulfoxide. UV irradiation

from the top of an open 0.2 ml reaction tube with a 25 W 254 nm UV lamp (UVGL-58; 115 V, 60 Hz and 0.16A) (2 cm distance) for 10 min at room temperature was used to crosslink the complex. 10 mM ABC was used to quench and stop the reaction.

3.23.3 Crosslinking with CBDPS

20 µM Hsp33 and 40 µM NPY were crosslinked by addition of 1 mM of an equimolar mixture of light and heavy isotopic forms of CBDPS dissolved in dimethyl sulfoxide. After incubation at room temperature for 15 min the reaction was stopped by addition of 10 mM ABC.

3.23.4 Proteolytic digest of *in vitro* crosslinking products

Trypsin (Promega) or proteinase K (Worthington Biochemical) were used at a 1:20 protease to protein ratio to digested crosslinked peptide for 18 h at 37 °C for 120 min at 37 °C, respectively. 10 mM 4-(2-aminoethyl)benzenesulfonyl fluoride hydrochloride (Sigma-Aldrich) was used to inhibit the proteases.

3.23.5 Peptide enrichment and sample desalting

ABAS and EDC crosslinked, and protease digested samples were desalted using ZipTip C18 (Merck Millipore) pipette tips. Samples crosslinked with CBDPS underwent an enrichment step by binding them to avidin beads (Pierce Biotechnology). Elution was conducted with a solution of 0.1% (v/v), trifluoroacetic acid 50% (v/v) acetonitrile (ACN). After desalting (ABAS and EDC samples) or elution from avidin beads (CBDPS samples) the resulting peptides were lyophilized until dry, and reduced with 10 mM tris-(2-carboxyethyl)-phosphine (TCEP) for 10 min at room temperature, and finally acidified to pH 2 with formic acid (FA).

3.23.6 LC/MS and data analysis of *in vitro* crosslinked peptides

Samples were suspected to mass spectrometric (MS) analysis on an Easy-nLC II nano-HPLC system (LC) (Thermo Fisher Scientific) coupled to the ESI-source (Nanospray Flex Ion Source; Thermo Fisher Scientific) of an Orbitrap

Velos Pro mass spectrometer (Thermo Fisher Scientific) (Petrotchenko, Makepeace et al. 2014). A self-prepared 100 µm ID, 360 µm OD 1-cm trap column packed with Magic C18AQ (Bruker-Michrom), 100 Å, 5 µm pore size was used for the liquid chromatography run. Samples were desalted by washing for 15 min with 0.1% (v/v) FA, and then separated using a 60 minute gradient (0–60 min: 4–40% B; 60–62 min: 40–80% B; 62–70 min: 80% B; with solvent B: 90% ACN, 10% water; and 0.1% FA) on a 75 µm ID, 360 µm OD 15 cm analytical, self-packed column with Magic C18AQ, 100 Å, 5 µm pore size with IntegraFrit (New Objective) equilibrated with 95% solvent A (2% (v/v) ACN, 98% water and 0.1% (v/v) FA). Xcalibur (version 2.1.0.1140) in data-dependent MS/MS mode was used for data analysis. The dynamic exclusion was set to 60 s. The respective repeat count was set to 2, and the repeat duration was set to 15 s. The resolutions for mass spectrometry scans (*m/z* 400–2,000 range) and MS/MS scans were set to 60,000 and 30,000 resolution, respectively. Collision-induced dissociation was applied for MS/MS fragmentation was performed (collision energy: 35%). Further settings included a Fourier transform mass spectrometry MSn automatic gain control target of 100,000 and a Fourier transform mass spectrometry full automatic gain control target of 1,000,000 and. Samples from EDC experiments where ^{15}N metabolically labelled Hsp33 was involved, were analyzed with a top 6 acquisition method. Samples crosslinked with isotopically labelled CBDPS-H8/D8 and ABAS-$^{12}C6/^{13}C6$, had Mass Tags setting for mass differences between light and heavy isotopic forms of 8.05 and 6.02, respectively (Petrotchenko, Makepeace et al. 2014). Spectra analysis and file coversion from RAW files to MGF files was done with Proteome Discoverer (version 1.4.0.288). The programs DXMSMS Match (Petrotchenko, Makepeace et al. 2014) of ICC-CLASS (Petrotchenko and Borchers 2010) and $^{14}N^{15}N$ DXMSMS Match (Petrotchenko, Serpa et al. 2014) were applied to analyze the data.

3.24 Quantum mechanics calculations and modelling

To generate a full-length Hsp33 model for quantum mechanics (QM) calculations as well as docking procedures I-TASSER (Roy, Kucukural et al.

2010) and ModRefiner (Xu and Zhang 2011) were employed. Truncated version of the Hsp33 model (PDB 1HW7) - residues 182–219 were omitted – was used for docking studies using Z-DOCK automated protein–protein docking (Pierce, Wiehe et al. 2014) between the Hsp33 variant and the conformational ensemble of NPY (Monks, Karagianis et al. 1996). No constraints were applied. UCSF Chimera 1.10 (Pettersen, Goddard et al. 2004) was used to visualize the M172S F187tFPA mutant I-TASSER model. For QM calculation purposes only residues surrounding tFPA were considered. Hydrogens were added to neutralize the system in Gaussview 5 (Gaussian). Subsequently, the structure was held constant using wb97 × d/6–31+G(d,p) with implicit water solvation while the tFPA side chain was rotated for optimized orientation. The chemical shifts were then calculated using gauge-independent atomic orbitals with the same calculation parameters in Gaussian 09 (Frisch, Trucks et al. 2009). The same methods for chemical shift referencing and conformational energy calculations were applied for trifluoroacetic acid.

4 Results and Discussion

4.1 Elucidating the substrate binding site of Hsp33

Results in **chapter 4.1** were published in: Groitl B, Horowitz S, Makepeace KA, Petrochenko EV, Borchers CH, Reichmann D, Bardwell JC, Jakob U. **Protein unfolding as a switch from self-recognition to high-affinity client binding**. Nat Commun. 2016 Jan 20;7:10357. I performed all of the experiments described in the manuscript except ^{15}N 2D HSQC NMR (Figure 4.1.5) and 19F NMR measurements in Figure 4.1.7, Figure 4.1.10, Figure 4.1.11 and Figure 4.1.12. Those experiments were conducted in collaboration Horowitz S. Mass spectrometry runs and subsequent analysis (Table 3) were performed in collaboration with Makepeace KA. The quantum mechanics calculations in Figure 4.1.8 A, B, and the computational docking model in Figure 4.1.16 was made by Horowitz S. The manuscript was written by Groitl B, Horowitz S, Bardwell JC and Jakob U. All subsequent figures are prepared by Groitl B.

4.1.1 Identification of Hsp33 interaction sites *in vivo*

For the determination of interaction sites between Hsp33 and substrate proteins under *in vivo* conditions, we genetically incorporated the non-canonical amino acid *p*-benzoyl-L-phenylalanine (BPA) into specific locations in Hsp33. Activation of the zero-crosslinker Bpa via UV irradiation (Chin and Schultz 2002) would then tether Hsp33 to any client proteins that came in close proximity of the respectibe Bpa residue.

Activation of Hsp33 normally requires the exposure of cells to hypochlorous acid (Winter, Ilbert et al. 2008). HOCl, however, is also known to elicit non-specific protein crosslinking. We therefore decided to introduce BPA into our temperature-regulated variant Hsp33^{M172S} instead of wild-type Hsp33 (Cremers, Reichmann et al. 2010). The behavior of Hsp33^{M172S} under oxidative unfolding conditions is like the one for wild-type Hsp33. This mutant, however, no longer requires HOCl treatment for its activation due to a destabilizing mutation in its N-terminus. Activation of the chaperone function of Hsp33^{M172S} is triggered by temperatures as low as 40 °C (Cremers, Reichmann et al. 2010). Using this variant enabled us

to activate Hsp33's chaperone function *in vivo* upon a simple temperature shift without the use of HOCl. The heat shock activated Hsp33^{M172S} variant binds a plethora of thermally unfolding proteins and sequesters them into insoluble aggregates (Cremers, Reichmann et al. 2010).

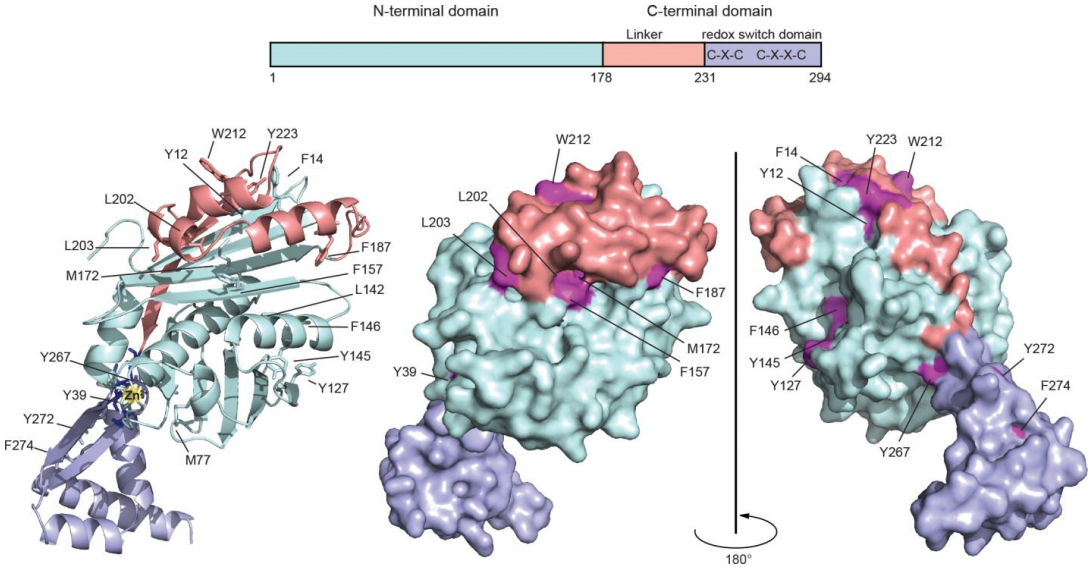

Figure 4.1.1: Location of sites for the identification of the Hsp33-client-binding site *in vivo*

Eighteen sites in Hsp33 were selected for the incorporation of unnatural amino acids as shown in the I-TASSER-based ribbon (left) and indicated in dark pink on the surface (right) models of reduced *E. coli* Hsp33. Hsp33 consists of an N-terminal domain (cyan), a metastable linker region (light pink) and a redox switch domain (purple), in which four thiolate anions arranged in a C_{232}-X-C_{234}-X_{31}-C_{265}-X-Y-C_{268} motif coordinate one zinc ion (yellow sphere) under reducing conditions. Only one monomer of the dimeric crystal structure is shown. In solution, reduced Hsp33 is monomeric (Graf, Martinez-Yamout et al. 2004).

Basis for the substitution of the phenylalanine-like BPA were sites with an existing aromatic amino acid (Phe, Tyr, Trp) or a residue that was found substituted for Phe in at least one known Hsp33 homologues. These substitutions would unlikely substantially affect Hsp33's tertiary structure. Thus, we chose eighteen different sites for BPA incorporation in Hsp33^{M172S} (Fig. 4.1.1). We conducted an individual replacement of the selected codons by an amber (TAG) stop codon, and cotransformed the respective Hsp33^{TAG}-containing plasmids together with the pEVOL single-vector construct. pEVOL contains two

copies of *M. jannaschii* aminoacyl-tRNA synthetases and an optimized suppressor $tRNA^{CUA}$ into a Hsp33-deletion mutant of *E. coli* (Young, Ahmad et al. 2010). As visualized by Western blotting using anti-Hsp33 antibodies, full-length Hsp33 was expressed only in the presence of BPA (Fig. 4.1.2). Strains expressing wild-type Hsp33 and $Hsp33^{M172S}$ were used as controls. Notably, strains expressing $Hsp33^{M172S}$ variants with amber mutations towards the C-terminus (Y223, Y267, Y272, and F274) showed an accumulation of truncated versions of the respective variants in the absence of BPA.

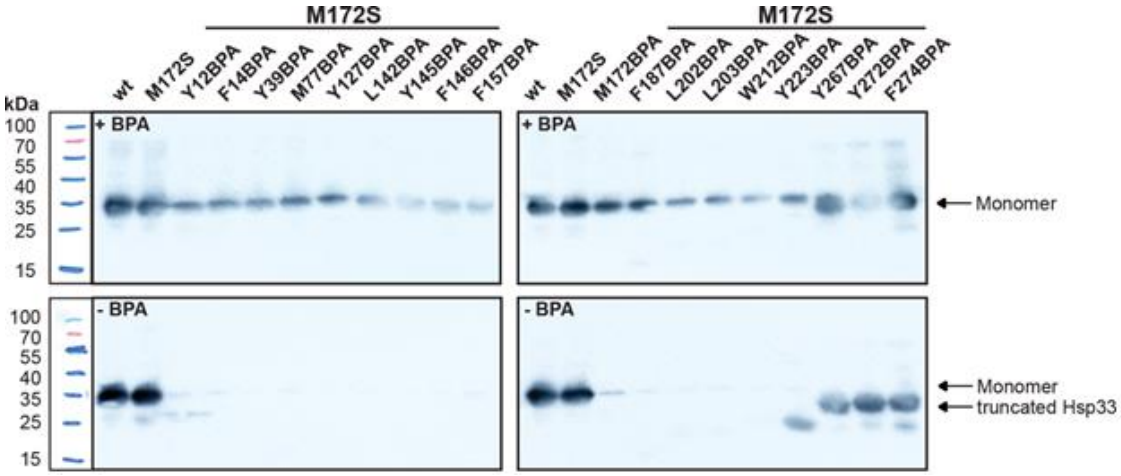

Figure 4.1.2: Expression of $Hsp33^{M172SBPA}$ variants in the presence or absence of BPA

The expression of $Hsp33^{M172SBPA}$ variants in the absence or presence of BPA (1 mM) was tested by western blot using anti-Hsp33 antibodies. Strains expressing $Hsp33^{M172S}$ variants with amber mutations at position Y223, Y267, Y272, or F274 accumulate truncated versions of the respective Hsp33 variants in the absence of BPA.

Live cells expressing the BPA-substituted Hsp33 variants were exposed to UV irradiation after shift to heat shock temperatures (43°C for 5, 10 or 20 min) (Fig 4.1.3A) or after a 20 min incubation at 30°C as a control (Fig. 4.1.3B). When we analyzed whole cell extracts by Western blotting using antibodies against Hsp33, we were able to monitor the extent and specificity of proteins crosslinked to Hsp33.

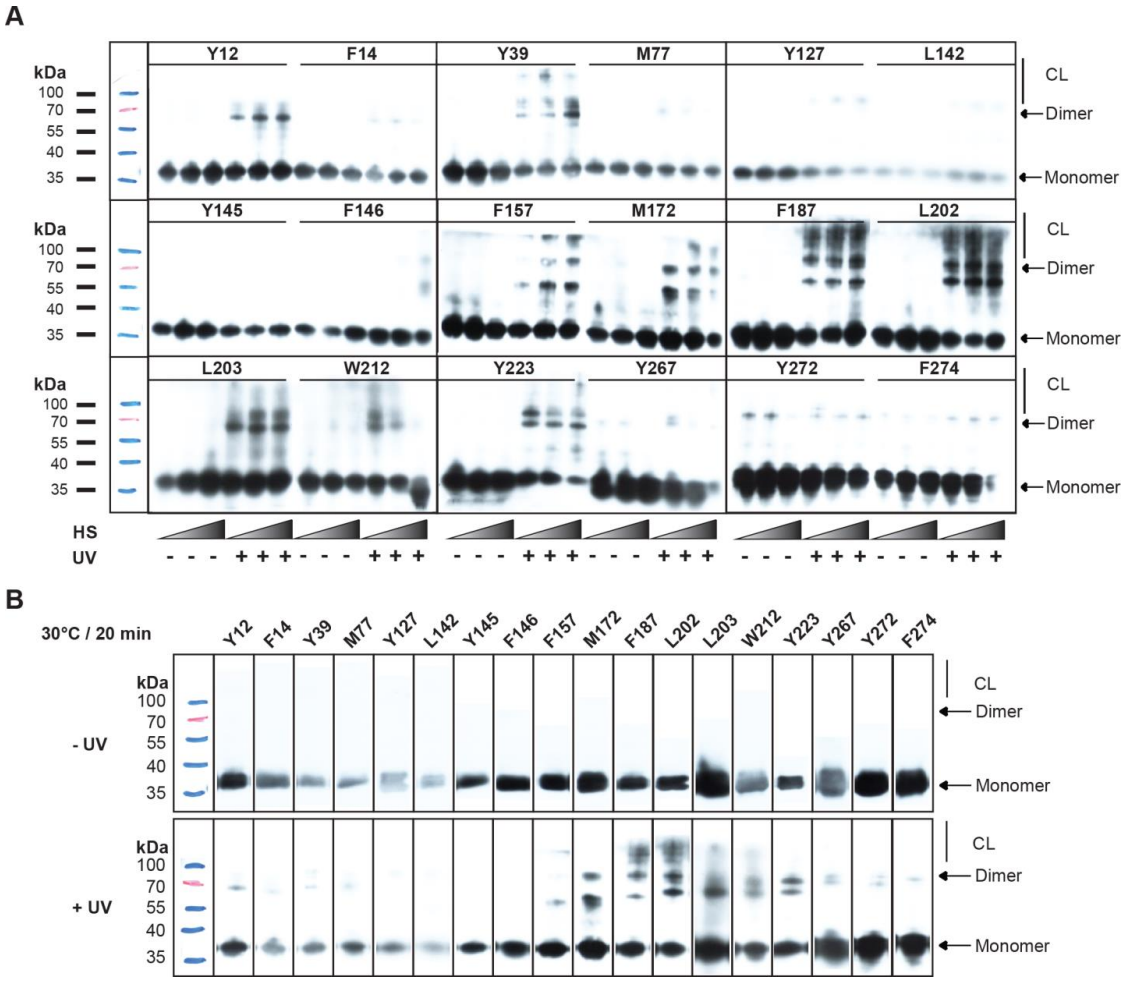

Figure 4.1.3: Western blots analysis of in vivo crosslinked Hsp33^{M172SBPA} variants at 30 °C or under heat-shock conditions (43 °C)

(**A**). *E. coli* cells overexpressing the Hsp33$^{M172S\text{-}BPA}$ variants were shifted from 30 °C to heat-shock conditions (43 °C for 5, 10 or 20 min) (HS). The cells were then either left untreated or exposed to UV irradiation for 10 min to induce crosslinking. Western blot analysis using anti-Hsp33 antibodies was used to visualize the crosslinking products (CL). (**B**). Western blot analysis of the *in vivo* crosslinking products at 30 °C (for details see Fig. 1b). After incubation of *E. coli* cells overexpressing the Hsp33^{M172SBPA} variants at 30 °C, the cells were exposed to UV irradiation for 10 min to induce crosslinking (CL). Controls were left untreated (no UV irradiation).

Mutants with BPA substitutions in and neighboring the flexible linker region (F157, M172, F187, L202, L203, W212, and Y223) revealed the strongest extent of crosslinking as visualized by Western blotting. Additional sites with moderate crosslinking were in the N-terminal region of Hsp33 (Y12, Y39). The majority of the remaining BPA incorporation sites did not show any substantial crosslinking. A summary of the findings is provided in Table 3.

Table 3: Summary of Hsp33-client interaction sites after limited proteolysis, in vivo crosslinking, in vitro crosslinking and ^{19}F NMR

All *in vivo* crosslinking-positive residues, all zero-length *in vitro* crosslinking sites, and ^{19}F NMR-positive sites are highlighted in red. Long- and medium-range *in vitro* crosslinking sites are marked in dark pink, and sites previously suggested to be involved in client binding by limited proteolysis experiments[16] are depicted in orange. Cell colors correspond to color scheme in Fig. 4.1.15B.

Hsp33 residues	Limited proteolysis[16]	*In vivo* crosslinking	*In vitro* crosslinking	Interactions ^{19}F NMR
M1			++	
R11	-			
Y12		++	++	
F14		-		
R20	-			
Y39		++		
K44	++		++	
K62	++		++	
M77		-		
R91	-			
R95	-			
E102			+++	
K107			++	
R126	-			
Y127		-		
L142		-		
Y145		-		-
F146		-		
R148	++			
E150			+++	
R155	-			
F157		++		+++
R159	++			
K166			++	
M172		++		
F187		+++		++
K198	++		+++	
L202		+++		+
L203		++		
W212		(+)		-
R213	-			
Y223		++		
K231	-		++	
Y267		-		
Y272		-		
F274		-		

To ascertain that the observed higher migrating band were in fact crosslinking products between Hsp33 and client proteins, and not crosslinks between Hsp33 molecules in higher oligomeric states, we recombinantly expressed and purified two BPA mutant variants,; Hsp33^{M172SY145BPA}, which did not show any *in vivo* crosslinking, and Hsp33^{M172SL202BPA}, which showed substantial *in vivo* crosslinking. We conducted *in vitro* crosslinking experiments by incubating the two mutant proteins at either 30°C or 45°C in the absence or presence of subsequent UV irradiation for 20 min. No higher migrating bands apart from Hsp33 dimers migrating at ~70 kDa were detected (Fig. 4.1.4A). These results indicate that the higher-migrating bands we observed in our *in vivo* crosslinking studies indeed represent crosslinks between activated Hsp33 and cellular client proteins. When we determined the location of the *in vitro* crosslinking sites that led to Hsp33-Hsp33 crosslinks, we noticed that aa 202 is far away from the other Hsp33 monomer in the reduced form, but comes into close proximity with the other subunit when the linker region of one subunit folds on top of the N-terminal linker-binding domain of the second subunit (Vijayalakshmi, Mukhergee et al. 2001) (Fig. 4.1.4B).

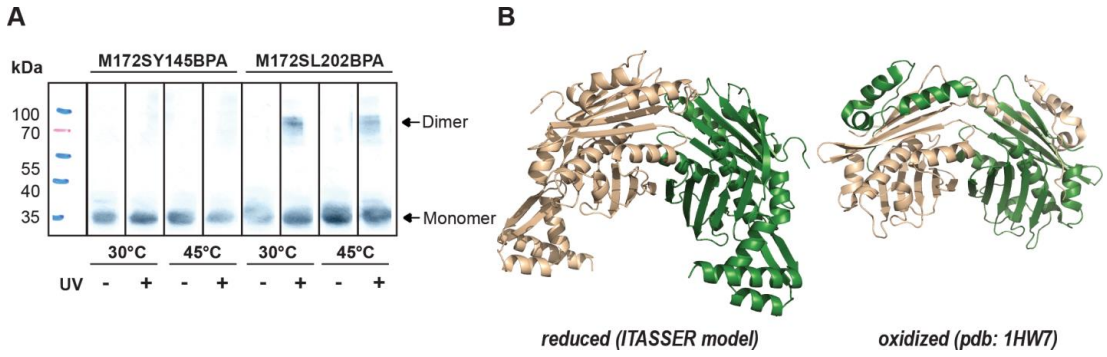

Figure 4.1.4: Western blot analysis of purified Hsp33^{M172SBPA} variants, and cartoon depiction of Hsp33$_{red}$ and Hsp33$_{ox}$

(**A**). Western blot analysis of purified Hsp33^{M172SY145BPA} (negative in *in vivo* crosslinking experiments) or Hsp33^{M172SL202BPA} (positive in *in vivo* crosslinking experiments) incubated at either 30°C or 45°C before and after UV-crosslinking. The 33 kDa monomer and the ~70 kDa Hsp33 dimer are indicated. Higher migrating bands were not detected. (**B**). Cartoon depiction of I-TASSER model (left) and domain-swapped model (right) of Hsp33 (PDB 1HW7).

Based on these and other experiments, we concluded that domain swapping accounts for most of the Hsp33-Hsp33 crosslinks that we observed *in vivo.* These results suggested that the same Hsp33-BPA substitutions could crosslink either with each other or with client proteins, and indicated that Hsp33 employs the same sites it uses to stabilize the linker region under non-stress conditions also for client binding under oxidative stress conditions. An alternative explanation could be that extended flexible loops in Hsp33 transiently come into close proximity to one another, resulting in crosslinks. We did not detect any substantial Hsp33-Hsp33 or Hsp33-client crosslinks for Hsp33 variants containing BPA in a region of the N-terminus opposite from the linker-binding surface (Y127, L142, Y145, F146). The same is true for residues in the C-terminal redox switch domain (Y267, Y272, F274), a finding fully in accordance with previous results, which indicated that the C-terminal redox switch domain has a primarily regulatory role and is not involved in substrate binding (Reichmann, Xu et al. 2012). In summary, our *in vivo* crosslinking studies gave a first hint as to the location of the client binding site in Hsp33, suggesting an involvement of both the hydrophobic linker-binding surface as well as the flexible linker region in client binding after chaperone activation.

4.1.2 Monitoring conformational changes in Hsp33 by ^{19}F-NMR

Our *in vivo* crosslinking results suggested that Hsp33 can interact both with client proteins as well as with itself during heat shock conditions *in vivo*. However, crosslinking studies have some drawbacks, such as the sensitivity to regions with some level of flexibility, non-equilibrium conditions, and the residue chemistry. By using an independent approach employing the novel application of *in vitro* ^{19}F NMR spectroscopy, we sought to overcome these issues and independently verify whether the identified residues truly interact with client proteins. The same amber stop codon positions we used for *in vivo* crosslinking offer the possibility of incorporating 4-(trifluoromethoxy)-phenylalanine (tFPA) (Hammill, Miyake-Stoner et al. 2007, Jackson, Hammill et al. 2007, Miyake-Stoner, Refakis et al. 2010) at our preselected Hsp33 sites for subsequent ^{19}F NMR studies. We decided to

focus on a select subset of our previously identified mutant variants, and use them to directly detect client binding by monitoring the ^{19}F NMR signal at these selected sites. ^{19}F features various advantages such as a signal sensitivity of 83% relative to that of ^{1}H, the most widely used isotope in protein NMR (Marsh and Suzuki 2014). Additionally, ^{19}F is the only natural isotope of fluorine and thus is present at 100% natural abundance. Furthermore, ^{19}F boasts a high chemical shift dispersion, is one of the most sensitive NMR nuclei available in nature, and is strong reporter on changes in local chemical environments, including solvent exposure (Gerig 1994). The combination of these traits with the mobility of the trifluoro-group make tFPA an excellent and highly sensitive chemical shift probe for studies on client binding or conformational changes (Cellitti, Jones et al. 2008, Peeler and Mehl 2012). The site-selectivity and the nature of the amber stop codon strategy furthermore ruled out ambiguities in resonance assignment, since only one amino acid is labeled at a time. We reasoned that use of a simple paramagnetic relaxation enhancement (PRE) experiment with our Hsp33-tFPA variants (see below for details) should be able to distinguish direct binding sites from areas of conformational changes within Hsp33. Employing ^{19}F NMR traits therefore makes the elucidation of structural changes in disordered proteins, whose NMR spectra are typically extremely challenging to interpret, possible How difficult it is to analyze disordered proteins became obvious when we recorded the ^{15}N 2D HSQC spectra of the reduced and oxidized Hsp33^{Y12E} mutant, a constitutively active variant. Although the peaks were dispersed in the reduced form (Fig. 4.1.5, left panel), about one third of the peaks were missing, hindering the residue assignment of both the reduced (Fig 4.1.5, left panel) and oxidized (Fig. 4.1.5, center panel) Hsp33^{Y12E} spectrum. Additionally, upon titration of the binding partner neuropeptide Y (NPY), only very minor changes in the spectrum were visible. As before, we found that many peaks overlap, impairing the assignment of the spectrum (Fig 4.1.5, right panel). Guided by the result of our *in vivo* crosslinking experiments, we picked several crosslinking-positive sites (Y12, Y39, F157, F187, and L202), one negative site (Y145), and one ambiguous site (W212) (Fig. 4.1.3A).

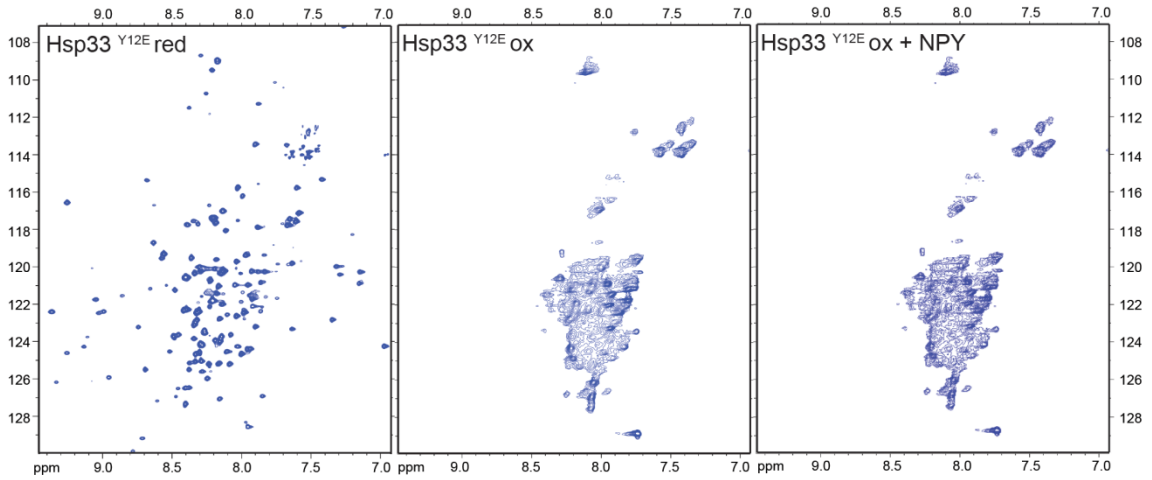

Figure 4.1.5: ^{15}N 2D HSQC NMR spectra of reduced and oxidized Hsp33^{Y12E}

Shown here are the ^{15}N 2D HSQC spectra of reduced ^{15}N-labeled Hsp33^{Y12E} (left panel), ^{15}N-labeled oxidized Hsp33^{Y12E} (center panel), and ^{15}N-labeled oxidized Hsp33^{Y12E} with the substrate neuropeptide Y (NPY) (right panel). This Hsp33 variant is known for its constitutively unfolded linker domain, which mediates full chaperone activity even in its reduced, zinc-coordinated form. It can therefore be considered to be the least unfolded variant of Hsp33 that shows full chaperone function. Although well dispersed, only one third of the expected peaks are well defined.

We were able to express and purify all of the proteins except the two Hsp33-variants harboring the non-natural amino acids tFPA at position Y12 or Y39. Next we evaluated the purified variants under both reducing and oxidizing conditions for their propensity to prevent the aggregation of chemically denatured citrate synthase (CS) at 20° C and 30° C, or thermally unfolded CS at 43° C (Fig. 4.1.6). In their oxidized and disulfide bonded form, all tested variants revealed wild-type-like activity, indicating that client binding was not substantially affected by the introduction of tFPA at these sites. In contrast, the activity of the reduced tFPA mutant variants was generally higher at 30 °C, with the exception of the Hsp33^{M172SY145tFPA} mutant, which did not maintain any degree of temperature-induced chaperone activation. These results suggested that the tFPA substitution introduces an additional destabilization of the linker region, which is known to increase the chaperone function of reduced Hsp33 (Cremers, Reichmann et al. 2010).

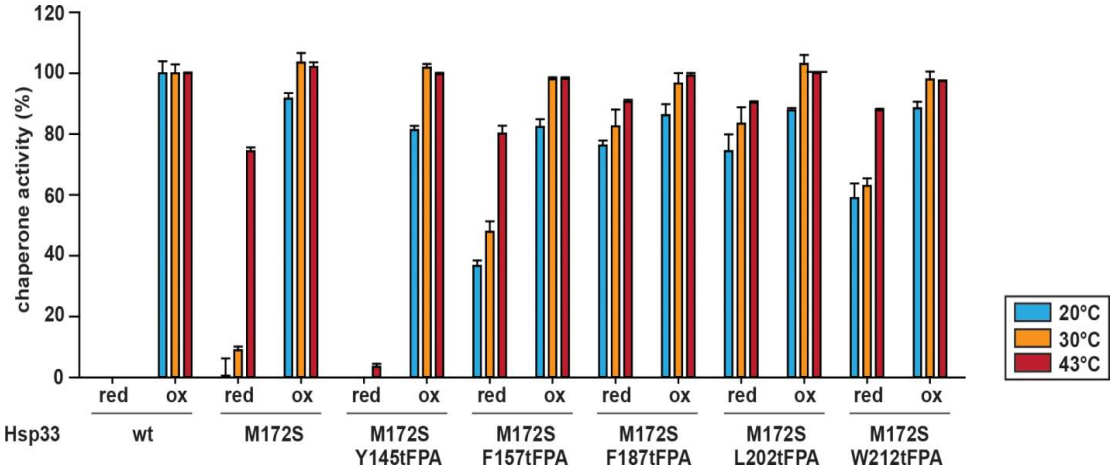

Figure 4.1.6: Chaperone activity of reduced, zinc-reconstituted or HOCl-activated wild-type Hsp33, Hsp33^{M172S} or Hsp33$^{M172S\text{-}tFPA}$ variants.

Chaperone activity was measured by testing the influence of a four-fold molar excess of Hsp33 on the aggregation of chemically unfolded CS at either 20 °C (blue bars) or 30 °C (orange bars) or on thermally unfolded CS at 43 °C (red bars). Chaperone activity of 0% is defined as the light-scattering signal 4 min after addition of CS in the absence of chaperones. Activity of 100% corresponds to the light-scattering signal of CS in the presence of a four-fold molar excess of wild-type Hsp33 that had been activated for 2 min in 200 µM HOCl at 30 °C. All experiments were conducted at least 3–5 times and the s.e.m. is shown.

These results suggested that the tFPA substitution introduces an additional destabilization of the linker region, which is known to increase the chaperone function of reduced Hsp33 (Cremers, Reichmann et al. 2010). This conclusion was in accordance with our findings that most of our crosslinking positive Hsp33-BPA mutants crosslinked with itself as well as with client proteins even at 30°C (Fig 4.1.3B). The Hsp33^{M172SY145tFPA} mutant, however, which was found to be fully chaperone-active when oxidized, apparently lost its temperature induced chaperone activation. This mutant variant did not exert any chaperone activity at either temperature in vitro, and did not reveal any crosslinking products at either 30 °C or 43 °C in vivo (Fig. 4.1.3). This finding suggested that the Y145tFPA mutation suppressed the temperature regulation of the Hsp33^{M172S} mutant variant. For our subsequent NMR studies, we therefore focused on the reduced version of our Hsp33^{M172StFPA} variants since we reasoned that we would be able to visualize the temperature-dependent activation and unfolding of Hsp33, and potentially also monitor client binding upon addition of a substrate.

When we conducted our ^{19}F NMR experiments, we found that only two of our mutant variants, Y145tFPA and W212tFPA, revealed a single peak in the ^{19}F NMR spectrum at 25°C as would be expected from a single labeled residue in a homogeneous environment (Fig. 4.1.7). The three remaining variants, however, each revealed two resonances in the spectra. These results were unexpected, and strongly suggested that the fluorinated residues, which reside in the linker region docking surface of Hsp33's N-terminus (F157) or the linker region (F187, L202), exist in at least two chemical environments that interchange slowly on the NMR timescale (millisecond exchange rate or slower). The chemical shifts of the up-field peaks were very similar to the chemical shifts of the unbound tFPA, suggesting that the up-field peak most likely corresponds to a surface-exposed conformation of tFPA.

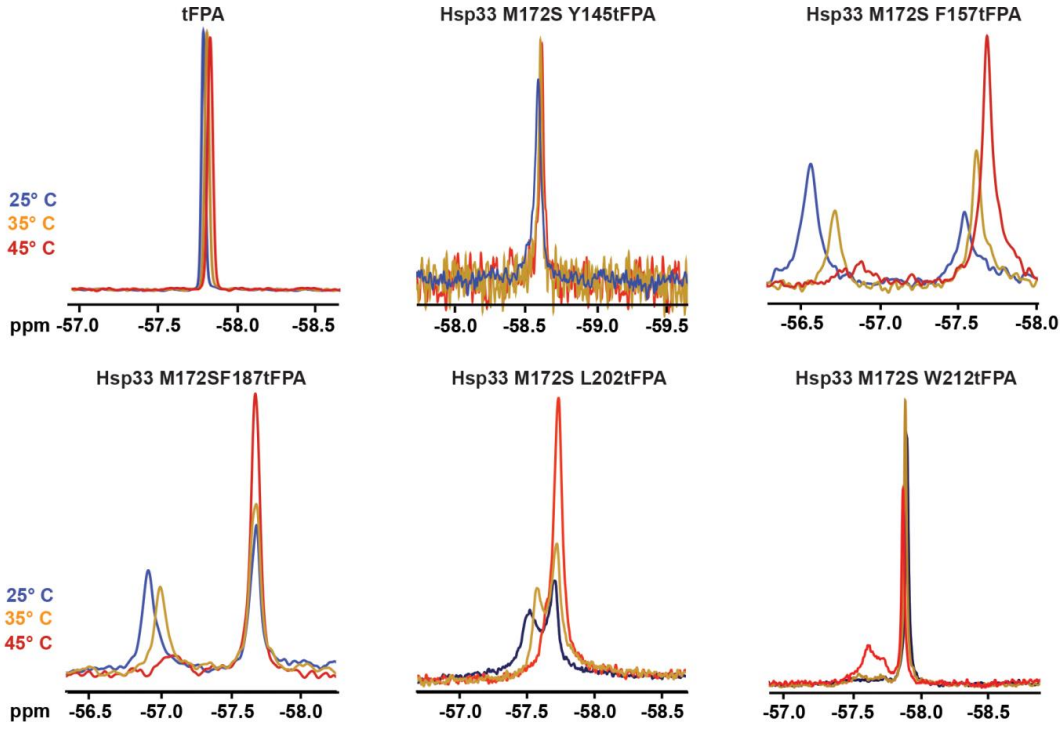

Figure 4.1.7: Temperature dependence of the ^{19}F NMR signal in select Hsp33$^{M172S\text{-}tFPA}$mutants.

^{19}F NMR spectra of tFPA alone or the indicated mutant variants were recorded at either 25 °C (blue), 35 °C (orange) or 45 °C (red).

The down-field peak, on the other hand, presents a conformation where the tFPA is in a more buried chemical environment (Fig. 4.1.7). One hypothesis is that the respective up-field resonances represent the unfolded, chaperone-active state of Hsp33, whereas the down-field peaks represent the folded, chaperone-inactive state of Hsp33. Further support for this theory was provided by quantum mechanics (QM) chemical shift calculations, which enabled us to quantify the effects of neighboring residues on chemical shifts. As exhibited by our QM calculations, small environmental or bond angle changes of our tFPA probe would result in measurable differences of the chemical shift (Fig 4.1.8A, B).

Our QM calculations agreed with our conclusions and revealed that the proximity of tFPA to the side chains of R155 and R159 in the folded state causes a down-field chemical shift change in the closed, inactive state (Fig. 4.1.8c, left) as compared to the open, active state (Fig. 4.1.8c, right). We further confirmed this result by monitoring the ^{19}F NMR signals of F157tFPA and F187tFPA as a function of temperature. The analysis of the spectra revealed that the area of the putative active state peak reversibly increased in size with rising temperature and hence unfolding, whereas the area of the putative folded, inactive state peak decreased (Fig. 4.1.7, compare blue and red traces). Unbound tFPA, however, was not subject to changes in peak area or height upon shift to higher temperatures. These results agree well with our previous findings (Cremers, Reichmann et al. 2010), which showed that the unfolding of the linker region in Hsp33^{M172S} is sufficient to activate the chaperone in a temperature-dependent manner. These results led us to conclude that the up-field resonance peaks for both F157 and F187 represent the chaperone active form of Hsp33 with the linker region freed from the surface of Hsp33. In turn, the down-field peaks represent the closed, inactive state of Hsp33, in which the binding site is buried and in close proximity to R155 and R159. Very similar results were obtained for the L202tFPA mutant variant. An increase in temperature of the W212-tFPA mutant variant, however, evoked the appearance of an additional down-field resonance peak, which could potentially represent a second active chemical environment (Fig 4.1.7).

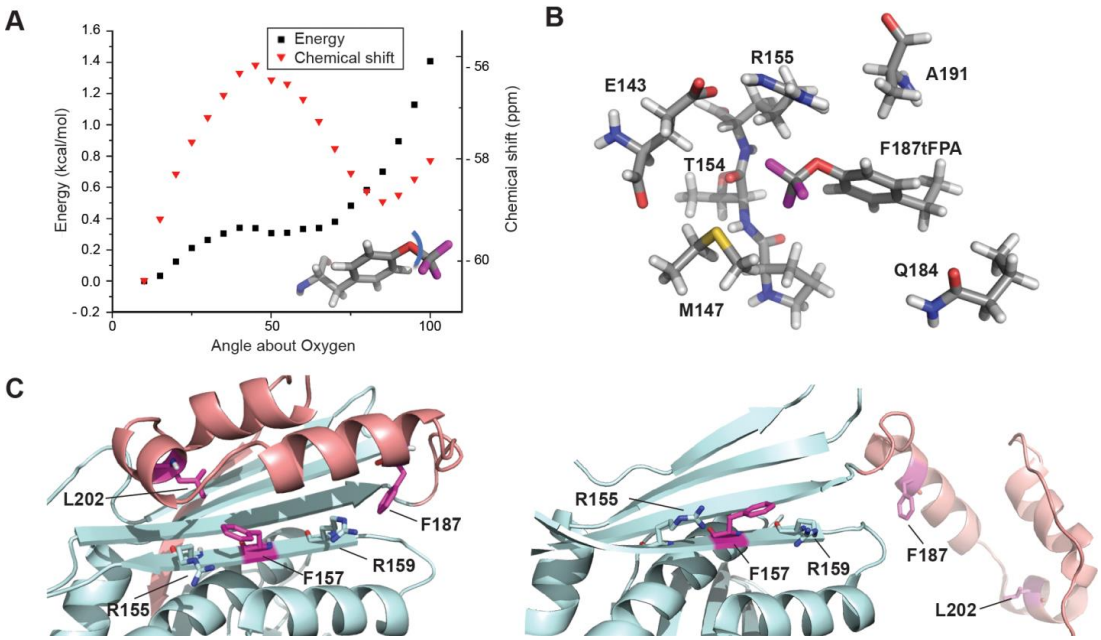

Figure 4.1.8: Chemical shift, conformational energy and QM model of tFPA in solution, or in inactive and active Hsp33

(**A**). Computational dihedral scan of tFPA chemical shift and conformational energy. The large chemical shift change combined with the low rotational barrier of the trifluoro group results in a high sensitivity of tFPA to binding or conformational changes. (**B**). QM model of F187tFPA substitution in the closed state. The adjacent positively charged R155 side chain causes a down-field change in the calculated ^{19}F chemical shift of tFPA. (**C**). N-terminal linker-docking surface (cyan) and the metastable linker region (pink) of *E. coli* Hsp33 in the inactive, closed state (left) (I-TASSER model) and in the activated, open state (right) (PDB 1HW7). The close proximity of F157 and F187 (and L202) to Arg155 and Arg159 in the closed state of Hsp33 is likely responsible for the distinctive down-field chemical shift change observed in the mutant variants under inactivating conditions.

4.1.3 Monitoring Hsp33-client interaction *in vitro*

Our temperature-dependent NMR experiments as well as the QM calculations helped us to identify the active and inactive states of our Hsp33 tFPA mutants. To test how client binding affects the chemical environment of our respective tFPA mutant variants, we conducted ^{19}F NMR spectroscopy in the presence of the soluble client peptide neuropeptide Y (NPY) as a Hsp33 substrate (Reichmann, Xu et al. 2012). Protein aggregation competition assay confirmed that all of our tFPA mutants were able to bind NPY (Fig 4.1.9). We reasoned that addition of binding partners that alter the environment of the ^{19}F-probe should cause a chemical shift change and/or line broadening, and hence should serve as a read-

out for protein dynamics as well as local changes surrounding the tFPA-labeled residues. When we titrated NPY into a solution containing the ^{19}F-labeled Hsp33 variants, we detected increased line broadening for the up-field active state peaks and distinct chemical shift changes for both F157 and F187 (Fig. 4.1.10). The inactive states (i.e., down-field peaks), in turn, displayed comparatively little to no line broadening or chemical shift changes. This result is in full agreement with previous results that showed that clients bind to the more unfolded, active state of Hsp33 (Reichmann, Xu et al. 2012). Furthermore, upon addition of NPY, the peak area of the presumed inactive state of both F157 and F187 slightly decreased, whereas the peak size of the presumed active state increased.

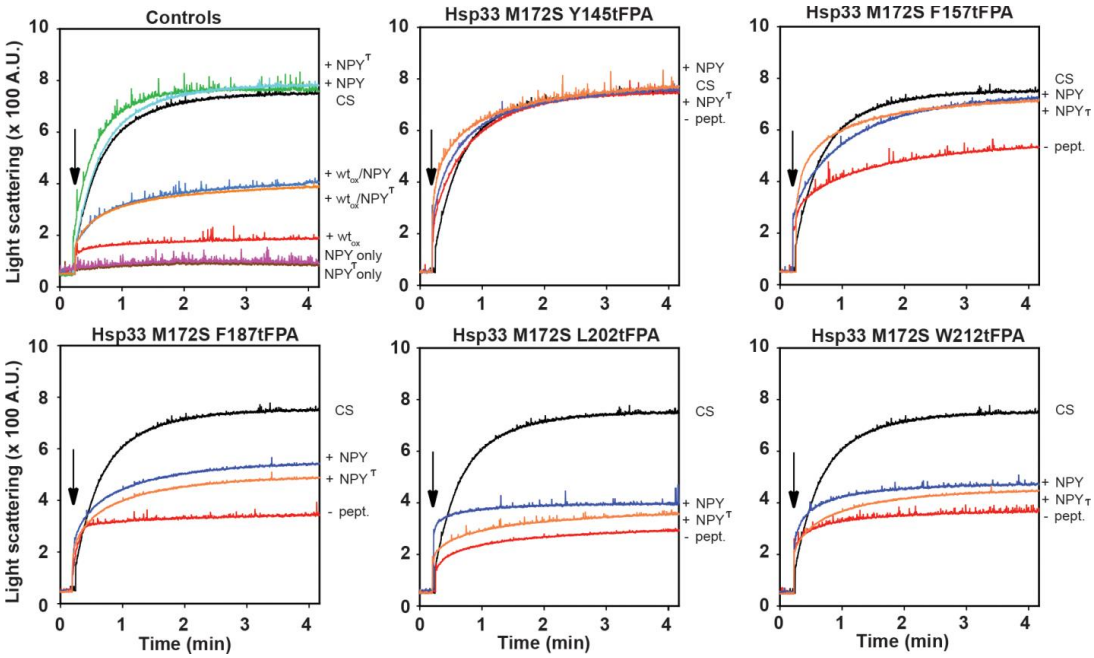

Figure 4.1.9: Peptide competition assays and ^{19}F NMR spectra of select Hsp33 tFPA variants.

The influence of a four-fold molar excess of oxidized, wild-type Hsp33 and reduced Hsp33^{M172StFPA} variants on the aggregation of chemically unfolded CS (150 nM) was monitored at 30 °C in the presence or absence of a ten-fold excess of NPY or NPY$^{D4C\text{-}IAM\text{-}TEMPO}$ (labeled NPY^T here) to CS. A loss in the prevention of aggregation of CS upon peptide addition indicates binding of NPY or NPY$^{D4C\text{-}IAM\text{-}TEMPO}$ to Hsp33.

These data suggest that the addition of the chaperone substrate NPY-PRE shifts the equilibrium in the direction of active client-bound Hsp33. We found no

chemical shift or line width changes mixing the Y145tFPA variant and NPY (Fig. 4.1.10), confirming that Hsp33^{M172SY145tFPA} is inactive under these conditions (Fig. 4.1.9). Significant protein aggregation and precipitation was observed for this mutant variant upon mixing peptide and chaperone, a likely explanation for the decrease in peak size (Fig. 4.1.10). In case of the L202tFPA and W212tFPA (Fig 4.1.10) variants, only very small chemical shift changes and no significant changes in the line width was observed, questioning their role in client binding.

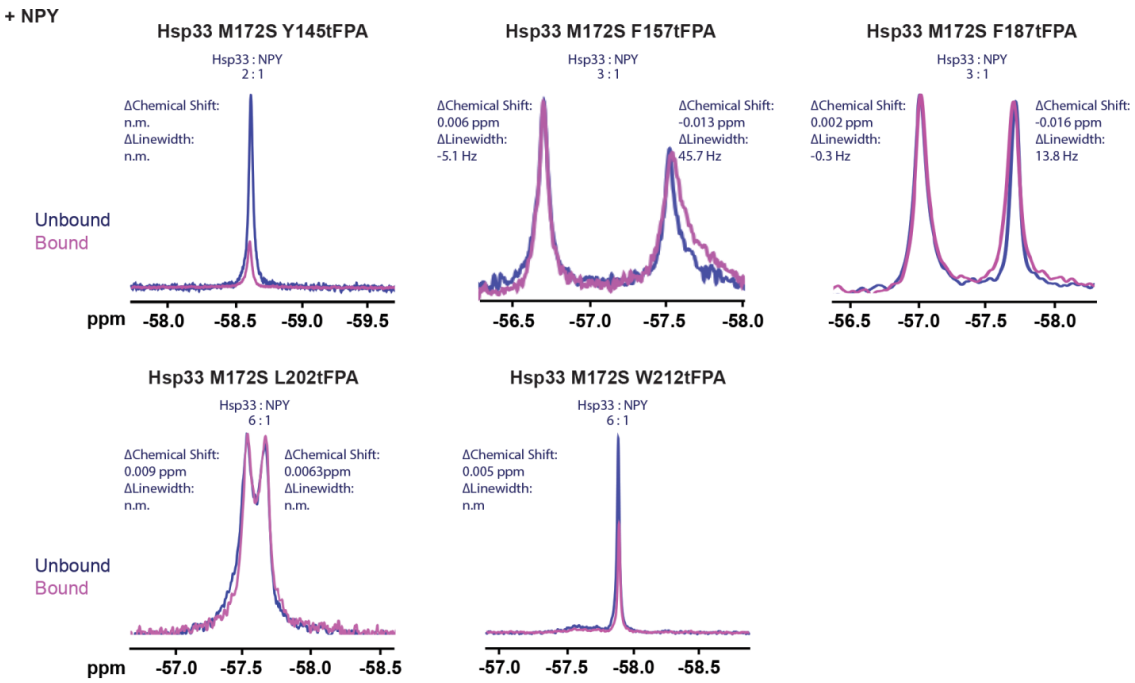

Figure 4.1.10: ^{19}F NMR spectra of select Hsp33^{M172StFPA} variants in the absence (blue) or presence (magenta) of NPY.

The incubation temperature was set to 35 °C. The decreased intensity of Hsp33^{M172SY145tFPA} is due to aggregation of the protein sample. All experiments were conducted at least three times.

To confirm that F157 and F187 and further evaluate the role of L202 and W212 in client binding, we decided to use a variant of NPY (NPY^{D4C}) labeled with a paramagnetic relaxation enhancement (PRE) tag. PRE tags line-broaden residues that are in close proximity to the tag, and are thus an immediate readout for a spatial relation between the tag and the affected residues (Clore and Iwahara 2009). Our tag of choice for this purpose was 4-(2-iodoacetamido)-

TEMPO (IAM-TEMPO), which we conjugated to an engineered cysteine residue in neuropeptide Y (NPY^{D4C}). Competition assays showed that the PRE tag had no substantial effect on binding of NPY to our mutant Hsp33 variants (Fig 4.1.9). By measuring the relative peak height change of the Hsp33 tFPA signals upon addition of the $NPY^{D4C\text{-}IAM\text{-}TEMPO}$ variant compared to unlabeled NPY revealed the line broadening effect of the PRE tag. Under the premise of exact normalization of peaks, an analysis of peak heights is equivalent to evaluating line broadening, a widely employed analysis method for PREs in biomolecular NMR (Clore and Iwahara 2009).

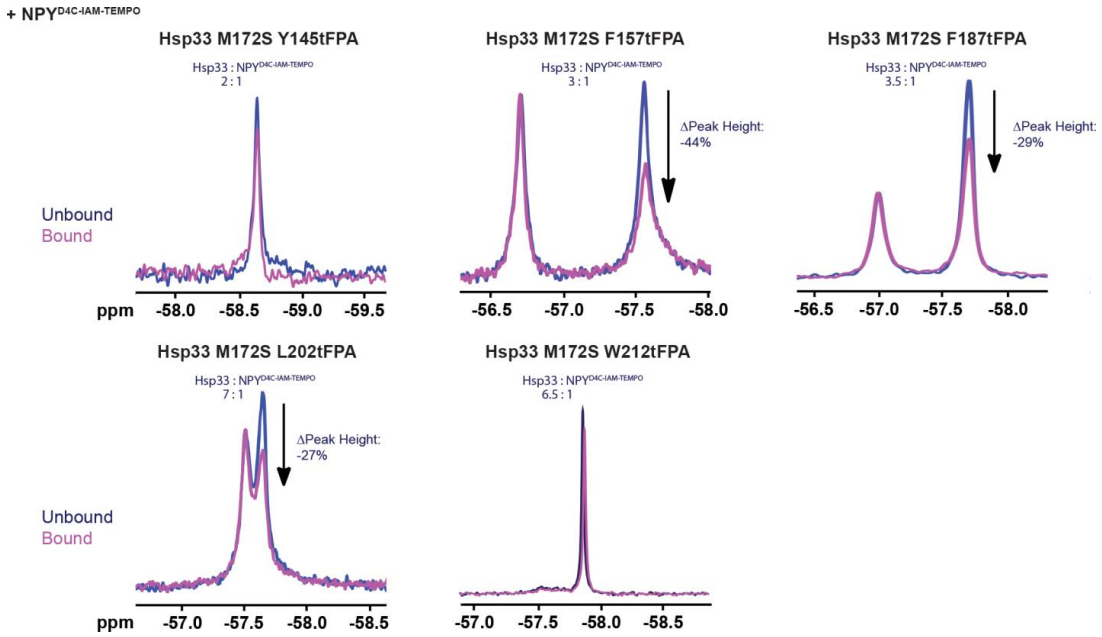

Figure 4.1.11: ^{19}F NMR spectra of select $Hsp33^{M172StFPA}$ variants in the absence (blue) or presence (magenta) of NPY labelled with the paramagnetic spin-label TEMPO.

The incubation temperature was set to 35 °C. All experiments were conducted at least three times. The lack of decreasing peak intensity upon addition of the paramagnetic TEMPO tag shown for $Hsp33^{M172SY145tFPA}$ and $Hsp33^{M172SW212tFPA}$ demonstrates that binding does not occur at these sites.

Addition of sub-stoichiometric concentrations of $NPY^{D4C\text{-}IAM\text{-}TEMPO}$ to either Hsp33 -F157tFPA or Hsp33-F187tFPA caused a substantial decrease in peak height for the active state resonances, indicative of direct client binding (Fig. 4.1.11). Titration of the $NPY^{D4C\text{-}IAM\text{-}TEMPO}$ peptide reproducibly led to decrease in the peak

height of the active state resonance dependent on the concentration of the peptide (Fig 4.1.12B, C). When we added buffer alone as a control, however, no pronounced change in the ratio between the active or inactive peak was observed (Fig 4.1.12A).

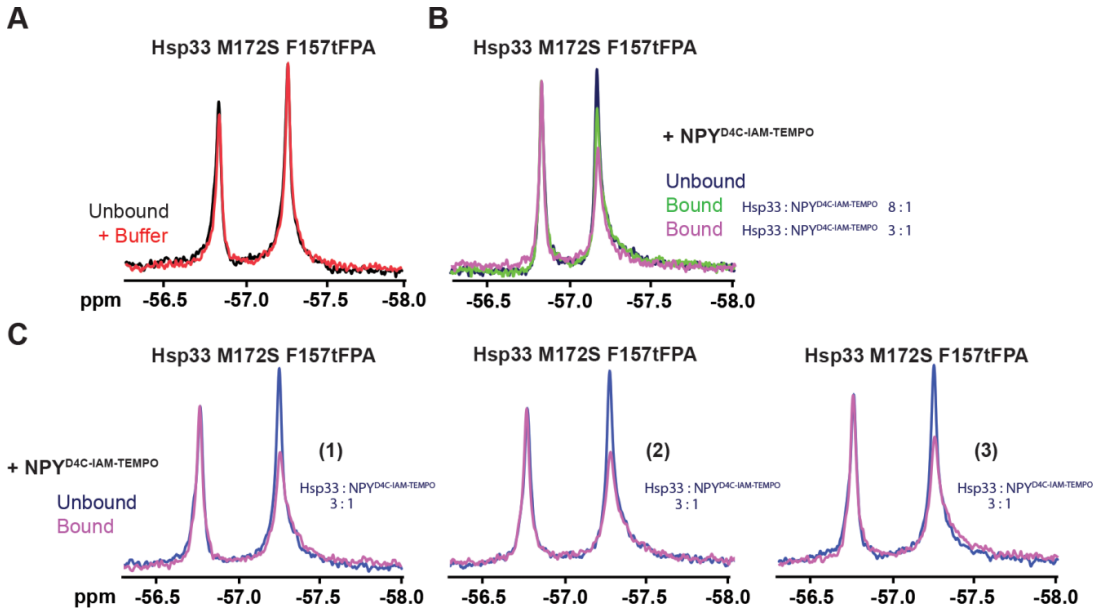

Figure 4.1.12: Buffer control, NMR titration experiment with NPY$^{D4C\text{-}IAM\text{-}TEMPO}$, and NMR data reproducibility as exemplified by Hsp33^{M172SF157tFPA}

(**A**). No substantial chemical shift changes were observed upon addition of NPY$^{D4C\text{-}IAM\text{-}TEMPO}$ buffer to Hsp33^{M172SF157tFPA}. (**B**). NMR titration experiment of increasing amounts of NPY$^{D4C\text{-}IAM\text{-}TEMPO}$ to Hsp33^{M172SF157tFPA} illustrates a concentration-dependent loss in peak intensity. (**C**). Reproducibility of peptide-dependent line broadening of the active state resonances as shown by using technical replicates of NPY$^{D4C\text{-}IAM\text{-}TEMPO}$ addition to Hsp33^{M172SF157tFPA}.

According to the extent of PRE line broadening and the stoichiometry of binding (Fig 4.1.11) (Gillespie and Shortle 1997), we were able to estimate an average interaction distance between NPY and residues F157 and F187 of about 13-15 Å. A comparative decrease in peak height and hence resulting PRE line broadening was also observed for the presumed active state peak of Hsp33-L202tFPA (Fig. 4.1.11). Such changes were not observed for the Y145tFPA or the W212tFPA variants upon addition of NPY$^{D4C\text{-}IAM\text{-}TEMPO}$, indicating that these two residues are not involved in substrate interaction (Fig 4.1.11). These findings emphasize the power of employing unnatural amino acid substitutions for *in vivo*

crosslinking, ^{19}F NMR, and spin-label experiments. These experiments provide us with insight into Hsp33's activation and client binding process, and helped identify at least three sites in Hsp33 that are indeed *bona fide* client interaction sites—one residue in the linker docking surface (F157) and two residues found in the linker region of Hsp33 (F187 and L202).

4.1.4 *In vitro* crosslinking reveals client binding sites in Hsp33

One limitation of *in vivo* crosslinking studies is the number and identity of residues selected for replacement in a protein. In order to overcome this constraint, we decided to use a parallel approach that is not reliant on amino acid substitutions. Our method of choice to complement our data was *in vitro* crosslinking followed by mass spectrometric analysis. The spacer distance of crosslinkers is a major factor that determines the outcome of *in vitro* crosslinking. Crosslinkers with greater spacer distance offer higher flexibility and do not require close contact between interaction partners. However, this flexibility may also lead to unspecific reactions between residues that are not in immediate spatial contact under normal conditions. Zero-length crosslinkers, in contrast, will only result in crosslinks after direct interaction of two binding partners but may be impaired if this binding interaction requires some degree of dynamic flexibility. Therefore, we decided to use three different crosslinking reagents that vary in their spacer distance (14 Å, 7 Å, 0 Å). We performed crosslinking experiments with reduced inactive or oxidized active wild-type Hsp33 using NPY or an engineered variant with an additional serine residue at the N-terminus SNPY as client peptides. A competition assay between citrate synthase and SNPY revealed that SNPY indeed competes with CS for binding to Hsp33, although to a lesser degree as its cognate peptide NPY (Fig 4.1.13 A). To identify Hsp33-NPY crosslinked peptides, we employed either isotopically-coded crosslinkers, such as collision-induced dissociation (CID)-cleavable amine-reactive 14 Å-length cyanur-biotin-dimercapto-propionyl-succinimide (CBDPS-H_8/D_8) (Petrotchenko, Serpa et al. 2011), or photoreactive 7 Å-length azido-benzoic-acid-succinimide (ABAS-$^{12}C_6$/$^{13}C_6$)(Brodie, Makepeace et al. 2015). Additionally, we used an

equimolar mixture of ^{14}N- and ^{15}N-metabolically labeled Hsp33 in the case of the zero-length crosslinker (3-dimethylaminopropyl)carbodiimide (EDC). After mixing Hsp33 in the presence (Fig 4.1.13B, lanes 1-6) or absence (Fig 4.1.13B, lanes 7-10) of crosslinkers, we separated the resulting samples by SDS-PAGE. We detected bands migrating higher than about 70 kDa (Hsp33 dimer) only in samples with crosslinker present, indicative of crosslinked complexes.

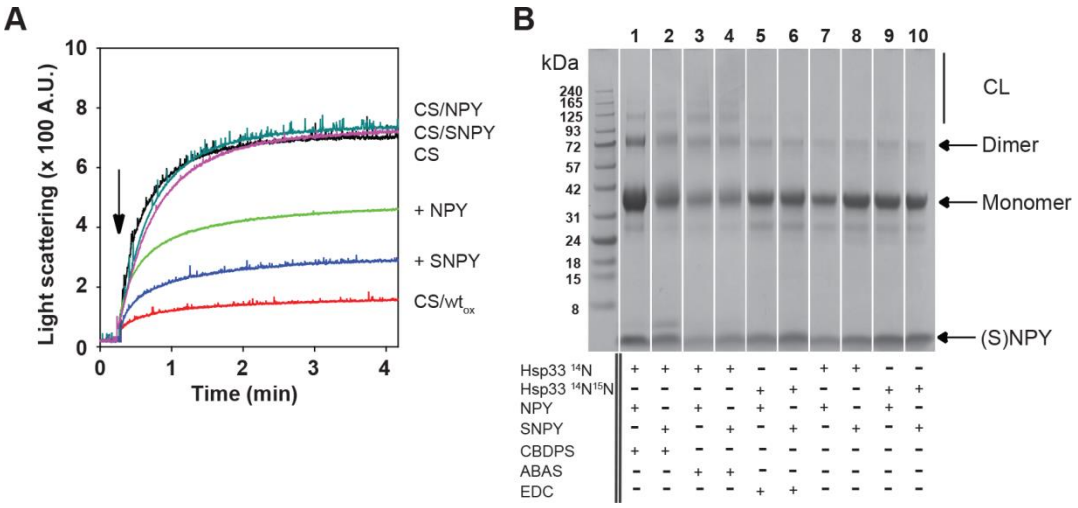

Figure 4.1.13 *In vitro* crosslinking procedure and scheme.

(**A**). Competition assays of NPY or SNPY. The influence of a four-fold molar excess of reduced, zinc-reconstituted as well as HOCl oxidized wild-type Hsp33 on the aggregation of chemically unfolded CS (150 nM) was monitored at 30 °C in the presence or absence of a ten-fold excess of NPY or SNPY. (**B**). SDS-PAGE gel of *in vitro* crosslinking conditions of Hsp33 and NPY or SNPY, which carries one additional Ser residue at the N-terminus.

After subsequent digestion of the protein mixtures with either protease K (PK) or trypsin (T), we identified the crosslinking products using MS/MS analysis. We detected a number of crosslinks between activated $Hsp33_{ox}$ and NPY, which we did not observe when we tested inactive $Hsp33_{red}$ (Table 4). Additionally, we detected several crosslinks between the peptide and either oxidized or reduced Hsp33, suggesting potential non-specific binding (Table 4).

Table 4: *In vitro* crosslinks between Hsp33 and (S)NPY: oxidized only (A), both oxidized & reduced (B), and reduced only (C)

	Crosslinker	Hsp33	Deconvoluted MS Peak (MH+) (L)	Experimental MS Peak (m/z) (L)	z (L)	Scan Identifier (L)	Error (ppm)	AA# Start (1)	AA# End (1)	AA# Modified (1)	AA-1 (1)	Peptide Sequence (1)	AA+1 (1)	Protein (2)	AA# Start (2)	AA# End (2)	AA# Modified (2)	AA-1 (2)	Peptide Sequence (2)	AA+1 (2)
A)	ABAS	Hsp33ox	2018.85545	1009.93164	2	1476	0	35	45	44	L	ENHDYPQPVKN	V	NPY	1	5	1	-	PAEDM	A
	ABAS	Hsp33ox	1372.57213	686.78998	2	1952	0.7	61	66	62	T	LKFDGD	I	NPY	1	5	1	-	PAEDM	A
	ABAS	Hsp33ox	1586.70445	793.85614	2	2318	0.2	61	68	62	T	LKFDGDIT	V	NPY	1	5	1	-	PAEDM	A
	ABAS	Hsp33ox	1763.77819	882.39301	2	1971	0.9	98	107	107	Q	GEIPENADLK	T	NPY	1	5	1	-	PAEDM	A
	ABAS	Hsp33ox	1269.56931	635.28857	2	1493	-1.6	194	198	198	L	TETIK	T	NPY	1	5	1	-	PAEDM	A
	CBDPS	Hsp33ox	2456.04295	1228.52539	2	3080	-1.1	12	20	12	R	YLFENFAVR	G	NPY	1	7	1	-	PAEDMAR	Y
	CBDPS	Hsp33ox	1592.59777	796.8028	2	2836	1.4	61	64	62	T	LKFD	G	NPY	1	5	1	-	PAEDM	A
	CBDPS	Hsp33ox	2155.85863	1078.43323	2	2616	-1.6	98	107	107	Q	GEIPENADLK	T	NPY	1	5	1	-	PAEDM	A
	CBDPS	Hsp33ox	1442.53429	721.77106	2	2227	-1.6	165	168	166	D	GKPA	A	NPY	1	5	1	-	PAEDM	A
	CBDPS	Hsp33ox	1435.57799	718.29291	2	2834	1.6	227	231	231	Q	DVEFK	C	NPY	10	12	10	Y	SAL	R
	EDC	Hsp33ox	2170.04716	724.02057	3	2332	-1	96	107	112	R	VQGEIPENADLK	T	SNPY	1	8	1	-	SPAEDMAR	Y
	EDC	Hsp33ox	1600.77395	534.26257	3	1797	0.9	149	155	150	R	SEQLPTR	L	NPY	1	7	1	-	PAEDMAR	Y
	EDC	Hsp33ox	2133.06263	711.69275	3	1901	0.5	196	210	198	E	TIKTEELLTLPANEV	L	NPY	2	5	3	P	AEDM	A
B)	ABAS	Hsp33ox	2036.93737	1018.9726	2	2803	0	244	255	244	L	KTLPDEEVDSIL	A	NPY	1	5	1	-	PAEDM	A
	ABAS	Hsp33red	2036.93687	1018.97235	2	2892	0.3	244	255	244	L	KTLPDEEVDSIL	A	NPY	1	5	1	-	PAEDM	A
	CBDPS	Hsp33ox	2703.12667	901.71411	3	2733	0.8	1	11	1	-	MIMPQHDQLHR	Y	NPY	1	7	1	-	PAEDMAR	Y
	CBDPS	Hsp33red	2703.12850	901.71472	3	2354	0.1	1	11	1	-	MIMPQHDQLHR	Y	NPY	1	7	1	-	PAEDMAR	Y
	CBDPS	Hsp33ox	2410.93407	1205.97095	2	2171	-1.4	35	45	44	L	ENHDYPQPVKN	V	NPY	1	5	1	-	PAEDM	A
	CBDPS	Hsp33red	2410.93235	1205.97009	2	2118	-0.6	35	45	44	L	ENHDYPQPVKN	V	NPY	1	5	1	-	PAEDM	A
	EDC	Hsp33ox	1901.90581	951.45697	2	3849	-0.2	244	255	249	L	KTLPDEEVDSIL	A	NPY	1	5	1	-	PAEDM	A
	EDC	Hsp33red	1901.90520	951.45673	2	3955	0.1	244	255	249	L	KTLPDEEVDSIL	A	NPY	1	5	1	-	PAEDM	A
	EDC	Hsp33ox	1988.93791	994.97278	2	3789	-0.3	244	255	249	L	KTLPDEEVDSIL	A	SNPY	1	6	1	-	SPAEDM	A
	EDC	Hsp33red	1988.93877	994.97266	2	3849	-0.7	244	255	249	L	KTLPDEEVDSIL	A	SNPY	1	6	1	-	SPAEDM	A
C)	CBDPS	Hsp33red	1866.66355	933.83569	2	2141	-0.2	232	236	235	K	CTCSR	E	NPY	1	7	1	-	PAEDMAR	Y

Several of the amino acids in $Hsp33_{ox}$ that we found to crosslink with NPY *in vitro* were independently identified using at least two different crosslinkers (Fig. 4.1.14A). The residues Y12, K44, K62, and K198 were of special interest since they were also identified as *in vivo* crosslinking sites in our study (Fig. 4.1.14B, Fig. 4.1.15A).

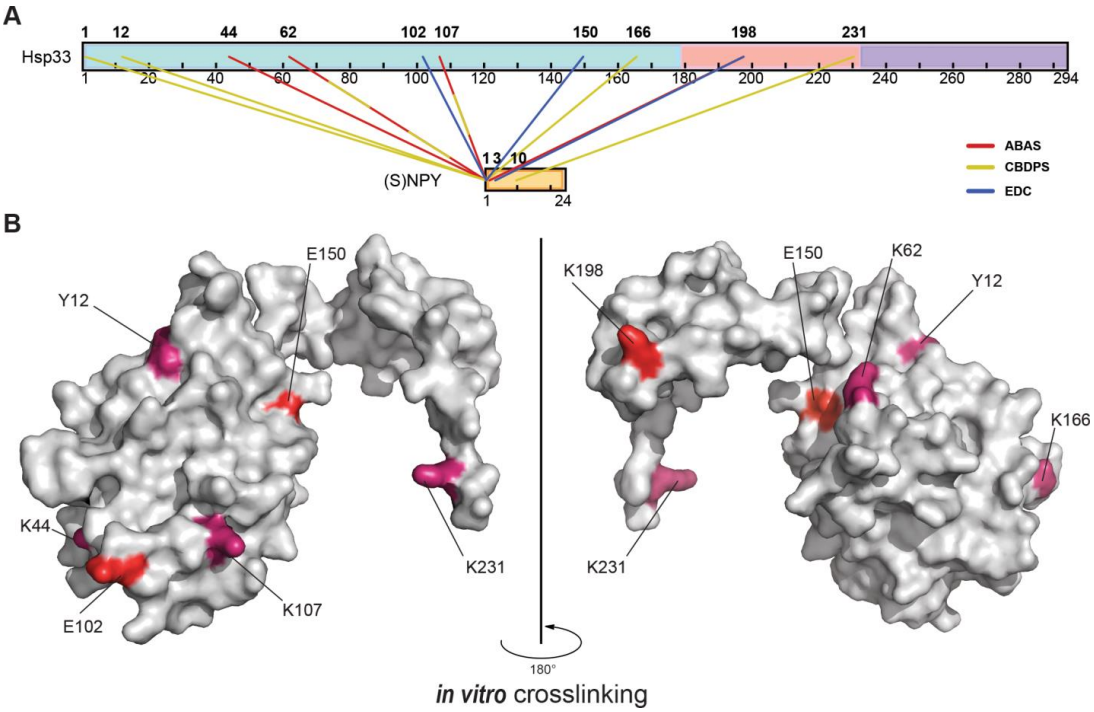

Figure 4.1.14: *In vitro* crosslinks between oxidized (activated) wild-type Hsp33 and (S)NPY-peptide

(**A**). Crosslinks displayed in a linear representation created with Cross-Link Viewer (Combe, Fischer et al. 2015) (SNPY is the NPY peptide containing one additional serine residue at the N-terminus). Residues that crosslinked with more than one crosslinker are shown as dashed lines in the respective colors (ABAS: red; CDBPS: yellow; and EDC: blue). (**B**). *In vitro* crosslinking sites are indicated on the crystal structure of oxidized, domain-swapped *E. coli* $Hsp33^{1-255}$ (PDB 1HW7). Only one of the two subunits that are found in the crystal structure is shown. Zero-length *in vitro* crosslinks with EDC are indicated in red; long- and medium-range crosslinks (CBDPS and ABAS) are shown in dark pink.

Additionally, these residues were also positively identified as potential client interacting residues of $Hsp33_{ox}$ in an earlier study (Reichmann, Xu et al. 2012). Here the authors compared the proteolytic sensitivity of oxidized Hsp33 alone or in complex with thermally unfolded luciferase, and found them to be protected when in complex with the client protein (Fig 4.1.15B, orange residues).

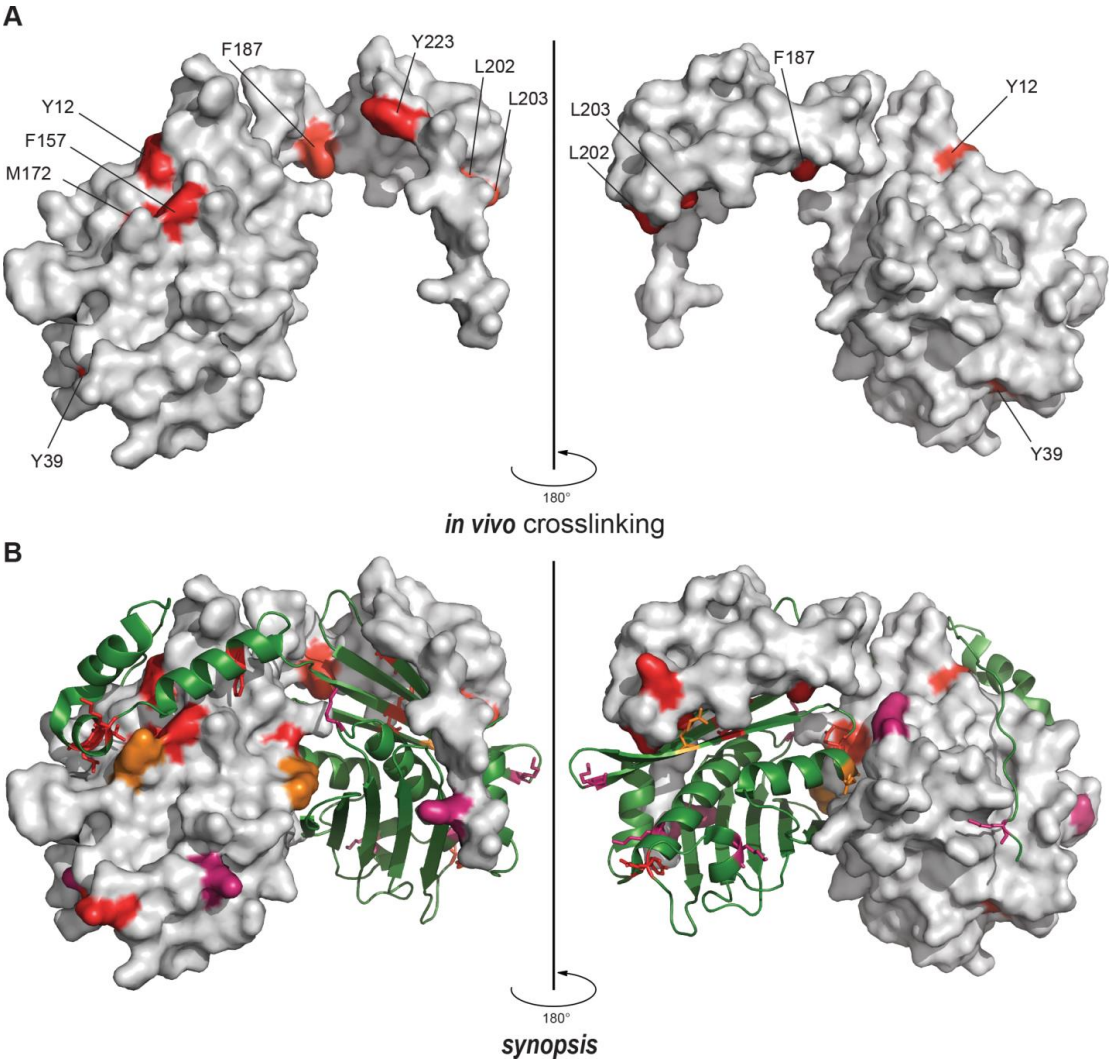

Figure 4.1.15: ***In vivo*** **crosslinking sites and synopsis of all residues identified in client binding**

(**A**). *In vivo* crosslinking sites are indicated in red on the crystal structure of oxidized, domain-swapped *E. coli* Hsp33$^{1\text{-}255}$ (PDB 1HW7). Only one of the two subunits that are found in the crystal structure is shown. (**B**). Structure of domain-swapped *E. coli* Hsp33$^{1\text{-}255}$ (PDB 1HW7) with one monomer in surface representation and the other one in cartoon depiction. All *in vivo* crosslinking-positive residues, all zero-length *in vitro* crosslinking sites, and ^{19}F NMR-positive sites are highlighted in red. Long- and medium-range *in vitro* crosslinking sites are marked in dark pink, and sites previously suggested to be involved in client binding by limited proteolysis experiments (Reichmann, Xu et al. 2012) are depicted in orange. Most identified client interaction sites overlap with interaction sites between Hsp33's linker-docking region and the linker region.

K198, a residue located in the linker region between Y187 and L202, was found to crosslink with the zero-length crosslinker EDC (Fig. 4.1.15A). This discovery

implicates a very close proximity between Hsp33's linker region and its client peptide, NPY. Most other crosslinks between $Hsp33_{ox}$ and NPY were found with residues of the linker-docking surface of the N-terminal domain (Fig. 4.1.14B, 4.1.15A). Taken together, these experiments provide independent evidence that the chaperone Hsp33 uses residues of its linker docking region as well as its natively disordered linker region to directly bind its unfolded client proteins (Fig 4.1.15B). Furthermore, we applied an *in silico* method to further verify our findings that the linker docking region indeed provides a favorable surface for the binding of client proteins. Computationally, we performed protein-protein docking simulations between NPY and an Hsp33 model in which the linker region of Hsp33 was removed, exposing the docking site to solvent (Fig. 4.1.16).

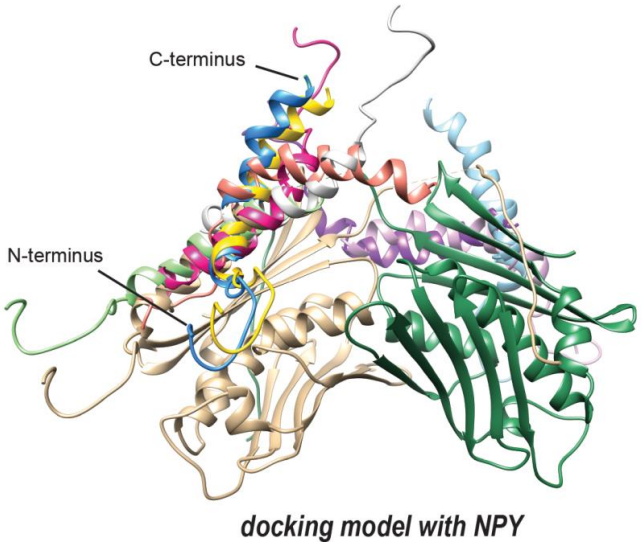

Figure 4.1.16: Computational docking model between Hsp33 and NPY

Docking model of NPY peptide (PDB 1RON) using the truncated oxidized Hsp33 model (residues 182–219 were removed from PDB 1HW7). The top ten docking models are shown in various colours. The Hsp33 subunits are depicted in green and gold, respectively.

Notably, when employing the default settings and thus performing a blind docking procedure with no experimental or computational constraints to identify the binding site, all of the top ten docking hits localized NPY to this linker docking region. This docking simulation complements our ^{19}F NMR binding data that the linker docking region provides a favorable surface for binding partially folded substrates.

4.1.5 Conclusion

Stress-induced chaperones like Hsp33, HdeA/HdeB, and small heat shock proteins are classified by their specific activation to functional chaperones by conformational changes, rearrangements in their folding status and/or alterations in the oligomerization states (Franzmann, Menhorn et al. 2008, Foit, George et al. 2013, Dahl, Koldewey et al. 2015). In their activated state, chaperones like Hsp33 efficiently and non-discriminatingly interact with protein folding intermediates and prevent their aggregation (Bardwell and Jakob 2012). Metastable regions in various proteins, e.g. the linker region in Hsp33, whose folding status is central to the activation process of Hsp33, have not only been found to be molecular switches controlling accessibility to potentially hydrophobic client binding sites (Graf, Martinez-Yamout et al. 2004, Foit, George et al. 2013, Dahl, Koldewey et al. 2015), but were also implicated in client binding itself. Gaining further insight into the underlying features of client binding has been impaired by the fact that methods monitoring structural changes rely on homogeneous and highly stable protein complexes, and require participants that are folded and well-behaved. As for many conditionally disordered chaperones, the folding status of neither the chaperone nor its client is locked into one position only, and thus there is no well-defined chaperone-client complex. Methodologies employed in the past to track down client protein binding sites in chaperones involved limited proteolysis and H/D exchange measurements combined with MS/MS analysis (Cheng, Basha et al. 2008, Reichmann, Xu et al. 2012, Graf, Lee et al. 2014). With these approaches, changes in the accessibility of proteolytic sites or degrees/rates of H/D exchange in the absence and presence of client proteins were used to monitor conformational changes in the chaperone that occur upon client binding (Reichmann, Xu et al. 2012). One limitation of these approaches is that they will not distinguish between direct binding events and structural changes in the chaperone due to client binding at another position in the protein. Limited proteolysis with Hsp33, for instance, revealed client-induced folding and unfolding events. However, these studies failed

to link direct interactions between client proteins and the conditionally disordered linker region (Reichmann, Xu et al. 2012).

This study sought to solve this question as to which regions in Hsp33 are involved in client-chaperone interaction, with the potential goal to elucidate a more common mechanism for client recognition by stress-induced chaperones. Thus, we designed a new approach, and incorporated unnatural amino acids into Hsp33 to perform both *in vivo* crosslinking and ^{19}F NMR experiments. Unbiased *in vitro* crosslinking experiments, complemented our studies and unambiguously unveiled a composite client-binding site in Hsp33 based of both polar residues from the flexible linker region as well as hydrophobic residues from the N-terminal linker docking surface of Hsp33 (Fig. 4.1.15B). The results of limited proteolysis and H/D exchange in a previous study provided further support to our data. These studies connected client binding to activated Hsp33 with a limited access of proteolytic sites accompanied by significant changes in the thermodynamic stability of the linker region, and proposed an involvement of the linker region in client binding (Reichmann, Xu et al. 2012). However, these studies failed to tie the involvement of the hydrophobic linker binding platform to client binding. Our crosslinking experiments, in turn, were able to fill this gap and revealed a substantial involvement of this region in Hsp33-client interactions. Our results strongly suggest that Hsp33 employs a composite binding site composed of a flexible polar linker region and a stable hydrophobic binding surface. This motif is highly reminiscent of the mechanism of substrate recognition by the canonical chaperone TRiC/CCT (Joachimiak, Walzthoeni et al. 2014), or of studies on the complex formation between Spy and Im7 (Koldewey, Stull et al. 2016). Electrostatic interactions between the chaperonin and its client protein confer specificity to binding while non-polar contacts allow for close interaction and serve to stabilize the complex. We hypothesize that Hsp33 analogously also employs its polar and highly flexible linker region to undergo initial charged-charged interactions with protein folding intermediates. This mechanism might help with steering clients to the non-polar N-terminal surface for additional hydrophobic interactions and increase the stability of the complex, potentially also by subsequent rearrangement and refolding of the linker region (Reichmann, Xu et al. 2012). Our studies added a

valuable piece to the puzzle as to how chaperones recognize and bind client proteins, and go beyond the idea of simple hydrophobic interactions, a force that has up to now been thought to drive most chaperone-client communication (Kim, Hipp et al. 2013). Moreover, we found that Hsp33 seems to employ a large number of interactions found between its linker region and the linker docking domain under reducing, non-stress conditions also when engaging with partially folded client proteins under oxidizing, activating conditions. Oxidized, active Hsp33 displays preferential binding to early unfolding clients proteins with substantial amounts of secondary structure elements (Reichmann, Xu et al. 2012), potentially mimicking the conformation of Hsp33's own linker region under reducing conditions. Interestingly, one commonality between the flexible linker region in the oxidized dimer and the peptide substrate model NPY in our docking model and in our *in vitro* experiments are the helical structure elements. Domain swapping in the oxidized Hsp33 dimers in the absence of clients also resembles client-chaperone interaction. It is conceivable that by binding of clients both by the linker docking platform as well as the flexible linker itself, and thus by extending the unfolded protein away from Hsp33's surface, shuttling of clients from Hsp33 to foldases (e.g. DnaK/DnaJ/GrpE) might be facilitated. The docking platform might here serve as a protective surface for hydrophobic residues of protein folding intermediates, whereas the flexible linker could aid in transferring the client to the refolding system.

By combining *in vitro* crosslinking methods with the incorporation of non-canonical amino acids for ^{19}F NMR as well as *in vivo* crosslinking we were able to provide an approach that was able to elucidate the client interaction sites in Hsp33, but could also be extended to untangle further the underlying biology behind chaperone-client interactions, whose elucidation has so far been hampered by difficult heterogeneous systems or dynamic experimental setups.

4.2 *Pseudomonas aeruginosa* defense systems against microbicidal oxidants

Mammalian host defense against invading pathogens is characterized by the employment of specific bactericidal oxidative agents, which are produced by dedicated haloperoxidases. Myeloperoxidase (MPO), which is released by activated neutrophils, produces hypochlorous acid (HOCl, bleach), hypobromous acid (HOBr) and hypothiocyanous acid (HOSCN). Despite some understanding of the molecular targets of these oxidants, little is known about their bacterical efficacies as well as the specific responses they elicit. Understanding these mechanisms is especially important for people suffering from the hereditary disease cystic fibrosis (CF), affecting about 30,000 people in the US alone (Cohen and Prince 2012). These patients experience reoccurring lower respiratory tract infections, chronic inflammation and progressive tissue damage in the lungs due to an imbalance in the amounts of HOCl and HOSCN (Rao and Grigg 2006). The defective cystic fibrosis transmembrane conductance regulator (CFTR) is also responsible for the transport of glutathione (GSH) (Kogan, Ramjeesingh et al. 2003) and SCN^- (Lorentzen, Durairaj et al. 2011), leading to decreased scavenging of HOCl. HOCl, in turn, is increased by elevated levels of MPO due to sustained airway neutrophilia, and even more so in patients with chronic *P. aeruginosa* infections where recruited neutrophils release substantial amounts of HOCl in their attempt to fight off the invading pathogen.

Results in **chapter 4.2** were submitted for publication on March 29th, 2017 in: Groitl B, Dahl JU, Schroeder JW, Jakob U. ***Pseudomonas aeruginosa* defense systems against microbicidal oxidants**. Mol. Microbiol. 2017. I performed all of the experiments except: The *in vivo* aggregation assay on *Pseudomonas aeruginosa* PA14 wt and *ppk*$^-$ in Figures 4.2.7 and 4.2.15A, the growth curves and survival assays after exposure of PA14 wt and select mutant to HOSCN in Figures 4.2.12 and 4.2.13, the polyphosphate extraction and quantification in Figure 4.2.14, and the quantitative real-time PCR results in Figure 4.2.14 were conducted by Dahl JU. The RNA sequencing analysis was performed by Schroeder JW. The manuscript was written by Groitl B, Dahl JU, Jakob U. All subsequent figures are prepared by Groitl B.

4.2.1 The antimicrobial efficacies of HOCl, HOBr, and HOSCN differ by growth conditions

Comparing the effects of oxidants in rich media can be hampered when the compounds to be tested do not just influence bacteria but also react with components in the media itself and thus alter their effective concentrations. For this reason, we decided to treat the bacteria with the oxidants HOCl, HOBr, and HOSCN in phosphate buffer, a buffer system that is known not to quench the concentrations of these oxidants.

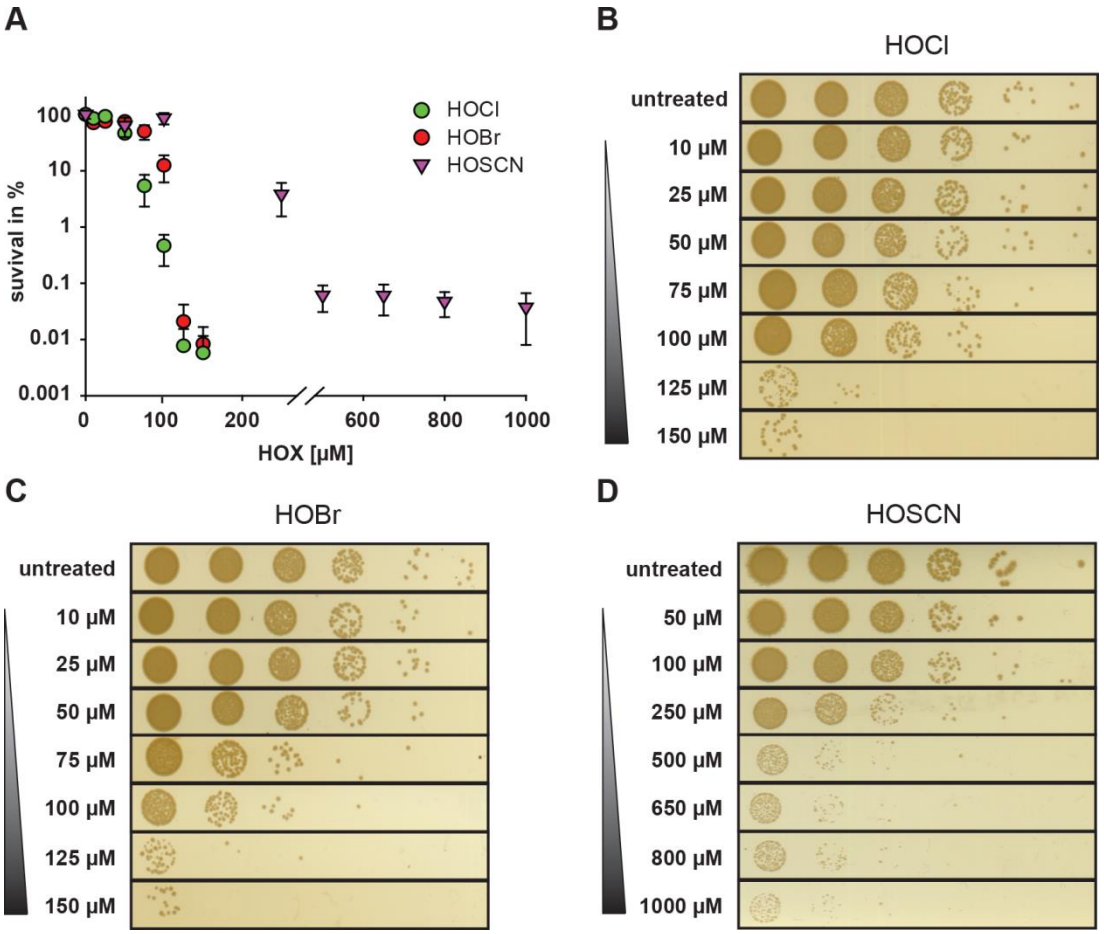

Figure 4.2.1: Comparison of the survival of PA14 after treatment with HOCl, HOBr, and HOSCN in PBS

(**A**). Survival of PA14 wild-type cells in response to treatment with various concentrations of HOCl, HOBr, and HOSCN for 30 min in PBS. All experiments were conducted at least three times and the s.e.m. is shown. Exponentially growing PA14 wild-type cells were incubated with various concentrations of HOCl (**B**), HOBr (**C**), or HOSCN (**D**) for 30 minutes in PBS, serially diluted, and spot-titered. A representative assay is shown.

We incubated *P. aeruginosa* PA14 in MOPS glucose media and grew the cells to mid-logarithmic phase, before we washed and resuspended them in PBS. We then exposed the bacteria to a treatment with various concentrations of the respective oxidants for 30 min. After quenching the oxidants and serially diluting the cells, we spotted the bacteria onto LB plates and monitored their survival after 14 h of incubation. Treatment with either HOCl or HOBr was similarly bactericidal. 100 to 125 µM of the respective oxidant was sufficient to reduce PA14 survival by about four orders of magnitude (Fig. 4.2.1A, B, C).

The same concentration of HOSCN, in turn, only resulted in about one log of killing, suggesting that HOSCN is much less bactericidal (Fig. 4.2.1A, D). A considerable fraction of bacteria still survived the treatment at even very high concentrations of HOSCN (i.e., 1 mM). However, when we conducted the treatment in MOPS-glucose medium, HOBr was most effective in killing PA14, followed by HOSCN and HOCl (Fig. 4.2.2, left column).

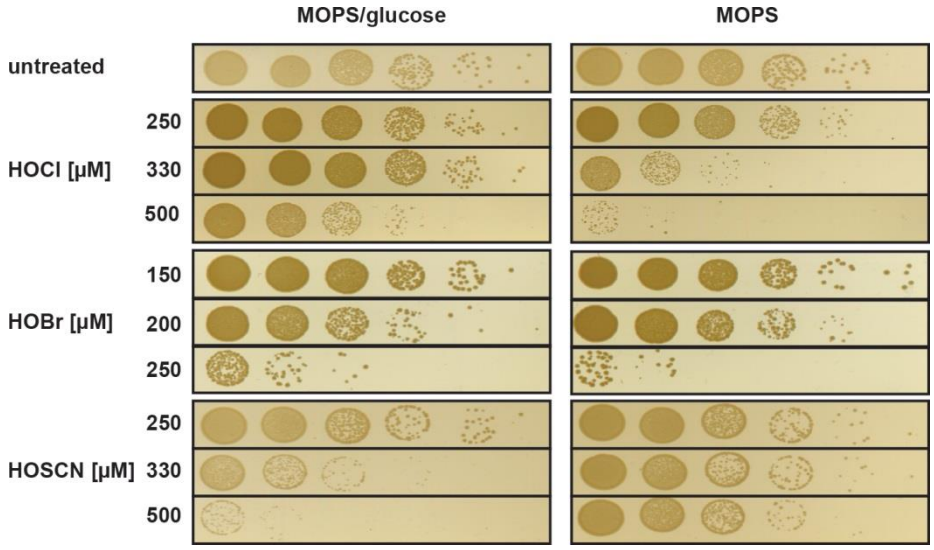

Figure 4.2.2: Comparison of the survival of PA14 after treatment with HOCl, HOBr, and HOSCN in MOPS-glucose or MOPS medium

Exponentially growing PA14 wild-type cells were grown in MOPS-glucose medium, transitioned to MOPS-gpucose or MOPS medium and incubated with various concentrations of HOCl for 30 minutes. Cells were serially diluted and spot-titered on LB plates for overnight growth. A representative assay is shown.

This result could possibly be explained by the fact that MOPS-glucose medium might differentially quench the respective oxidants. However, an alternative

explanation was that the three oxidants might act differently on metabolically active bacteria grown in MOPS/glucose media or non-growing bacteria resuspended in PBS buffer. To dissect between these scenarios, we grew PA14 in MOPS-glucose and transferred the cells to either fresh MOPS-glucose or MOPS media immediately before the subsequent stress treatment (Fig. 4.2.2).

This method enabled us to directly compare the growth status of the bacteria depending on the metabolic activity since glucose is considered to be inert towards the reaction with any of these oxidants. Interestingly, we found that HOCl and HOBr were more effective in killing non-growing *P. aeruginoasa,* whereas HOSCN treatment was significantly more effective in killing actively growing cells (Fig. 4.2.2). Treating the cells with 0.5 mM HOSCN reduced cell survival in MOPS/glucose media by 4 orders of magnitude while no substantial killing was observed when the same treatment was conducted in MOPS media. HOCl and HOBr, in turn, elicited major killing in non-growing bacteria at concentrations that presented actively metabolizing bacteria with little threat (Fig. 4.2.2). These results give a good explanation why HOCl and HOBr are more and HOSCN less effective in killing non-growing *P. aeruginosa* incubated in PBS buffer. In summary, these findings also suggest a different killing mechanism for the three oxidants and/or that they affect different *in vivo* targets. It is predicted that, when used in combination, the oxidants will be highly bactericidal for both actively growing and dormant cells.

4.2.2 PA14 transcriptional changes in response to HOCl, HOBr and HOSCN treatment

Transcriptional response to changes in their environment such as the exposure to oxidative stress is necessary for bacteria to rapidly adapt to the stress and ensure survival. To gain insights into the physiological consequences of treatment with the physiologically relevant oxidants HOCl, HOBr or HOSCN, we tested gene expression changes in PA14 treated with sublethal concentrations of the respective compound. We incubated logarithmically growing wild-type PA14 in MOPS-glucose medium in the presence of 0.5 mM HOCl, 0.15 mM HOBr or 0.25 mM HOSCN for

20 min. These concentrations triggered a 1-1.5 h growth arrest, after which PA14 recovered and returned to normal growth without killing the cells (Fig. 4.2.3 A, B).

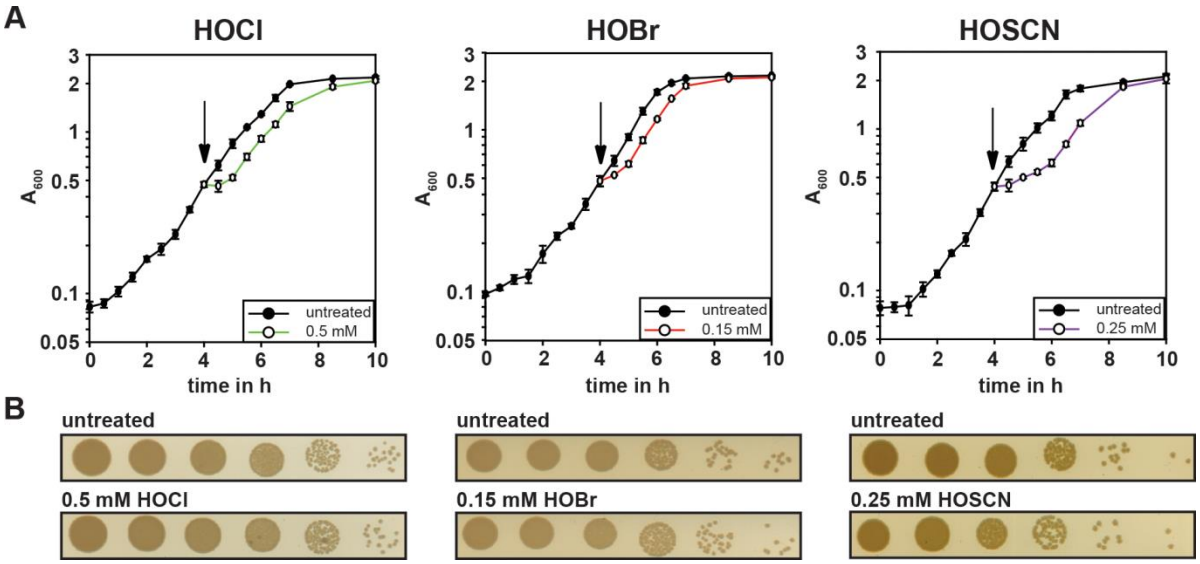

Figure 4.2.3: Treatment of PA14 wild-type with sublethal doses of HOCl, HOBr and HOSCN

(**A**). Growth curves of PA14 wild-type in response to 0.5 mM HOCl, 0.15 mM HOBr and 0.25 mM HOSCN show recovery of cells in response to treatment after a growth delay of 1-1.5 hr. (**B**). Survival assay of PA14 wild-type after treatment with to 0.5 mM HOCl, 0.15 mM HOBr and 0.25 mM HOSCN. Cells were serially diluted and spot-titered on LB plates for overnight growth. No decrease in survival is visible in comparison to the untreated cells.

After the extraction of total RNA from the stress-treated cells, we conducted an RNA_{seq} analysis to monitor global changes in gene expression in PA14 in response to each of the three oxidants. All experiments were conducted in triplicates. For the transcriptome analysis, we included all genes annotated in the NCBI database and compared the expression values of the stress treated cells to non-stress treated controls. The threshold for significance we defined as a *p*-value of <0.005, and transcriptional changes of $\log_2$ fold change of >1.5 we considered upregulated, whereas a $\log_2$ fold change of < -1.5 we considered as downregulated. A complete list of all genes and expression data is available in: Groitl B, Dahl JU, Schroeder JW, Jakob U. ***Pseudomonas aeruginosa* defense systems against microbicidal oxidants**. Mol. Microbiol. Mar 2017 (under review). When we conducted a principal component analysis of the data sets, we found that gene expression changes in all three replicates treated with either HOCl or HOBr clustered in one dimension

(Fig. 4.2.4A, green and red diamonds), while PA14 cells exposed to HOSCN showed distinctly different gene expression changes and clustered in two dimensions (Fig. 4.2.4A, purple diamonds). These data suggest that samples treated with HOCl and HOBr are more closely related to each other in the gene response as those treated with HOSCN. This became apparent when we analyzed of all up- and downregulated genes in the three treatment groups in more depth and discovered a >85% overlap between HOBr and HOCl regulated genes while less than a 50% overlap existed between differentially regulated genes in PA14 treated with HOCl/HOBr and HOSCN (Fig.4.2.4B).

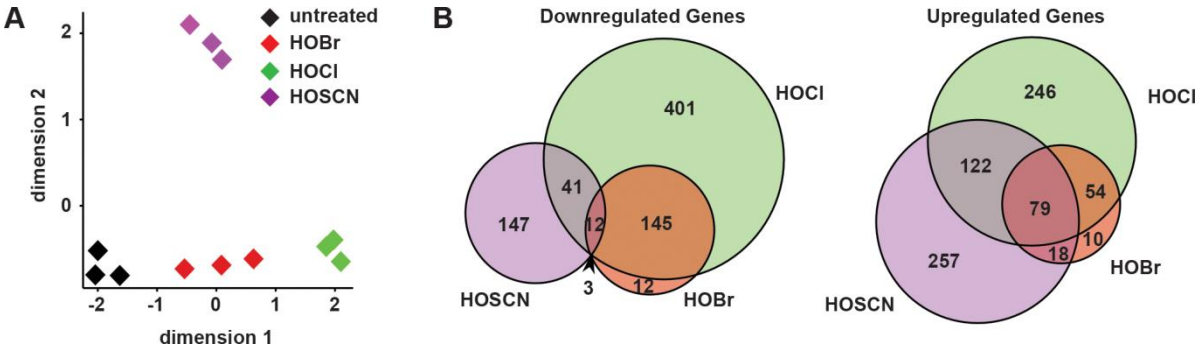

Figure 4.2.4: Global gene expression changes in PA14 in response to HOCl, HOBr or HOSCN treatments.

RNA sequencing analysis after extraction of RNA from exponentially growing PA14 wild-type cells exposed to a sublethal concentration of HOCl (0.5 mM), HOBr (0.15 mM), or HOSCN (0.25 mM) for 15 min. Reads were aligned to the *P. aeruginosa* UCBPP-PA14 reference genome (Accession number: NC_008463.1). (**A**). Principal Component analysis revealed distinct clustering of transcriptomes between untreated PA14 (black) and PA14 treated with HOCl (green), HOBr (red), or HOSCN (purple). (**B**). Venn diagram shows the number of upregulated or downregulated genes upon treatment with HOCl (green), HOBr (red), or HOSCN (purple) and a potential overlap between treatments.

All three antimicrobials tested classify as oxidants, and as such we found the expected increase in expression of genes involved in oxidant detoxification (e.g., catalase, methionine sulfoxide reductase, alkyl hydroperoxide reductase) and restoration of redox homeostasis (e.g. glutathione peroxidase, glutathione reductase) for all three compounds tested (Fig. 4.2.5A). We found striking differences in the proportion of upregulated genes in the functional categories of molecular chaperones. Our analysis revealed that a total of 12 and 9 genes (e.g.,

ibpA, dnaK, groES, hslU/V) were significantly upregulated in response to HOCl and HOBr, respectively.

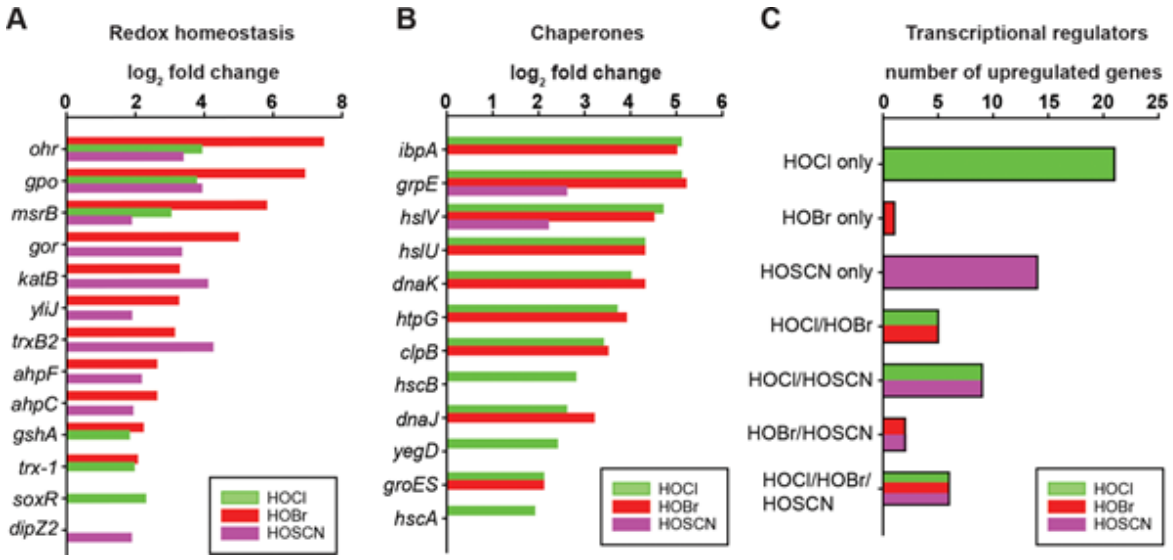

Figure 4.2.5: Upregulated genes involved in redox homeostasis, protein folding and transcriptional regulation

(**A**). Log_2-fold change in genes involved in redox homeostasis. (**B**). Log_2-fold change in chaperones/heat shock genes. (**C**). Number of genes in the functional group of transcriptional regulators. Each condition was tested in triplicate. Significance was defined by a false discovery rate <0.005 and absolute value of log_2-fold change of >1.5.

In contrast, we only detected two heat shock genes (i.e., *grpE, hslV*) to be upregulated in response to HOSCN (Fig. 4.2.5B). Looking more closely into the transcript levels for both of these genes, we found them to be about 6-fold less abundant in HOSCN-treated cells as compared to HOCl treated cells (Fig. 4.2.5B). In the group of transcriptional regulators that were upregulated by the three different treatments, we detected a significant overlap between all three oxidants, although HOCl/HOBr and HOSCN each appeared to upregulate specific sets of transcriptional regulators as well (Table 4.2.5C). Other functional categories that were specifically and significantly more upregulated in response to HOCl/HOBr as compared to HOSCN included genes involved in motility and attachment, chemotaxis, and nucleotide biosynthesis.

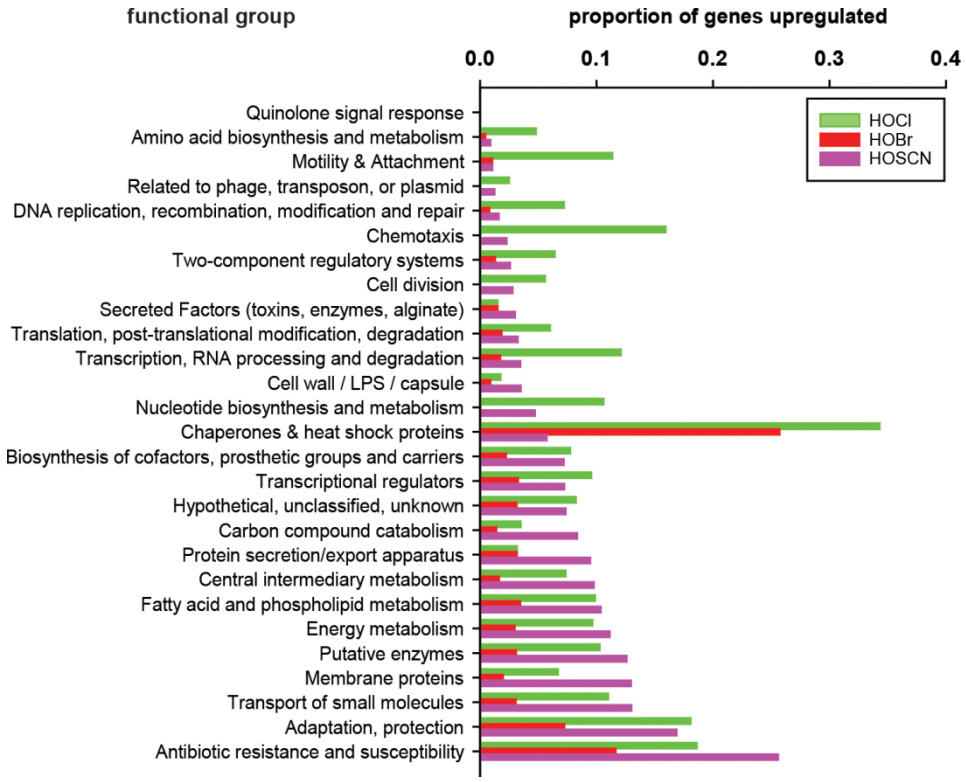

Figure 4.2.6: Proportion of upregulated genes with regards to all functional groups.

Proportion of upregulated genes within each functional groups according to a gene classification by (Lee, Urbach et al. 2006) after treatment with HOCl (0.5 mM), HOBr (0.15 mM), or HOSCN (0.25 mM) for 15 min. Significance was defined by a false discovery rate <0.005 and absolute value of $\log_2$-fold change of >1.5.Functionally classified genes

In turn, proportionally more genes involved in antibiotic resistance or encoding membrane proteins were upregulated in response to HOSCN as compared to HOCl and HOBr, suggesting that HOSCN might target membrane proteins (Fig. 4.2.6). These data led us to the conclusion that all three oxidants affect the redox homeostasis of the cell, but each of them elicits its own oxidant-specific effects.

4.2.3 Effects of HOCl, HOBr and HOSCN on the PA14 proteome

HOCl has previously been demonstrated to elicit extensive protein unfolding and aggregation (Winter, Ilbert et al. 2008). The underlying mechanism is presumably its propensity to quickly react with a plethora of different amino acid side chains, oxidizing them and thereby shifting the equilibrium of proteins more to their aggregation prone state (Winter, Ilbert et al. 2008, Dahl, Gray et al. 2015). Protein aggregation caused by HOCl-induced unfolding is the likely explanation for the

upregulation of members of the heat shock regulon, whose expression is triggered by the accumulation of unfolded proteins (Arsene, Tomoyasu et al. 2000). Based on the observed increase in HOCl resistance by chaperone-mediated prevention of protein aggregation, we previously concluded that protein unfolding is one mechanism of HOCl induced bacterial killing (Winter, Ilbert et al. 2008). It is conceivable that HOBr, like HOCl, leads to global protein aggregation due to the similar chemical character of HOCl and HOBr.

HOSCN's high cysteine specificity raised the question whether it kills bacteria by different means (Skaff, Pattison et al. 2009, Barrett, Pattison et al. 2012, Chandler, Nichols et al. 2013). To allow for a direct comparison of the amount and targets of HOX-mediated protein aggregation, we treated wild-type PA14 with our previously established sublethal concentrations of HOCl (0.5 mM), HOBr (0.15 mM) or HOSCN (0.25 mM) (Fig. 4.2.3A, B). We lysed the cells 30 min after the stress treatment and analyzed the aggregated proteins by SDS-PAGE (Fig. 4.2.7).

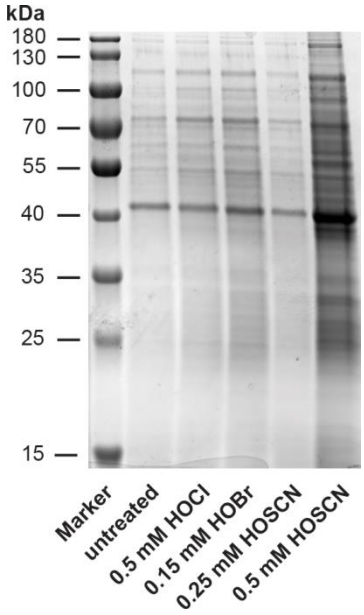

Figure 4.2.7: Effects of HOCl, HOBr or HOSCN on the PA14 wild-type proteome.

Exponentially growing PA14 wild-type cells in MOPS-glucose medium were either left untreated or exposed to HOCl (0.5 mM), HOBr (0.15 mM), or HOSCN (0.25 mM, 0.5 mM) for 30 min. Incubation was stopped by the addition of 10 mM thiosulfate to quench excess of HOX. Cells were lysed, and the aggregated proteins were separated from the soluble fractions by centrifugation. The insoluble proteins were analyzed by SDS-PAGE. Experiments were performed independently at least three times and a representative result is shown.

Exposure to sublethal concentrations of HOCl and HOBr resulted in moderate protein aggregation involving many different PA14 proteins, whereas we detected no significant protein aggregation when cells were treated with growth-delaying concentrations (i.e., 0.25 mM) of HOSCN. These data were in full agreement with our RNA_{seq} data that showed no induction of the heat shock response at these HOSCN concentrations. Thus, we concluded that the observed HOSCN-induced growth arrest presumably is not caused by general protein aggregation. Lethal doses of HOSCN evoked considerable protein aggregation, suggesting that HOSCN exerts either directly or indirectly proteotoxic effects as well.

4.2.4 *In vitro* activation of *E. coli* and PA14 Hsp33 by hypohalous acids

Previous studies have shown that Hsp33 is activated by the oxidative unfolding action of HOCl (Winter, Ilbert et al. 2008). We therefore tested the effects of all three oxidants on the activation of *E. coli* Hsp33.

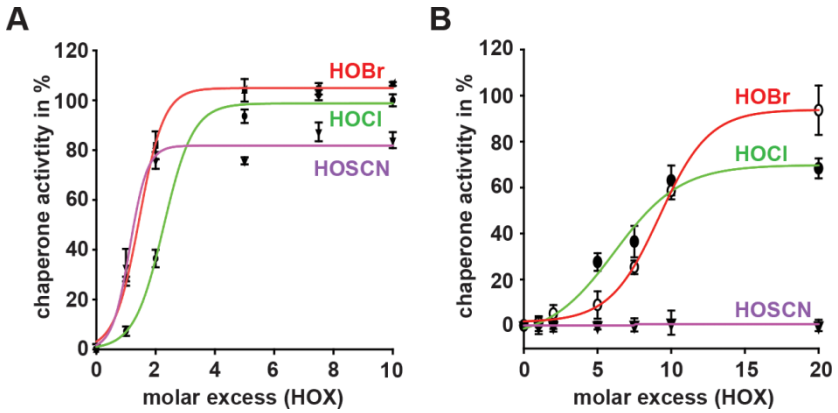

Figure 4.2.8: *E.coli* Hsp33 and PA14 Hsp33 chaperone activity assay

To test the effects of HOX on the *in vitro* activation of *E.coli*-Hsp33 (**A**) and PA14-Hsp33 (**B**), 12 µM chemically denatured citrate synthase was diluted 160-fold into 40 mM HEPES, pH 7.5 at 30 °C in the presence and absence of $Hsp33_{HOX}$. Light scattering was monitored with excitation and emission wavelength set to 360 nm. The light scattering signal of citrate synthase incubated in the presence of 10-fold molar excess of HOCl-activated E.coli Hsp33 (**A**) or a 20-fold molar excess of HOBr-activated PA14-Hsp33 (**B**) was set to 100% activity while the light scattering signal of CS in the absence of any Hsp33 was set to 0% chaperone activity.

Reduced inactive *E. coli* Hsp33 could be turned into an active chaperone upon treatment with either HOCl, HOBr, or HOSCN (Fig. 4.2.8A). In contrast, only HOCl and HOBr activate PA14 Hsp33's chaperone function while HOSCN failed to do so

(Fig. 4.2.8B). Hsp33's zinc-binding domain is a sensitive redox-regulator, and therefore it is conceivable that HOSCN also evokes disulfide bond formation and potential concomitant unfolding of the linker region. But despite this fact, PA14 Hsp33, unlike *E.coli* Hsp33, was not activated by HOSCN.

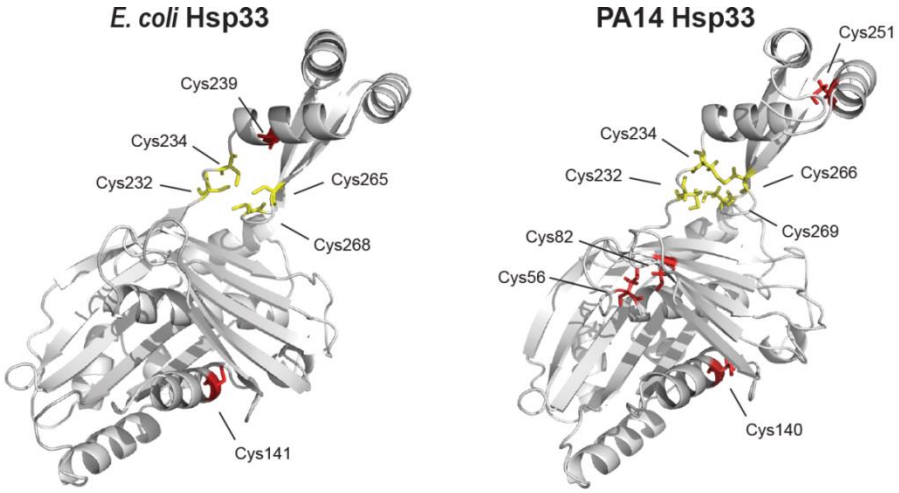

Figure 4.2.9: iTASSER model of *E.coli* Hsp33 and PA14 Hsp33

Models of E.coli Hsp33 (left) and PA14 Hsp33 were produced using iTASSER protein structure prediction software (Roy, Kucukural et al. 2010). Shown in yellow are the zinc-binding cysteines, other cysteines in red. PA14 Hsp33 contains two additional cysteines (Cys56 and Cys82) compared to *E.coli* Hsp33 that come in close proximity.

One discernable difference between the two homologues is the presence of two additional cysteine residues in PA14-Hsp33 that are located in very close proximity to the active site C-X-C motif. It is conceivable that these additional cysteines might interfere with the correct disulfide bond formation in HOSCN-treated PA14-Hsp33 (Fig. 4.2.9). Further studies, such as the substitution of these two cysteines, are needed to give a definitive answer as to the underlying mechanistic differences in their activation.

4.2.5 *In vitro* effect of hypohalous acids on protein stability and function

To further test our hypothesis that HOCl/HOBr and HOSCN exert different effects on protein stability, we monitored the influence of the three oxidants on the protein structure and function of different purified proteins *in vitro*. Citrate synthase (CS) was previously shown to be sensitive to HOCl-mediated protein unfolding and

aggregation (Winter, Ilbert et al. 2008). We therefore monitored the changes in the secondary structure of CS by far-UV CD, and followed CS aggregation by light scattering after treatment with a 150-fold molar excess of HOX. We observed that both the treatment with HOCl and HOBr equally caused a substantial loss in secondary structure and led to protein unfolding and aggregation. In contrast, however, treatment with HOSCN triggered only a minor loss in the secondary structure suggesting that the selective reactivity of HOSCN with cysteines does not lead to the unfolding of CS and aggregation (Fig. 4.2.10A,B).

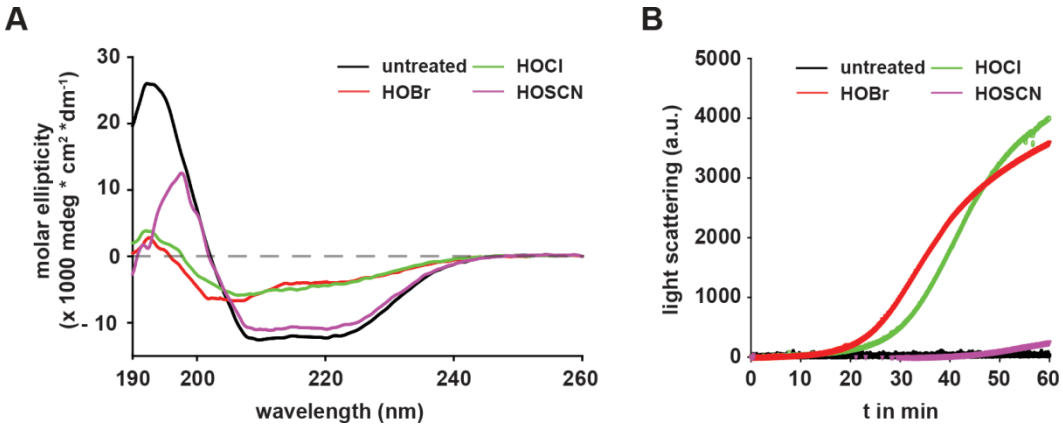

Figure 4.2.10: HOCl and HOBr promote secondary structure changes and aggregation *in vitro*

(**A**). Far-UV CD spectra of CS (3 µM) in the absence of oxidants (black) or after 30 min incubation in the presence of a 150-fold excess (450 µM) of HOCl (green), HOBr (red), or HOSCN (pink) were recorded at 30°C. (**B**). Light-scattering measurements of CS (3 µM) were performed with 450 µM HOCl (green), 450 µM HOBr (red), or 450 µM HOSCN (pink) at 30°C. The excitation and emission wavelength was set to 360nm.

We obtained very similar data with the Immunity protein 7 (Im7), which is another commonly used chaperone client protein but lacks cysteines. As before, treatment with HOCl and HOBr caused substantial protein unfolding while HOSCN had no considerable effect (Fig. 4.2.11). The structure of wild-type Im7 upon treatment with either HOCl and HOBr closely resembled the structure of the known partially unfolded Im7 variant Im7 L53A I54A (Friel, Smith et al. 2009), suggesting that HOCl and HOBr lead to at least partial unfolding of wild-type Im7. Based on our data on our test proteins, HOCl and HOBr elicit protein unfolding and lead to a loss in

protein secondary structure, while HOSCN, at least *in vitro*, does not directly trigger general protein unfolding or aggregation.

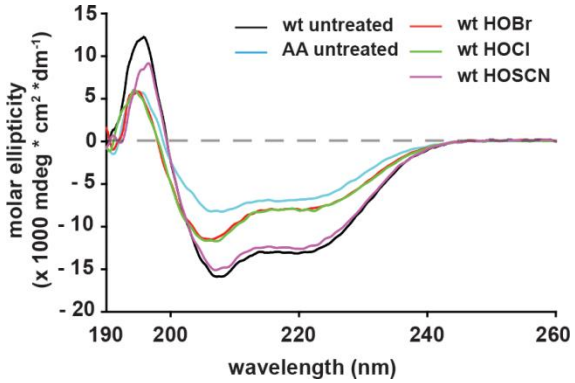

Figure 4.2.11: HOCl and HOBr cause structural changes in Im7

Far-UV CD spectra of wild-type Im7 (20 µM) in the absence of oxidants (black) or after 30 min incubation in the presence of a 10-fold excess (200 µM) of HOCl (green), HOBr (red), or HOSCN (pink) were recorded at 30°C. The Far-UV CD spectrum of the partially unfolded variant Im7 L53A I54A (20 µM) is shown in light blue.

4.2.6 Polyphosphate – the universal defense system against oxidative protein unfolding

To deal with oxidative stress-mediated protein aggregation, *E. coli* has been shown to employ both protein based mechanisms such as the post-translational activation of the redox-regulated chaperone Hsp33, as well as non-protein based chaperone strategies including the conversion of ATP into the chemical chaperone polyphosphate (Dahl, Gray et al. 2015). Hsp33 is inactive under non-stress conditions but becomes rapidly activated as a molecular chaperone upon oxidative stress conditions that lead to widespread protein unfolding (Winter, Ilbert et al. 2008). Oxidative stress conditions lead to an inactivation of the exo-polyphosphatase (PPX). In part this inactivation is responsible for a subsequent accumulation of polyphosphate under these conditions. PolyP is then able to act as a protein–stabilizing chaperone by binding unfolding proteins and preventing *in vivo* aggregation (Gray, Wholey et al. 2014). Thus, we decided to evaluate the degree as to which Hsp33 and/or polyP participate in protecting *P. aeruginosa* against the three physiologically relevant oxidants. For this purpose we deleted either the Hsp33 encoding gene *hslO*, the polyphosphate kinase encoding gene *ppk*, or both

hslO and *ppk* genes in PA14. We then exposed the strains to HOX-treatment in MOPS-glucose media, and monitored their growth in liquid culture after treatment (Fig. 4.2.12) as well as their survival (Fig. 4.2.13).

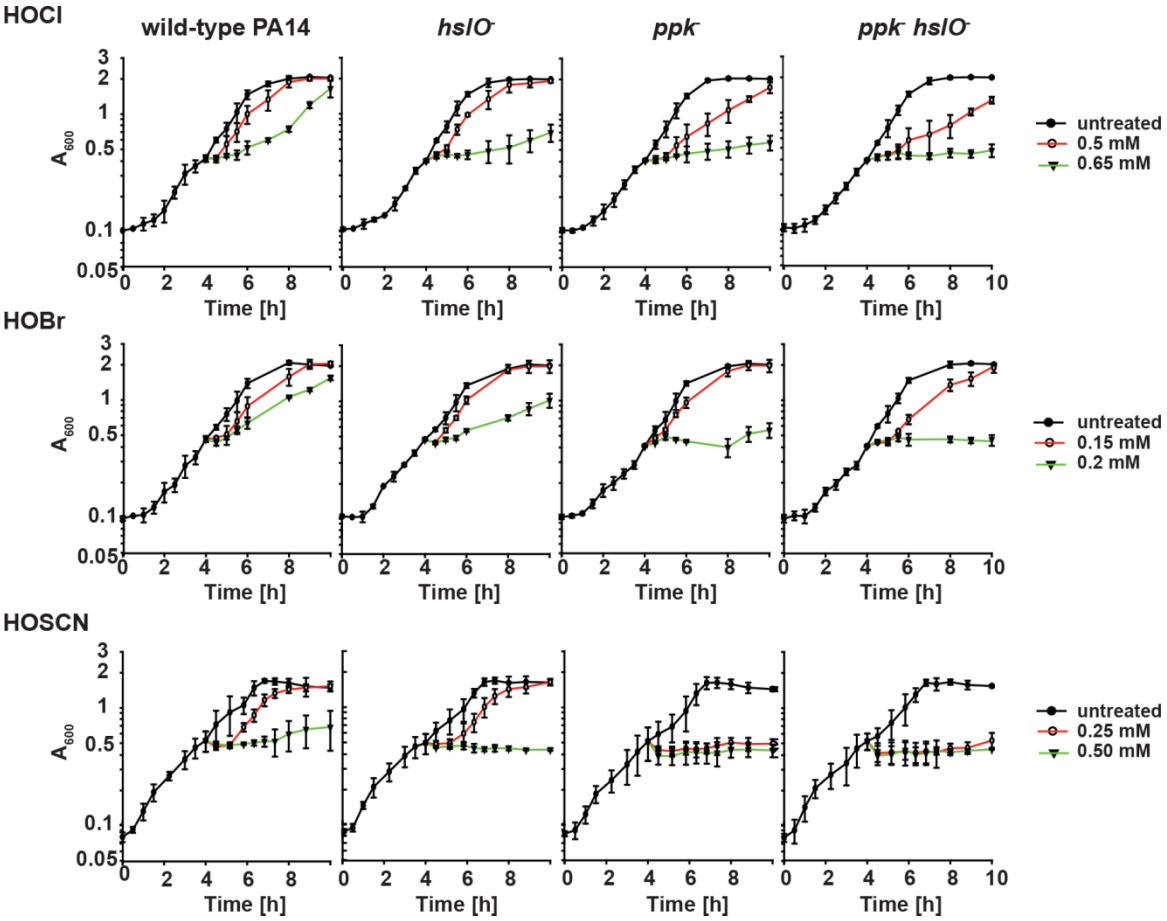

Figure 4.2.12: Growth curves of HOCl, HOBr and HOSCN treated wild-type PA14 and select mutant strains

Logarithmically growing PA14 wild-type, *ppk*$^-$, *hslO*$^-$ or *ppk*$^-$*hslO*$^-$ cells in MOPS-glucose medium were incubated with the indicated concentrations of either HOCl, or HOBr, or HOSCN. Growth was recorded every 30 min for 6 h post treatment.

Deletion of the *hslO* gene in PA14 led to a substantial increase in the sensitivity of PA14 towards HOCl and HOBr treatment but showed no effects upon exposure to HOSCN (Fig. 4.2.12, Fig. 4.2.13). These results were in excellent agreement with our in vitro activation data of Hsp33, and our finding that 0.25 mM HOSCN does cause significant protein unfolding in PA14 wild-type cells. These results indicated that Hsp33 is not involved in the HOSCN defense of PA14.

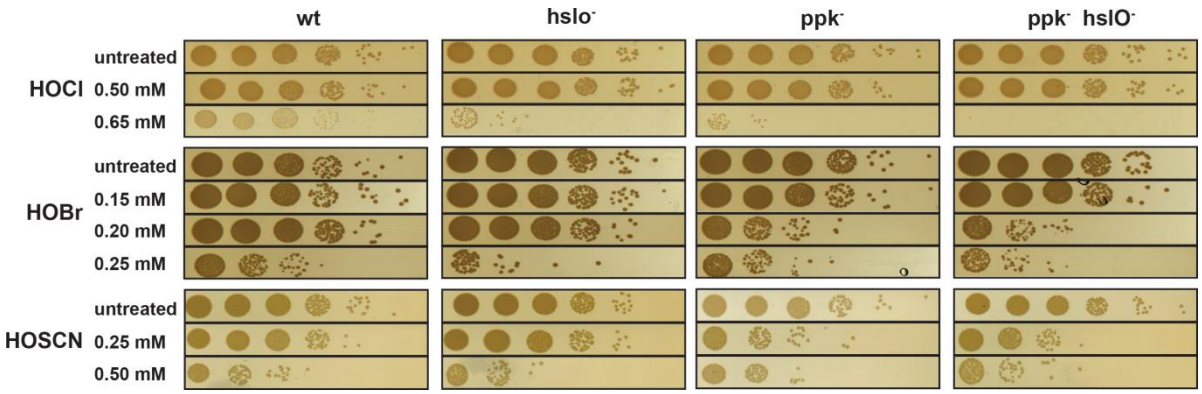

Figure 4.2.13: Post HOX-exposure survival of wild-type PA14 and select mutant strains

Exponentially growing PA14 wild-type, *ppk*$^{-}$, *hslO*$^{-}$, and *ppk*$^{-}$*hslO*$^{-}$ cells were incubated with the indicated concentrations of HOCl, HOBr, or HOSCN for 30 min. Subsequently, 10 mM thiosulfate was used to quench residual oxidants, and cells were serially diluted with 0.85% NaCl, spot-titered onto LB agar plates, and incubated overnight at 37°C. The experiments were repeated at least three independent times and a representative data set is shown.

Deletion of the *ppk* gene, however, caused a dramatic increase in the sensitivity of PA14 towards HOSCN treatment. Upon treatment of the *ppk* deletion mutant with 0.25 mM HOSCN, we did not observe any recovery of PA14 (Fig. 4.2.12) and survival was decreased by 2 orders of magnitude (Fig. 4.2.13). The deletion of *hslO* in the *ppk*$^{-}$ *hslO*$^{-}$ double mutant had no additional effect on the HOSCN sensitivity of PA14, confirming that Hsp33 is indeed dispensable for HOSCN survival. The deletion of the *ppk* gene also increased the sensitivity of PA14 towards HOCl and HOBr, and even more so in the background of the *hslO* deletion (Fig. 4.2.12, Fig. 4.2.13). When we compared the polyP levels in HOCl, HOBr and HOSCN-treated wild-type PA14 we found that all three treatments elicited a comparable increase in polyP level (Fig. 4.2.14), ruling out that polyP's apparently more substantial influence on HOSCN resistance is due to higher amounts of polyP. Instead, our results suggested that polyP accumulation is either sufficient to deal with HOSCN-mediated protein unfolding, explaining the lack of heat shock gene induction and failed activation of Hsp33, or that polyP prevents HOSCN-mediated damage of other cellular targets, such as DNA. In either case, our data implicated polyP to be the global stress response system for the protection of PA14 against all three neutrophilic oxidants.

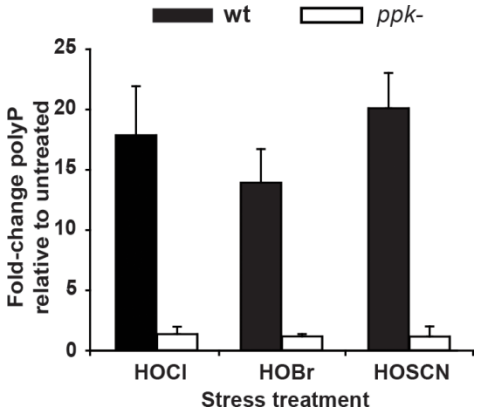

Figure 4.2.14: Determination of polyP concentration in wild-type PA14 and PA14 *ppk*⁻

Exponentially growing PA14 wild-type and *ppk*⁻ cells were incubated with sublethal concentrations of HOCl (0.5 mM), HOBr (0.15 mM), or HOSCN (0.25 mM) for 2.5 hours. After polyP extraction and quantification the resulting amount was normalized to the respective protein amount in each sample. Experiments were performed independently at least three times. Data represent means ± s.d.

4.2.7 *In vivo* protein unfolding propensity of HOCl and HOSCN

To elucidate the underlying mechanism by which polyP protects PA14 against HOSCN-mediated damage, we monitored the protein aggregation in the *ppk* deletion strain after exposure to HOCl, HOBr and HOSCN. Our hypothesis was that in case polyP indeed prevented HOSCN-mediated protein damage in PA14, the deletion of the polyP-synthesizing enzyme PPK would lead to a dramatic increase in protein aggregation. If, however, polyP's effects were independent of protein unfolding, the aggregation pattern would be unaffected. Exposure of the PA14 *ppk*⁻ to 0.25 mM HOSCN for 20 minutes – this concentration did not trigger any detectable protein aggregation in the wild-type strain (Fig. 4.2.7) - caused significant accumulation of unfolded and aggregated proteins in the *ppk* deletion strain (Fig. 4.2.15A). Moreover, analysis of heat shock gene expression (*ibpA*, *dnaK*, *rpoH*) by qRT-PCR showed that the *ppk* deletion strain responded to HOSCN stress with significant heat shock gene induction, suggesting that cells attempt to overcome the lack of polyP by inducing chaperone production (Fig. 4.2.15B). In summary, we could show that HOSCN indeed leads to protein aggregation of a plethora of proteins, but our data suggest that endogenous polyP levels sufficiently prevent HOSCN-mediated protein damage in PA14. In turn, when we treated the *ppk*

deletion strain with HOCl we detected a comparable extent of protein aggregation with several proteins being affected by HOSCN and not HOCl treatment (Fig. 5, arrows). Future studies, e.g. by using SILAC experiments, will reveal whether particularly cysteine-rich proteins or proteins with other specific features are prone to HOSCN-mediated protein aggregation.

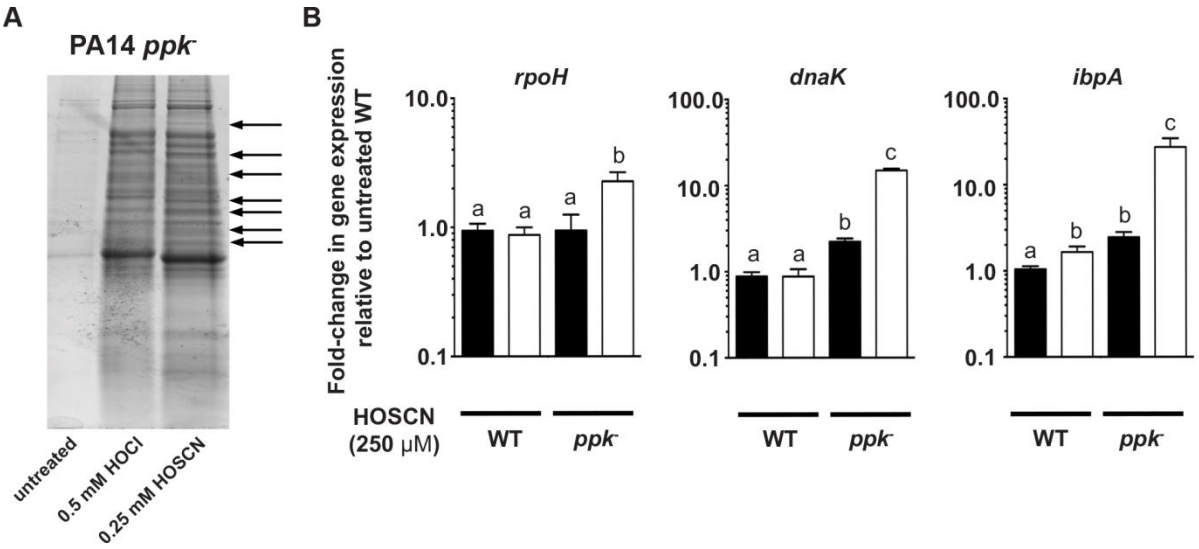

Figure 4.2.15 Effects of lack of polyp on protein aggregation and heat shock gene expression

(**A**). Exponentially growing PA14 *ppk*⁻ cells were incubated in the absence of oxidants or in the presence of HOCl (0.5 mM) or HOSCN (0.25 mM) in MOPS glucose medium for 30 min. Residual oxidants were quenched with 10 mM thiosulfate, and the cells were lysed. Aggregated proteins were separated and visualized by SDS-PAGE. Arrows represent changes in the aggregation pattern between HOCl- and HOSCN-treated samples. Shown here is a representative gel. (**B**). Exponentially growing PA14 wild-type and *ppk*⁻ cells were exposed to 0.25 mM HOSCN for 20 min. Incubation was stopped by the addition of ice-cold methanol. Total RNA was extracted, reverse-transcribed into cDNA, and RT-qPCR was performed using primers for detection of heat-shock genes *rpoH*, *dnaK*, and *ibpA*. Gene expression was normalized to the expression of *rrsD* (encoding 16S rRNA), which did not change under the conditions tested, and fold-changes were calculated relative to the expression of each gene in untreated PA14 wild-type using the ΔΔCT method. Data represent the mean of three independent experiments ± s.d. Two-way ANOVA analysis was conducted with a = n.s.; b = 0.01<*p*<0.05; c: 0.001<*p*<0.01.

4.2.8 Mesalamine increases PA14 sensitivity towards neutrophil derived oxidants

Our data revealed that the accumulation of polyP serves as an efficient posttranslational stress response system that protects bacteria against the

deleterious effects of the three major neutrophilic oxidants. Recent work from our lab showed that mesalamine, the standard treatment for patients with mild to moderate ulcerative colitis, decreases bacterial polyP levels in a wide range of different physiologically relevant bacteria, including *P. aeruginosa* PA14 (Dahl, Gray et al. 2017). We therefore wondered whether mesalamine treatment sensitizes PA14 towards the three physiological oxidants, making it potentially a powerful drug to combat *P. aeruginoasa* infections in chronically inflamed environments. As before, we exposed logarithmically growing PA14 wild-type and *ppk* deletion mutant that were cultivated in MOPS-glucose medium in the presence or absence of mesalamine, to a 30-min treatment of HOCl, HOBr or HOSCN, and monitored survival (Fig. 4.2.16). Indeed, we found that wild-type cells treated with 500 µM mesalamine were about two orders of magnitude more susceptible to the treatment with the three oxidants than cells, lacking the mesalamine pretreatment. As expected, the same treatment with mesalamine did not cause any further change in the oxidant sensitivity of the *ppk* deletion strain. These results demonstrate that a decrease in polyphosphate levels sensitizes *P. aeruginosa* towards HOSCN, and also suggest that polyphosphate is the universal bacterial defense system employed to prevent HOX mediated killing.

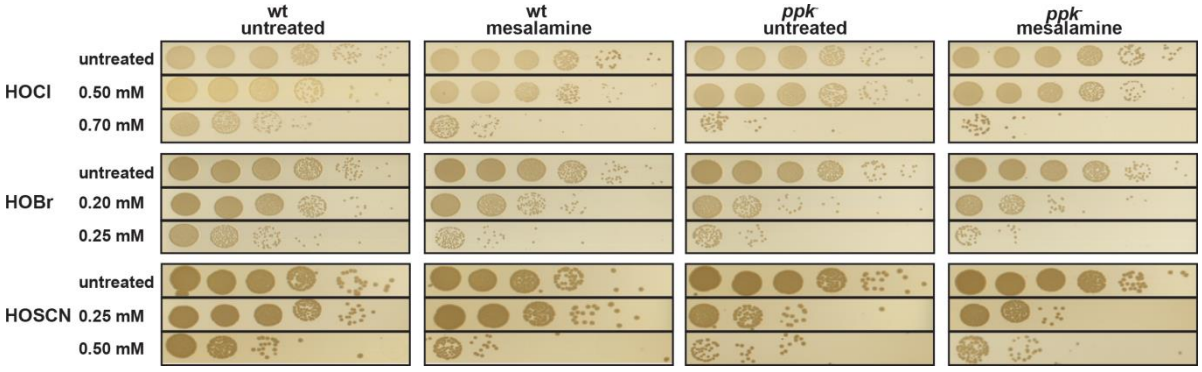

Figure 4.2.16: Mesalamine-treatment increases HOX sensitivity of wild-type PA14 by targeting polyP homeostasis.

Exponentially growing PA14 wild-type and *ppk*⁻ cells in MOPS-glucose medium were either left untreated or pretreated with 0.5 mM mesalamine for 120 min. Subsequently, cells were exposed to the indicated concentrations of HOCl, HOBr or HOSC, and after 30 min of incubation, residual oxidants were quenched with 10 mM thiosulfate. Cells were serially diluted with 0.85% NaCl, spot-titered onto LB agar plates, and incubated overnight at 37 °C. The experiments were repeated at least three independent times.

4.2.9 Conclusion

This study sought to investigate the cellular effects of HOCl, HOBr, and HOSCN on the pathogenic bacterium *P. aeruginosa*, one of the most prevalent microorganisms found in patients suffering from cystic fibrosis. The lungs of these patient show signs of chronic inflammation caused by an imbalance in the levels of HOCl to HOSCN, the former being abnormally elevated and the latter reduced (Rada 2017). We reasoned that the identification of bacterial defense mechanisms, and targeted attenuation or even silencing of those, could open new avenues to fight chronic infections, such as those of *P. aeruginosa* in CF patients.

When we examined the bactericidal effects of HOCl, HOBr and HOSCN on actively metabolizing as well as dormant cells, we found that HOCl and HOBr exerted a stronger killing effect in non-growing cells, which were treated in buffers/media devoid of a carbon source like sugar, such as PBS buffer or MOPS medium. Both HOCl and HOBr are highly promiscuous in their reactivity with many chemicals, so it is conceivable that at least in part organic compounds secreted from actively growing cells quench and thus detoxify these two oxidants. In turn, HOSCN exerted a higher toxicity on metabolically active cells, suggesting a mechanism by which HOSCN targets systems involved in metabolism and/or growth. Indeed, studies in bacterial and mammalian cells have previously shown that HOSCN modifies thiol-containing proteins involved in metabolisms and glycolysis (e.g. fructose bisphosphate aldolase and glyceraldehyde-3-phosphate dehydrogenase), as well as protein folding and redox homeostasis. This drop in glycolytic activity has been suggested to contribute to HOSCN-mediated cell death (Love, Barrett et al. 2016). A variety of bacteria show altered metabolic activity upon HOSCN, such as impaired uptake of nutrients (e.g. glucose and amino acids), conceivably due to the modification of membrane proteins involved in import and export of these compounds (Chandler and Day 2015). In line with these findings, the results of our RNA_{seq} experiment showed a significant upregulation of genes encoding membrane associated proteins and transporters upon HOSCN exposure. These data suggest that HOCl/HOBr and HOSCN elicit their own and distinctly different effects on bacteria. Well balanced levels of these oxidants, as found in healthy indiviuals, thus

appear to be well suited to combat both metabolically active and dormant cells; unlike in CF patients, where elevated levels of HOCl foster chronic inflammations.

We identified a universal response system to HOCl/HOBr and HOSCN in *P. aeruginosa*, polyphosphate. Increased levels of polyP triggered by the exposure to these oxidants increased bacterial survival, and deleting the gene encoding for polyphosphate kinase rendered PA14 substantially more susceptible to all three oxidants. Previous studies underlined polyP's highly conserved nature as a high energy molecule, able to protect a wide spectrum of cellular proteins from oxidative stress mediated unfolding (Gray, Wholey et al. 2014). Unlike HOCl treatment, HOSCN did not lead to increased protein aggregation or an upregulation of chaperone genes in wild-type PA14. In a polyphosphate kinase deficient strain, however, we found significant protein aggregation also in response to HOSCN treatment. We found no discernable difference in the amounts of polyP in response to the exposure of wild-type PA14 to HOSCN vs. HOCl/HOBr, leading us to conclude that polyP is well suited to deal with HOSCN-mediated protein unfolding but fails to prevent aggregation caused by the fast acting oxidants HOCl and HOBr. These finding are again in accordance with our results on the model proteins citrate synthase and Im7, as well as previous *in vivo* and *in vitro* results showing that the high reactivity of HOCl with a variety of amino acids leads to protein unfolding (Winter, Ilbert et al. 2008). Due to its high thiol specificity, first line targets of HOSCN will mostly likely be solvent-exposed cysteine residues (Skaff, Pattison et al. 2009), whose oxidation is unlikely to initiallycause massive protein unfolding. Only upon prolonged exposure, more widespread unfolding might occur.

The levels of polyP in the cell will increase both upon HOCl/HOBr and HOSCN exposure as the oxidative modification of a surface-exposed cysteine in the exopolyphosphatase PPX stalls polyphosphate degradation (Gray, Wholey et al. 2014). However, it is conceivable that polyP generation will not be enogh to counter the fast action of HOCl and its triggered sudden onset of protein. This would also explain why cells employ the redox-regulated chaperone Hsp33 with its extremely fast activation for additional protection. Why PA14 Hsp33 is activated by HOCl/HOBr but not by HOSCN still needs further investigation. It is possible that the

two additional cysteine in PA14 Hsp33 interfere with the correct disulfide bonding and/or that HOSCN's unfolding power is not sufficient enough to activate Hsp33. Alternatively, it is possine that HOSCN only secondarily elicits aggregation by inactivating a few crucial redox-sensitive cellular proteins (e.g. chaperones with cysteine residues important for their activity). Inactivation of such proteins presumably would subsequently lead to aggregation across a broad spectrum of proteins. Overall, polyP appears to be the universal bacterial answer to oxidative stress elicited by all three oxidants, and Hsp33 is only needed for the fast acting stressors HOCl and HOBr. Both systems will prevent protein aggregation by HOCl/HOBr and HOSCN, which each cause aggregation in a specific subset of cellular proteins. Thus, polyP production could be a potential target for the treatment of cystic fibrosis patients with chronic *P. aeruginosa* infections in their lungs, whose clearance is often hampered by the high antibiotic resistance of *P. aeruginosa* (Lister, Wolter et al. 2009). We could show that mesalamine, which has previously been implicated in lowering endogenous polyP levels in *E. coli*, V*. cholarae* and *P. aeruginosa,* increased the susceptibility of PA14 to all three oxidants. Validating and expanding these findings in an animal model would be a next step to prove the feasibility of mesalamine as a future drug in the fight against chronic infections. Taken together, these finding could open new avenues to develop novel treatment regimens aimed to improve the host defense of patients, and eventually their quality of life.

5 Supplementary Section

5.1 Publications

Thiol-based redox switches.
Groitl B, Jakob U.
Biochim Biophys Acta. 2014 Aug;1844(8):1335-43.

Protein unfolding as a switch from self-recognition to high-affinity client binding.
Groitl B, Horowitz S, Makepeace KA, Petrotchenko EV, Borchers CH, Reichmann D, Bardwell JC, Jakob U.
Nat Commun. 2016 Jan 20;7:10357. doi: 10.1038/ncomms10357.

Pseudomonas aeruginosa defense systems against microbicidal oxidants
Groitl B, Dahl JU, Schroeder JW, Jakob U.
Mol Microbiol. Mar 2017(under revision)

5.2 Poster presentations

21st Annual Midwest Stress Response and Molecular Chaperone Meeting
(January 2016)
Northwestern University, Evanston, IN
Protein unfolding as a switch from self-recognition to high-affinity client binding.
Groitl B, Horowitz S, Makepeace KA, Petrotchenko EV, Borchers CH, Reichmann D, Bardwell JC, Jakob U

1st Genetic Code Expansion Conference
(August 2016)
Oregon State University, Corvallis, OR
Protein unfolding as a switch from self-recognition to high-affinity client binding.
Groitl B, Horowitz S, Makepeace KA, Petrotchenko EV, Borchers CH, Reichmann D, Bardwell JC, Jakob U

5.3 Oral presentation

University of Michigan – Department of Molecular, Cellular and Developmental Biology - Retreat
(January 2016)
Northwestern University, Evanston, IN
Characterization of the effects of hypohalous acids in P. aeruginosa.

6 Acknowledgements

First of all, I would like to express my gratitude to my mentor and PhD advisor Prof. Ursula Jakob who helped me grow as a scientist. Her encouragement, support and advice over the years have gotten me where I am today. Her expertise in biochemistry and molecular biology was an inspiring source and an enormous motivation. Thank you very much for giving me the opportunity to learn and strive in your lab under your guidance and supervision. I would also like to thank Prof. Johannes Buchner for his support and for being my advisor in Munich, without whose help this work would not have been possible.

For their collegiality and great atmosphere I would like to thank the entire Jakob lab. Doing research in such an amazing atmosphere was truly inspiring. I'm especially grateful for all the help and input from my friend and colleague Claudia Cremers, who introduced me to all there is to know about Hsp33. I'd also like to thank Jan-Ulrik Dahl and Daniela Knöfler for the fruitful discussions and collaboration, but most importantly for your friendship. Thank you also to Wilhelm Voth, Justine Lempart, Anke Kaufmann, François Beaufay, Lihan Xie, Filipa Teixera, and all the other members of the Jakob lab for your support. Special thanks also to our lab manager and work studies for making scientific work in the lab possible.
I want to thank Prof. James Bardwell for critical input and inspiration, and also his lab for constant help. Thanks to Christopher Lennon and Scott Horrowitz for the great cooperation. Special thanks to Antje Schickert and Veronika Sachsenhauser for their constant support both scientifically and personally.

I'm also extremely thankful to my first cohort and fun crew - Nicolette Ognjanovski, Kaitlyn Norman, Justin Randall, Scott Scholz, and William Hirst – for all their advice, support and fun activities together over all those years. Thank you for walking the way with me. You made Michigan a special place for me.

I would also like to thank my friends back in Germany and other friends here for their constant support over the years, for being there when I needed them:

Thomas Seyferth, Sabrina Habler, Stefanie Reichinger, Josef Auburger, Katarina Seidlmaier, Annabelle Winter, Steven Beuder, Jeremiah Powers, Amelia McKitterick, Brendan O'Hara, and Ethan Shuman.

Zuletzt möchte ich auch meinen Eltern, meinen Großeltern und meinem Bruder Simon einen riesigen Dank aussprechen. Eure beständige Unterstützung hat mich erst soweit gebracht, und ihr seid die beste Familie, die man sich denken kann.

7 References

Altuvia, S., D. WeinsteinFischer, A. X. Zhang, L. Postow and G. Storz (1997). "A small, stable RNA induced by oxidative stress: Role as a pleiotropic regulator and antimutator." Cell **90**(1): 43-53.
Arsene, F., T. Tomoyasu and B. Bukau (2000). "The heat shock response of Escherichia coli." Int J Food Microbiol **55**(1-3): 3-9.

Asahi, T., Y. Nakamura, Y. Kato and T. Osawa (2015). "Specific role of taurine in the 8-brominated-2 '-deoxyguanosine formation." Archives of Biochemistry and Biophysics **586**: 45-50.

Ashby, M. T. (2008). "Inorganic chemistry of defensive peroxidases in the human oral cavity." J Dent Res **87**(10): 900-914.

Aslund, F., M. Zheng, J. Beckwith and G. Storz (1999). "Regulation of the OxyR transcription factor by hydrogen peroxide and the cellular thiol - disulfide status." Proceedings of the National Academy of Sciences of the United States of America **96**(11): 6161-6165.

Atichartpongkul, S., P. Vattanaviboon, R. Wisitkamol, J. Jaroensuk, S. Mongkolsuk and M. Fuangthong (2016). "Regulation of Organic Hydroperoxide Stress Response by Two OhrR Homologs in Pseudomonas aeruginosa." PLoS One **11**(8): e0161982.

Bae, Y. S., M. K. Choi and W. J. Lee (2010). "Dual oxidase in mucosal immunity and host-microbe homeostasis." Trends Immunol **31**(7): 278-287.

Barbirz, S., U. Jakob and M. O. Glocker (2000). "Mass spectrometry unravels disulfide bond formation as the mechanism that activates a molecular chaperone." J Biol Chem **275**(25): 18759-18766.

Bardwell, J. C. and U. Jakob (2012). "Conditional disorder in chaperone action." Trends Biochem Sci **37**(12): 517-525.

Barrett, T. J., D. I. Pattison, S. E. Leonard, K. S. Carroll, M. J. Davies and C. L. Hawkins (2012). "Inactivation of thiol-dependent enzymes by hypothiocyanous acid: role of sulfenyl thiocyanate and sulfenic acid intermediates." Free Radic Biol Med **52**(6): 1075-1085.

Beissinger, M. and J. Buchner (1998). "How chaperones fold proteins." Biol Chem **379**(3): 245-259.

Benjamini, Y. and Y. Hochberg (1995). "Controlling the False Discovery Rate - a Practical and Powerful Approach to Multiple Testing." Journal of the Royal Statistical Society Series B-Methodological **57**(1): 289-300.

Berndt, C., C. H. Lillig and A. Holmgren (2007). "Thiol-based mechanisms of the thioredoxin and glutaredoxin systems: implications for diseases in the cardiovascular system." Am J Physiol Heart Circ Physiol **292**(3): H1227-1236.

Berridge, M.J. (2014) Cell Signalling Biology; doi:10.1042/csb0001002

Bhave, G., C. F. Cummings, R. M. Vanacore, C. Kumagai-Cresse, I. A. Ero-Tolliver, M. Rafi, J. S. Kang, V. Pedchenko, L. I. Fessler, J. H. Fessler and B. G. Hudson (2012). "Peroxidasin forms sulfilimine chemical bonds using hypohalous acids in tissue genesis." Nat Chem Biol **8**(9): 784-790.

Biteau, B., J. Labarre and M. B. Toledano (2003). "ATP-dependent reduction of cysteine-sulphinic acid by S. cerevisiae sulphiredoxin." Nature **425**(6961): 980-984.

Blanchard, J. L., W. Y. Wholey, E. M. Conlon and P. J. Pomposiello (2007). "Rapid changes in gene expression dynamics in response to superoxide reveal SoxRS-dependent and independent transcriptional networks." PLoS ONE **2**(11): e1186.

Bliss, R. E. and K. A. Oconnell (1984). "Problems with Thiocyanate as an Index of Smoking Status - a Critical-Review with Suggestions for Improving the Usefulness of Biochemical Measures in Smoking Cessation Research." Health Psychology **3**(6): 563-581.

Boschi-Muller, S., A. Gand and G. Branlant (2008). "The methionine sulfoxide reductases: Catalysis and substrate specificities." Arch Biochem Biophys **474**(2): 266-273.

Brandes, H. K., F. W. Larimer, M. K. Geck, C. D. Stringer, P. Schurmann and F. C. Hartman (1993). "Direct Identification of the Primary Nucleophile of Thioredoxin-F." Journal of Biological Chemistry **268**(25): 18411-18414.

Brodie, N. I., K. A. Makepeace, E. V. Petrotchenko and C. H. Borchers (2015). "Isotopically-coded short-range hetero-bifunctional photo-reactive crosslinkers for studying protein structure." J Proteomics **118**: 12-20.

Bruel, N., M. P. Castanie-Cornet, A. M. Cirinesi, G. Koningstein, C. Georgopoulos, J. Luirink and P. Genevaux (2012). "Hsp33 controls elongation factor-Tu stability and allows Escherichia coli growth in the absence of the major DnaK and trigger factor chaperones." J Biol Chem **287**(53): 44435-44446.

Carr, A. C., J. J. van den Berg and C. C. Winterbourn (1996). "Chlorination of cholesterol in cell membranes by hypochlorous acid." Arch Biochem Biophys **332**(1): 63-69.

Cellitti, S. E., D. H. Jones, L. Lagpacan, X. Hao, Q. Zhang, H. Hu, S. M. Brittain, A. Brinker, J. Caldwell, B. Bursulaya, G. Spraggon, A. Brock, Y. Ryu, T. Uno, P. G. Schultz and B. H. Geierstanger (2008). "In vivo incorporation of unnatural amino acids to probe structure, dynamics, and ligand binding in a large protein by nuclear magnetic resonance spectroscopy." J Am Chem Soc **130**(29): 9268-9281.

Ceragioli, M., M. Mols, R. Moezelaar, E. Ghelardi, S. Senesi and T. Abee (2010). "Comparative transcriptomic and phenotypic analysis of the responses of Bacillus cereus to various disinfectant treatments." Appl Environ Microbiol **76**(10): 3352-3360.

Chandler, J. D. and B. J. Day (2015). "Biochemical mechanisms and therapeutic potential of pseudohalide thiocyanate in human health." Free Radic Res **49**(6): 695-710.

Chandler, J. D., E. Min, J. Huang, D. P. Nichols and B. J. Day (2013). "Nebulized thiocyanate improves lung infection outcomes in mice." Br J Pharmacol **169**(5): 1166-1177.
Chandler, J. D., D. P. Nichols, J. A. Nick, R. J. Hondal and B. J. Day (2013). "Selective metabolism of hypothiocyanous acid by mammalian thioredoxin reductase promotes lung innate immunity and antioxidant defense." J Biol Chem **288**(25): 18421-18428.

Chen, D. H., D. Madan, J. Weaver, Z. Lin, G. F. Schroder, W. Chiu and H. S. Rye (2013). "Visualizing GroEL/ES in the act of encapsulating a folding protein." Cell **153**(6): 1354-1365.

Cheng, G., E. Basha, V. H. Wysocki and E. Vierling (2008). "Insights into small heat shock protein and substrate structure during chaperone action derived from hydrogen/deuterium exchange and mass spectrometry." J Biol Chem **283**(39): 26634-26642.

Chi, B. K., K. Gronau, U. Mader, B. Hessling, D. Becher and H. Antelmann (2011). "S-bacillithiolation protects against hypochlorite stress in Bacillus subtilis as revealed by transcriptomics and redox proteomics." Mol Cell Proteomics **10**(11): M111 009506.

Chiang, S. M. and H. E. Schellhorn (2012). "Regulators of oxidative stress response genes in Escherichia coli and their functional conservation in bacteria." Archives of Biochemistry and Biophysics.

Chin, J. W. and P. G. Schultz (2002). "In vivo photocrosslinking with unnatural amino Acid mutagenesis." Chembiochem **3**(11): 1135-1137.

Choe, J. K., D. H. Richards, C. J. Wilson and W. A. Mitch (2015). "Degradation of Amino Acids and Structure in Model Proteins and Bacteriophage MS2 by Chlorine, Bromine, and Ozone." Environmental Science & Technology **49**(22): 13331-13339.

Choi, H.-I., S. P. Lee, K. S. Kim, C. Y. Hwang, Y.-R. Lee, S.-K. Chae, Y.-S. Kim, H. Z. Chae and K.-S. Kwon (2006). "Redox-regulated cochaperone activity of the human DnaJ homolog Hdj2." Free Radical Biology and Medicine **40**(4): 651-659.

Choi, H., S. Kim, P. Mukhopadhyay, S. Cho, J. Woo, G. Storz and S. E. Ryu (2001). "Structural basis of the redox switch in the OxyR transcription factor." Cell **105**(1): 103-113.

Christman, M. F., R. W. Morgan, F. S. Jacobson and B. N. Ames (1985). "Positive control of a regulon for defenses against oxidative stress and some heat-shock proteins in Salmonella typhimurium." Cell **41**(3): 753-762.

Clore, G. M. and J. Iwahara (2009). "Theory, practice, and applications of paramagnetic relaxation enhancement for the characterization of transient low-population states of biological macromolecules and their complexes." Chem Rev **109**(9): 4108-4139.

Cohen, T. S. and A. Prince (2012). "Cystic fibrosis: a mucosal immunodeficiency syndrome." Nat Med **18**(4): 509-519.

Combe, C. W., L. Fischer and J. Rappsilber (2015). "xiNET: cross-link network maps with residue resolution." Mol Cell Proteomics **14**(4): 1137-1147.

Cook, K. M. and P. J. Hogg (2013). "Post-translational control of protein function by disulfide bond cleavage." Antioxid Redox Signal **18**(15): 1987-2015.

Cremers, C. M., D. Reichmann, J. Hausmann, M. Ilbert and U. Jakob (2010). "Unfolding of metastable linker region is at the core of Hsp33 activation as a redox-regulated chaperone." J Biol Chem **285**(15): 11243-11251.

Cussiol, J. R., S. V. Alves, M. A. de Oliveira and L. E. Netto (2003). "Organic hydroperoxide resistance gene encodes a thiol-dependent peroxidase." J Biol Chem **278**(13): 11570-11578.

Dahl, J. U., M. J. Gray, D. Bazopoulou, F. Beaufay, J. Lempart, M. J. Koenigsknecht, Y. Wang, J. R. Baker, W. L. Hasler, V. B. Young, D. Sun and U. Jakob (2017). "The anti-inflammatory drug mesalamine targets bacterial polyphosphate accumulation." Nat Microbiol **2**: 16267.

Dahl, J. U., M. J. Gray and U. Jakob (2015). "Protein quality control under oxidative stress conditions." J Mol Biol **427**(7): 1549-1563.

Dahl, J. U., P. Koldewey, L. Salmon, S. Horowitz, J. C. Bardwell and U. Jakob (2015). "HdeB functions as an acid-protective chaperone in bacteria." J Biol Chem **290**(16): 9950.

Dahl, J. U., P. Koldewey, L. Salmon, S. Horowitz, J. C. Bardwell and U. Jakob (2015). "HdeB functions as an acid-protective chaperone in bacteria." J Biol Chem **290**(1): 65-75.

Das, D., P. K. De and R. K. Banerjee (1995). "Thiocyanate, a plausible physiological electron donor of gastric peroxidase." Biochem J **305 (Pt 1)**: 59-64.

Davies, M. J. (2011). "Myeloperoxidase-derived oxidation: mechanisms of biological damage and its prevention." J Clin Biochem Nutr **48**(1): 8-19.

Davies, M. J., C. L. Hawkins, D. I. Pattison and M. D. Rees (2008). "Mammalian heme peroxidases: from molecular mechanisms to health implications." Antioxid Redox Signal **10**(7): 1199-1234.

Day, A. M., J. D. Brown, S. R. Taylor, J. D. Rand, B. A. Morgan and E. A. Veal (2012). "Inactivation of a peroxiredoxin by hydrogen peroxide is critical for thioredoxin-mediated repair of oxidized proteins and cell survival." Mol Cell **45**(3): 398-408.

Dinarvand, P., S. M. Hassanian, S. H. Qureshi, C. Manithody, J. C. Eissenberg, L. Yang and A. R. Rezaie (2014). "Polyphosphate amplifies proinflammatory responses of nuclear proteins through interaction with receptor for advanced glycation end products and P2Y1 purinergic receptor." Blood **123**(6): 935-945.

Drazic, A., H. Miura, J. Peschek, Y. Le, N. C. Bach, T. Kriehuber and J. Winter (2013). "Methionine oxidation activates a transcription factor in response to oxidative stress." Proc Natl Acad Sci U S A **110**(23): 9493-9498.

Drazic, A., A. Tsoutsoulopoulos, J. Peschek, J. Gundlach, M. Krause, N. C. Bach, K. M. Gebendorfer and J. Winter (2013). "Role of cysteines in the stability and DNA-binding activity of the hypochlorite-specific transcription factor HypT." PLoS One **8**(10): e75683.

Du, Y., H. Zhang, X. Zhang, J. Lu and A. Holmgren (2013). "Thioredoxin 1 is inactivated due to oxidation induced by peroxiredoxin under oxidative stress and reactivated by the glutaredoxin system." J Biol Chem **288**(45): 32241-32247.

Dukan, S., S. Dadon, D. R. Smulski and S. Belkin (1996). "Hypochlorous acid activates the heat shock and soxRS systems of Escherichia coli." Appl Environ Microbiol **62**(11): 4003-4008.

Dyson, H. J., A. Holmgren and P. E. Wright (1989). "Assignment of the proton NMR spectrum of reduced and oxidized thioredoxin: sequence-specific assignments, secondary structure, and global fold." Biochemistry **28**(17): 7074-7087.

Foit, L., J. S. George, B. W. Zhang, C. L. Brooks, 3rd and J. C. Bardwell (2013). "Chaperone activation by unfolding." Proc Natl Acad Sci U S A **110**(14): E1254-1262.

Franzmann, T. M., P. Menhorn, S. Walter and J. Buchner (2008). "Activation of the chaperone Hsp26 is controlled by the rearrangement of its thermosensor domain." Mol Cell **29**(2): 207-216.

Friel, C. T., D. A. Smith, M. Vendruscolo, J. Gsponer and S. E. Radford (2009). "The mechanism of folding of Im7 reveals competition between functional and kinetic evolutionary constraints." Nat Struct Mol Biol **16**(3): 318-324.

Frisch, M. J., G. W. Trucks, H. B. Schlegel, G. E. Scuseria, M. A. Robb, J. R. Cheeseman, G. Scalmani, V. Barone, B. Mennucci, G. A. Petersson, H. Nakatsuji, M. Caricato, X. Li, H. P. Hratchian, A. F. Izmaylov, J. Bloino, G. Zheng, J. L. Sonnenberg, M. Hada, M. Ehara, K. Toyota, R. Fukuda, J. Hasegawa, M. Ishida, T. Nakajima, Y. Honda, O. Kitao, H. Nakai, T. Vreven, J. Montgomery, J. A., J. E. Peralta, F. Ogliaro, M. Bearpark, J. J. Heyd, E. Brothers, K. N. Kudin, V. N. Staroverov, R. Kobayashi, J. Normand, K. Raghavachari, A. Rendell, J. C. Burant, S. S. Iyengar, J. Tomasi, M. Cossi, N. Rega, J. M. Millam, M. Klene, J. E. Knox, J. B. Cross, V. Bakken, C. Adamo, J. Jaramillo, R. Gomperts, R. E. Stratmann, O. Yazyev, A. J. Austin, R. Cammi, C. Pomelli, J. W. Ochterski, R. L. Martin, K. Morokuma, V. G. Zakrzewski, G. A. Voth, P. Salvador, J. J. Dannenberg, S. Dapprich, A. D.

Daniels, O. Farkas, J. B. Foresman, J. V. Ortiz, J. Cioslowski and D. J. Fox (2009). Gaussian 09. Wallingford, CT.
Fu, X., X. Shi, L. Yin, J. Liu, K. Joo, J. Lee and Z. Chang (2013). "Small heat shock protein IbpB acts as a robust chaperone in living cells by hierarchically activating its multi-type substrate-binding residues." J Biol Chem **288**(17): 11897-11906.

Fuangthong, M., S. Atichartpongkul, S. Mongkolsuk and J. D. Helmann (2001). "OhrR is a repressor of ohrA, a key organic hydroperoxide resistance determinant in Bacillus subtilis." J Bacteriol **183**(14): 4134-4141.

Furtmuller, P. G., M. Zederbauer, W. Jantschko, J. Helm, M. Bogner, C. Jakopitsch and C. Obinger (2006). "Active site structure and catalytic mechanisms of human peroxidases." Arch Biochem Biophys **445**(2): 199-213.

Gaut, J. P., G. C. Yeh, H. D. Tran, J. Byun, J. P. Henderson, G. M. Richter, M. L. Brennan, A. J. Lusis, A. Belaaouaj, R. S. Hotchkiss and J. W. Heinecke (2001). "Neutrophils employ the myeloperoxidase system to generate antimicrobial brominating and chlorinating oxidants during sepsis." Proc Natl Acad Sci U S A **98**(21): 11961-11966.
Gebendorfer, K. M., A. Drazic, Y. Le, J. Gundlach, A. Bepperling, A. Kastenmuller, K. A. Ganzinger, N. Braun, T. M. Franzmann and J. Winter (2012). "Identification of a hypochlorite-specific transcription factor from Escherichia coli." J Biol Chem **287**(9): 6892-6903.

Gerig, J. T. (1994). "Fluorine Nmr of Proteins." Progress in Nuclear Magnetic Resonance Spectroscopy **26**: 293-370.

Gerschman, R., D. L. Gilbert, S. W. Nye, P. Dwyer and W. O. Fenn (1954). "Oxygen poisoning and x-irradiation: a mechanism in common." Science **119**(3097): 623-626.

Gillespie, J. R. and D. Shortle (1997). "Characterization of long-range structure in the denatured state of staphylococcal nuclease. I. Paramagnetic relaxation enhancement by nitroxide spin labels." J Mol Biol **268**(1): 158-169.

Gonzalez-Flecha, B. and B. Demple (1997). "Homeostatic regulation of intracellular hydrogen peroxide concentration in aerobically growing Escherichia coli." J Bacteriol **179**(2): 382-388.

Graf, C., C. T. Lee, L. Eva Meier-Andrejszki, M. T. Nguyen and M. P. Mayer (2014). "Differences in conformational dynamics within the Hsp90 chaperone family reveal mechanistic insights." Front Mol Biosci **1**: 4.

Graf, P. C., M. Martinez-Yamout, S. VanHaerents, H. Lilie, H. J. Dyson and U. Jakob (2004). "Activation of the redox-regulated chaperone Hsp33 by domain unfolding." J Biol Chem **279**(19): 20529-20538.

Graf, P. C. F. (2004). "Activation of the Redox-regulated Chaperone Hsp33 by Domain Unfolding." Journal of Biological Chemistry **279**(19): 20529-20538.

Graumann, J., H. Lilie, X. Tang, K. A. Tucker, J. H. Hoffmann, J. Vijayalakshmi, M. Saper, J. C. Bardwell and U. Jakob (2001). "Activation of the redox-regulated molecular chaperone Hsp33--a two-step mechanism." Structure **9**(5): 377-387.

Gray, M. J. and U. Jakob (2015). "Oxidative stress protection by polyphosphate--new roles for an old player." Curr Opin Microbiol **24**: 1-6.

Gray, M. J., Y. Li, L. I. O. Leichert, Z. H. Xu and U. Jakob (2015). "Does the Transcription Factor NemR Use a Regulatory Sulfenamide Bond to Sense Bleach?" Antioxidants & Redox Signaling **23**(9): 747-754.

Gray, M. J., W. Y. Wholey, B. W. Parker, M. Kim and U. Jakob (2013). "NemR is a bleach-sensing transcription factor." J Biol Chem **288**(19): 13789-13798.

Gray, M. J., W. Y. Wholey, N. O. Wagner, C. M. Cremers, A. Mueller-Schickert, N. T. Hock, A. G. Krieger, E. M. Smith, R. A. Bender, J. C. Bardwell and U. Jakob (2014). "Polyphosphate is a primordial chaperone." Mol Cell **53**(5): 689-699.

Griffith, K. L., I. M. Shah and R. E. Wolf, Jr. (2004). "Proteolytic degradation of Escherichia coli transcription activators SoxS and MarA as the mechanism for reversing the induction of the superoxide (SoxRS) and multiple antibiotic resistance (Mar) regulons." Mol Microbiol **51**(6): 1801-1816.

Grimaud, R., B. Ezraty, J. K. Mitchell, D. Lafitte, C. Briand, P. J. Derrick and F. Barras (2001). "Repair of oxidized proteins. Identification of a new methionine sulfoxide reductase." J Biol Chem **276**(52): 48915-48920.

Groitl, B. and U. Jakob (2014). "Thiol-based redox switches." Biochim Biophys Acta **1844**(8): 1335-1343.

Ha, E. M. (2005). "A Direct Role for Dual Oxidase in Drosophila Gut Immunity." Science **310**(5749): 847-850.

Hall, A., K. Nelson, L. B. Poole and P. A. Karplus (2011). "Structure-based insights into the catalytic power and conformational dexterity of peroxiredoxins." Antioxid Redox Signal **15**(3): 795-815.

Hammill, J. T., S. Miyake-Stoner, J. L. Hazen, J. C. Jackson and R. A. Mehl (2007). "Preparation of site-specifically labeled fluorinated proteins for 19F-NMR structural characterization." Nat Protoc **2**(10): 2601-2607.

Hampton, M. B., A. J. Kettle and C. C. Winterbourn (1998). "Inside the neutrophil phagosome: oxidants, myeloperoxidase, and bacterial killing." Blood **92**(9): 3007-3017.

Haslbeck, M., A. Ignatiou, H. Saibil, S. Helmich, E. Frenzl, T. Stromer and J. Buchner (2004). "A domain in the N-terminal part of Hsp26 is essential for chaperone function and oligomerization." J Mol Biol **343**(2): 445-455.

Hausladen, A., C. T. Privalle and J. S. Stamler (1996). "Direct activation of the prokaryotic transcription factor oxyR by S-nitrosylation." Biology of Nitric Oxide, Pt 5 **10**: 28-28.

Hawkins, C. L. and M. J. Davies (1998). "Hypochlorite-induced damage to proteins: formation of nitrogen-centred radicals from lysine residues and their role in protein fragmentation." Biochem J **332 (Pt 3)**: 617-625.

Hawkins, C. L., P. E. Morgan and M. J. Davies (2009). "Quantification of protein modification by oxidants." Free Radic Biol Med **46**(8): 965-988.

Hernandez-Ruiz, L., I. Gonzalez-Garcia, C. Castro, J. A. Brieva and F. A. Ruiz (2006). "Inorganic polyphosphate and specific induction of apoptosis in human plasma cells." Haematologica **91**(9): 1180-1186.

Hidalgo, E., J. M. Bollinger, Jr., T. M. Bradley, C. T. Walsh and B. Demple (1995). "Binuclear [2Fe-2S] clusters in the Escherichia coli SoxR protein and role of the metal centers in transcription." J Biol Chem **270**(36): 20908-20914.

Hidalgo, E. and B. Demple (1994). "An iron-sulfur center essential for transcriptional activation by the redox-sensing SoxR protein." EMBO J **13**(1): 138-146.

Hmelo, L. R., B. R. Borlee, H. Almblad, M. E. Love, T. E. Randall, B. S. Tseng, C. Lin, Y. Irie, K. M. Storek, J. J. Yang, R. J. Siehnel, P. L. Howell, P. K. Singh, T. Tolker-Nielsen, M. R. Parsek, H. P. Schweizer and J. J. Harrison (2015). "Precision-engineering the Pseudomonas aeruginosa genome with two-step allelic exchange." Nat Protoc **10**(11): 1820-1841.

Hoffmann, J. H., K. Linke, P. C. Graf, H. Lilie and U. Jakob (2004). "Identification of a redox-regulated chaperone network." EMBO J **23**(1): 160-168.

Hofmann, B., H. J. Hecht and L. Flohe (2002). "Peroxiredoxins." Biol Chem **383**(3-4): 347-364.

Holmgren, A. (1988). "Thioredoxin and glutaredoxin: small multi-functional redox proteins with active-site disulphide bonds." Biochem Soc Trans **16**(2): 95-96.

Holmgren, A. (1989). "Thioredoxin and Glutaredoxin Systems." Journal of Biological Chemistry **264**(24): 13963-13966.

Holyoak, T. and T. Nowak (2001). "Structural investigation of the binding of nucleotide to phosphoenolpyruvate carboxykinase by NMR." Biochemistry **40**(37): 11037-11047.

Horowitz, S., L. Salmon, P. Koldewey, L. S. Ahlstrom, R. Martin, S. Quan, P. V. Afonine, H. van den Bedem, L. Wang, Q. Xu, R. C. Trievel, C. L. Brooks, 3rd and J. C. Bardwell (2016). "Visualizing chaperone-assisted protein folding." Nat Struct Mol Biol **23**(7): 691-697.

Ilbert, M., J. Horst, S. Ahrens, J. Winter, P. C. Graf, H. Lilie and U. Jakob (2007). "The redox-switch domain of Hsp33 functions as dual stress sensor." Nat Struct Mol Biol **14**(6): 556-563.

Imlay, J. A. (2008). "Cellular defenses against superoxide and hydrogen peroxide." Annu Rev Biochem **77**: 755-776.

Jackson, J. C., J. T. Hammill and R. A. Mehl (2007). "Site-specific incorporation of a (19)F-amino acid into proteins as an NMR probe for characterizing protein structure and reactivity." J Am Chem Soc **129**(5): 1160-1166.

Jacquier-Sarlin, M. R., K. Fuller, A. T. Dinh-Xuan, M. J. Richard and B. S. Polla (1994). "Protective effects of hsp70 in inflammation." Experientia **50**(11-12): 1031-1038.

Jakob, U. (2000). "Redox Switch of Hsp33 Has a Novel Zinc-binding Motif." Journal of Biological Chemistry **275**(49): 38302-38310.

Jakob, U., M. Eser and J. C. Bardwell (2000). "Redox switch of hsp33 has a novel zinc-binding motif." J Biol Chem **275**(49): 38302-38310.

Jakob, U., W. Muse, M. Eser and J. C. Bardwell (1999). "Chaperone activity with a redox switch." Cell **96**(3): 341-352.

Janda, I., Y. Devedjiev, U. Derewenda, Z. Dauter, J. Bielnicki, D. R. Cooper, P. C. Graf, A. Joachimiak, U. Jakob and Z. S. Derewenda (2004). "The crystal structure of the reduced, Zn2+-bound form of the B. subtilis Hsp33 chaperone and its implications for the activation mechanism." Structure **12**(10): 1901-1907.

Jang, H. H., K. O. Lee, Y. H. Chi, B. G. Jung, S. K. Park, J. H. Park, J. R. Lee, S. S. Lee, J. C. Moon, J. W. Yun, Y. O. Choi, W. Y. Kim, J. S. Kang, G. W. Cheong, D. J. Yun, S. G. Rhee, M. J. Cho and S.

Y. Lee (2004). "Two enzymes in one; two yeast peroxiredoxins display oxidative stress-dependent switching from a peroxidase to a molecular chaperone function." Cell **117**(5): 625-635.

Jaya, N., V. Garcia and E. Vierling (2009). "Substrate binding site flexibility of the small heat shock protein molecular chaperones." Proceedings of the National Academy of Sciences **106**(37): 15604-15609.

Joachimiak, L. A., T. Walzthoeni, C. W. Liu, R. Aebersold and J. Frydman (2014). "The structural basis of substrate recognition by the eukaryotic chaperonin TRiC/CCT." Cell **159**(5): 1042-1055.

Kettenhofen, N. J. and M. J. Wood (2010). "Formation, reactivity, and detection of protein sulfenic acids." Chem Res Toxicol **23**(11): 1633-1646.

Khor, H. K., M. T. Fisher and C. Schoneich (2004). "Potential role of methionine sulfoxide in the inactivation of the chaperone GroEL by hypochlorous acid (HOCl) and peroxynitrite (ONOO-)." J Biol Chem **279**(19): 19486-19493.

Kim, Y. E., M. S. Hipp, A. Bracher, M. Hayer-Hartl and F. U. Hartl (2013). "Molecular chaperone functions in protein folding and proteostasis." Annu Rev Biochem **82**: 323-355.

Klebanoff, S. J. (1980). "Oxygen metabolism and the toxic properties of phagocytes." Ann Intern Med **93**(3): 480-489.

Klebanoff, S. J. (1999). "Myeloperoxidase." Proc Assoc Am Physicians **111**(5): 383-389.

Klebanoff, S. J. (2005). "Myeloperoxidase: friend and foe." J Leukoc Biol **77**(5): 598-625.

Klion, A. D. and T. B. Nutman (2004). "The role of eosinophils in host defense against helminth parasites." J Allergy Clin Immunol **113**(1): 30-37.

Knoops, B., E. Loumaye and V. Van Der Eecken (2007). "Evolution of the peroxiredoxins." Subcell Biochem **44**: 27-40.

Kogan, I., M. Ramjeesingh, C. Li, J. F. Kidd, Y. Wang, E. M. Leslie, S. P. Cole and C. E. Bear (2003). "CFTR directly mediates nucleotide-regulated glutathione flux." EMBO J **22**(9): 1981-1989.

Koldewey, P., F. Stull, S. Horowitz, R. Martin and J. C. Bardwell (2016). "Forces Driving Chaperone Action." Cell **166**(2): 369-379.

Koo, M. S., J. H. Lee, S. Y. Rah, W. S. Yeo, J. W. Lee, K. L. Lee, Y. S. Koh, S. O. Kang and J. H. Roe (2003). "A reducing system of the superoxide sensor SoxR in Escherichia coli." EMBO J **22**(11): 2614-2622.

Kornberg, A., N. N. Rao and D. Ault-Riche (1999). "Inorganic polyphosphate: a molecule of many functions." Annu Rev Biochem **68**: 89-125.

Kullik, I., J. Stevens, M. B. Toledano and G. Storz (1995). "Mutational analysis of the redox-sensitive transcriptional regulator OxyR: regions important for DNA binding and multimerization." J Bacteriol **177**(5): 1285-1291.

Kumsta, C. and U. Jakob (2009). "Redox-regulated chaperones." Biochemistry **48**(22): 4666-4676.

Kumsta, C., M. Thamsen and U. Jakob (2011). "Effects of oxidative stress on behavior, physiology, and the redox thiol proteome of Caenorhabditis elegans." Antioxid Redox Signal **14**(6): 1023-1037.

Lambrecht, J. A., J. M. Flynn and D. M. Downs (2012). "Conserved YjgF protein family deaminates reactive enamine/imine intermediates of pyridoxal 5'-phosphate (PLP)-dependent enzyme reactions." J Biol Chem **287**(5): 3454-3461.

Lau, D. and S. Baldus (2006). "Myeloperoxidase and its contributory role in inflammatory vascular disease." Pharmacol Ther **111**(1): 16-26.

Lee, D. G., J. M. Urbach, G. Wu, N. T. Liberati, R. L. Feinbaum, S. Miyata, L. T. Diggins, J. He, M. Saucier, E. Deziel, L. Friedman, L. Li, G. Grills, K. Montgomery, R. Kucherlapati, L. G. Rahme and F. M. Ausubel (2006). "Genomic analysis reveals that Pseudomonas aeruginosa virulence is combinatorial." Genome Biol **7**(10): R90.

Lee, T. H., S. U. Kim, S. L. Yu, S. H. Kim, D. S. Park, H. B. Moon, S. H. Dho, K. S. Kwon, H. J. Kwon, Y. H. Han, S. Jeong, S. W. Kang, H. S. Shin, K. K. Lee, S. G. Rhee and D. Y. Yu (2003). "Peroxiredoxin II is essential for sustaining life span of erythrocytes in mice." Blood **101**(12): 5033-5038.

Leichert, L. I., F. Gehrke, H. V. Gudiseva, T. Blackwell, M. Ilbert, A. K. Walker, J. R. Strahler, P. C. Andrews and U. Jakob (2008). "Quantifying changes in the thiol redox proteome upon oxidative stress in vivo." Proc Natl Acad Sci U S A **105**(24): 8197-8202.

Lemire, J. A., J. J. Harrison and R. J. Turner (2013). "Antimicrobial activity of metals: mechanisms, molecular targets and applications." Nat Rev Microbiol **11**(6): 371-384.

Lennon, C. W., W. Ross, S. Martin-Tumasz, I. Toulokhonov, C. E. Vrentas, S. T. Rutherford, J. H. Lee, S. E. Butcher and R. L. Gourse (2012). "Direct interactions between the coiled-coil tip of DksA and the trigger loop of RNA polymerase mediate transcriptional regulation." Genes Dev **26**(23): 2634-2646.

Lesser, M. P. (2006). "Oxidative stress in marine environments: biochemistry and physiological ecology." Annu Rev Physiol **68**: 253-278.

Li, H. and R. Durbin (2009). "Fast and accurate short read alignment with Burrows-Wheeler transform." Bioinformatics **25**(14): 1754-1760.

Li, H., B. Handsaker, A. Wysoker, T. Fennell, J. Ruan, N. Homer, G. Marth, G. Abecasis and R. Durbin (2009). "The Sequence Alignment/Map format and SAMtools." Bioinformatics **25**(16): 2078-2079.

Ligeza, A., A. N. Tikhonov, J. S. Hyde and W. K. Subczynski (1998). "Oxygen permeability of thylakoid membranes: electron paramagnetic resonance spin labeling study." Biochim Biophys Acta **1365**(3): 453-463.

Lister, P. D., D. J. Wolter and N. D. Hanson (2009). "Antibacterial-resistant Pseudomonas aeruginosa: clinical impact and complex regulation of chromosomally encoded resistance mechanisms." Clin Microbiol Rev **22**(4): 582-610.

Lo Conte, M. and K. S. Carroll (2013). "The redox biochemistry of protein sulfenylation and sulfinylation." J Biol Chem **288**(37): 26480-26488.

Lorentzen, D., L. Durairaj, A. A. Pezzulo, Y. Nakano, J. Launspach, D. A. Stoltz, G. Zamba, P. B. McCray, Jr., J. Zabner, M. J. Welsh, W. M. Nauseef and B. Banfi (2011). "Concentration of the antibacterial precursor thiocyanate in cystic fibrosis airway secretions." Free Radic Biol Med **50**(9): 1144-1150.

Love, D. T., T. J. Barrett, M. Y. White, S. J. Cordwell, M. J. Davies and C. L. Hawkins (2016). "Cellular targets of the myeloperoxidase-derived oxidant hypothiocyanous acid (HOSCN) and its role in the inhibition of glycolysis in macrophages." Free Radic Biol Med **94**: 88-98.

Lowther, W. T., H. Weissbach, F. Etienne, N. Brot and B. W. Matthews (2002). "The mirrored methionine sulfoxide reductases of Neisseria gonorrhoeae pilB." Nat Struct Biol **9**(5): 348-352.

Lu, J. and A. Holmgren (2014). "The thioredoxin antioxidant system." Free Radic Biol Med **66**: 75-87.

Mahawar, M., V. Tran, J. S. Sharp and R. J. Maier (2011). "Synergistic roles of Helicobacter pylori methionine sulfoxide reductase and GroEL in repairing oxidant-damaged catalase." J Biol Chem **286**(21): 19159-19169.

Marsh, E. N. and Y. Suzuki (2014). "Using (19)F NMR to probe biological interactions of proteins and peptides." ACS Chem Biol **9**(6): 1242-1250.

Martin, J. L. (1995). "Thioredoxin--a fold for all reasons." Structure **3**(3): 245-250.

McKenna, S. M. and K. J. Davies (1988). "The inhibition of bacterial growth by hypochlorous acid. Possible role in the bactericidal activity of phagocytes." Biochem J **254**(3): 685-692.

Miyake-Stoner, S. J., C. A. Refakis, J. T. Hammill, H. Lusic, J. L. Hazen, A. Deiters and R. A. Mehl (2010). "Generating permissive site-specific unnatural aminoacyl-tRNA synthetases." Biochemistry **49**(8): 1667-1677.

Monks, S. A., G. Karagianis, G. J. Howlett and R. S. Norton (1996). "Solution structure of human neuropeptide Y." J Biomol NMR **8**(4): 379-390.

Moon, J. C., G. M. Kim, E. K. Kim, H. N. Lee, B. Ha, S. Y. Lee and H. H. Jang (2013). "Reversal of 2-Cys peroxiredoxin oligomerization by sulfiredoxin." Biochem Biophys Res Commun **432**(2): 291-295.

Morgan, P. E., D. I. Pattison, J. Talib, F. A. Summers, J. A. Harmer, D. S. Celermajer, C. L. Hawkins and M. J. Davies (2011). "High plasma thiocyanate levels in smokers are a key determinant of thiol oxidation induced by myeloperoxidase." Free Radic Biol Med **51**(9): 1815-1822.

Morris, J. C. (1966). "The Acid Ionization Constant of HOCl from 5 to 35°." The Journal of Physical Chemistry **70**(12): 3798-3805.

Morrissey, J. H., S. H. Choi and S. A. Smith (2012). "Polyphosphate: an ancient molecule that links platelets, coagulation, and inflammation." Blood **119**(25): 5972-5979.

Moskovitz, J., J. M. Poston, B. S. Berlett, N. J. Nosworthy, R. Szczepanowski and E. R. Stadtman (2000). "Identification and characterization of a putative active site for peptide methionine sulfoxide reductase (MsrA) and its substrate stereospecificity." J Biol Chem **275**(19): 14167-14172.

Moskovitz, J., M. A. Rahman, J. Strassman, S. O. Yancey, S. R. Kushner, N. Brot and H. Weissbach (1995). "Escherichia coli peptide methionine sulfoxide reductase gene: regulation of expression and role in protecting against oxidative damage." J Bacteriol **177**(3): 502-507.

Moskovitz, J., H. Weissbach and N. Brot (1996). "Cloning the expression of a mammalian gene involved in the reduction of methionine sulfoxide residues in proteins." Proc Natl Acad Sci U S A **93**(5): 2095-2099.

Mossner, E., M. Huber-Wunderlich, A. Rietsch, J. Beckwith, R. Glockshuber and F. Aslund (1999). "Importance of redox potential for the in vivo function of the cytoplasmic disulfide reductant thioredoxin from Escherichia coli." J Biol Chem **274**(36): 25254-25259.

Muller, A., S. Langklotz, N. Lupilova, K. Kuhlmann, J. E. Bandow and L. I. Leichert (2014). "Activation of RidA chaperone function by N-chlorination." Nat Commun **5**: 5804.

Neumann, C. A., D. S. Krause, C. V. Carman, S. Das, D. P. Dubey, J. L. Abraham, R. T. Bronson, Y. Fujiwara, S. H. Orkin and R. A. Van Etten (2003). "Essential role for the peroxiredoxin Prdx1 in erythrocyte antioxidant defence and tumour suppression." Nature **424**(6948): 561-565.

Nisbet, E. G. and N. H. Sleep (2001). "The habitat and nature of early life." Nature **409**(6823): 1083-1091.

Nunoshiba, T., T. deRojas-Walker, J. S. Wishnok, S. R. Tannenbaum and B. Demple (1993). "Activation by nitric oxide of an oxidative-stress response that defends Escherichia coli against activated macrophages." Proc Natl Acad Sci U S A **90**(21): 9993-9997.

Nunoshiba, T., E. Hidalgo, C. F. Amabile Cuevas and B. Demple (1992). "Two-stage control of an oxidative stress regulon: the Escherichia coli SoxR protein triggers redox-inducible expression of the soxS regulatory gene." J Bacteriol **174**(19): 6054-6060.

Parker, B. W., E. A. Schwessinger, U. Jakob and M. J. Gray (2013). "The RclR protein is a reactive chlorine-specific transcription factor in Escherichia coli." J Biol Chem **288**(45): 32574-32584.

Pattison, D. I. and M. J. Davies (2001). "Absolute rate constants for the reaction of hypochlorous acid with protein side chains and peptide bonds." Chem Res Toxicol **14**(10): 1453-1464.

Peeler, J. C. and R. A. Mehl (2012). "Site-specific incorporation of unnatural amino acids as probes for protein conformational changes." Methods Mol Biol **794**: 125-134.

Peeters, E., A. Sass, E. Mahenthiralingam, H. Nelis and T. Coenye (2010). "Transcriptional response of Burkholderia cenocepacia J2315 sessile cells to treatments with high doses of hydrogen peroxide and sodium hypochlorite." BMC Genomics **11**: 90.

Peschek, J., N. Braun, J. Rohrberg, K. C. Back, T. Kriehuber, A. Kastenmuller, S. Weinkauf and J. Buchner (2013). "Regulated structural transitions unleash the chaperone activity of alphaB-crystallin." Proc Natl Acad Sci U S A **110**(40): E3780-3789.

Petrotchenko, E. V. and C. H. Borchers (2010). "ICC-CLASS: isotopically-coded cleavable crosslinking analysis software suite." BMC Bioinformatics **11**: 64.

Petrotchenko, E. V., K. A. Makepeace and C. H. Borchers (2014). "DXMSMS Match Program for Automated Analysis of LC-MS/MS Data Obtained Using Isotopically Coded CID-Cleavable Cross-Linking Reagents." Curr Protoc Bioinformatics **48**: 8 18 11-19.

Petrotchenko, E. V., K. A. Makepeace, J. J. Serpa and C. H. Borchers (2014). "Analysis of protein structure by cross-linking combined with mass spectrometry." Methods Mol Biol **1156**: 447-463.

Petrotchenko, E. V., J. J. Serpa and C. H. Borchers (2011). "An isotopically coded CID-cleavable biotinylated cross-linker for structural proteomics." Mol Cell Proteomics **10**(2): M110 001420.

Petrotchenko, E. V., J. J. Serpa, K. A. Makepeace, N. I. Brodie and C. H. Borchers (2014). "(14)N(15)N DXMSMS Match program for the automated analysis of LC/ESI-MS/MS crosslinking data from experiments using (15)N metabolically labeled proteins." J Proteomics **109**: 104-110.

Pettersen, E. F., T. D. Goddard, C. C. Huang, G. S. Couch, D. M. Greenblatt, E. C. Meng and T. E. Ferrin (2004). "UCSF Chimera--a visualization system for exploratory research and analysis." J Comput Chem **25**(13): 1605-1612.

Pfaffl, M. W. (2001). "A new mathematical model for relative quantification in real-time RT-PCR." Nucleic Acids Res **29**(9): e45.

Pierce, B. G., K. Wiehe, H. Hwang, B. H. Kim, T. Vreven and Z. Weng (2014). "ZDOCK server: interactive docking prediction of protein-protein complexes and symmetric multimers." Bioinformatics **30**(12): 1771-1773.

Poole, L. B. (2007). "The catalytic mechanism of peroxiredoxins." Subcell Biochem **44**: 61-81.
Poole, L. B., P. A. Karplus and A. Claiborne (2004). "Protein sulfenic acids in redox signaling." Annu Rev Pharmacol Toxicol **44**: 325-347.

Poynton, R. A. and M. B. Hampton (2014). "Peroxiredoxins as biomarkers of oxidative stress." Biochim Biophys Acta **1840**(2): 906-912.
Prutz, W. A. (1996). "Hypochlorous acid interactions with thiols, nucleotides, DNA, and other biological substrates." Arch Biochem Biophys **332**(1): 110-120.

Quan, S., P. Koldewey, T. Tapley, N. Kirsch, K. M. Ruane, J. Pfizenmaier, R. Shi, S. Hofmann, L. Foit, G. Ren, U. Jakob, Z. Xu, M. Cygler and J. C. Bardwell (2011). "Genetic selection designed to stabilize proteins uncovers a chaperone called Spy." Nat Struct Mol Biol **18**(3): 262-269.

Rada, B. (2017). "Interactions between Neutrophils and Pseudomonas aeruginosa in Cystic Fibrosis." Pathogens **6**(1).

Rao, N. N., M. R. Gomez-Garcia and A. Kornberg (2009). "Inorganic polyphosphate: essential for growth and survival." Annu Rev Biochem **78**: 605-647.

Rao, S. and J. Grigg (2006). "New insights into pulmonary inflammation in cystic fibrosis." Arch Dis Child **91**(9): 786-788.

Reichmann, D., Y. Xu, C. M. Cremers, M. Ilbert, R. Mittelman, M. C. Fitzgerald and U. Jakob (2012). "Order out of disorder: working cycle of an intrinsically unfolded chaperone." Cell **148**(5): 947-957.

Rhee, S. G., H. Z. Chae and K. Kim (2005). "Peroxiredoxins: a historical overview and speculative preview of novel mechanisms and emerging concepts in cell signaling." Free Radic Biol Med **38**(12): 1543-1552.

Rhee, S. G., W. Jeong, T. S. Chang and H. A. Woo (2007). "Sulfiredoxin, the cysteine sulfinic acid reductase specific to 2-Cys peroxiredoxin: its discovery, mechanism of action, and biological significance." Kidney Int Suppl(106): S3-8.

Rietsch, A., P. Bessette, G. Georgiou and J. Beckwith (1997). "Reduction of the periplasmic disulfide bond isomerase, DsbC, occurs by passage of electrons from cytoplasmic thioredoxin." J Bacteriol **179**(21): 6602-6608.

Ritchie, M. E., B. Phipson, D. Wu, Y. Hu, C. W. Law, W. Shi and G. K. Smyth (2015). "limma powers differential expression analyses for RNA-sequencing and microarray studies." Nucleic Acids Res **43**(7): e47.

Robinson, M. D., D. J. McCarthy and G. K. Smyth (2010). "edgeR: a Bioconductor package for differential expression analysis of digital gene expression data." Bioinformatics **26**(1): 139-140.

Romsang, A., S. Atichartpongkul, W. Trinachartvanit, P. Vattanaviboon and S. Mongkolsuk (2013). "Gene expression and physiological role of Pseudomonas aeruginosa methionine sulfoxide reductases during oxidative stress." J Bacteriol **195**(15): 3299-3308.

Roos, G., N. Foloppe and J. Messens (2013). "Understanding the pK(a) of redox cysteines: the key role of hydrogen bonding." Antioxid Redox Signal **18**(1): 94-127.

Rosen, H., S. J. Klebanoff, Y. Wang, N. Brot, J. W. Heinecke and X. Fu (2009). "Methionine oxidation contributes to bacterial killing by the myeloperoxidase system of neutrophils." Proc Natl Acad Sci U S A **106**(44): 18686-18691.

Roy, A., A. Kucukural and Y. Zhang (2010). "I-TASSER: a unified platform for automated protein structure and function prediction." Nat Protoc **5**(4): 725-738.

Rutala, W. A. and D. J. Weber (1997). "Uses of inorganic hypochlorite (bleach) in health-care facilities." Clin Microbiol Rev **10**(4): 597-610.

Ryu, J. H., E. M. Ha and W. J. Lee (2010). "Innate immunity and gut-microbe mutualism in Drosophila." Dev Comp Immunol **34**(4): 369-376.

Sanz, M. L., A. Parra, I. Prieto, I. Dieguez and A. K. Oehling (1997). "Serum eosinophil peroxidase (EPO) levels in asthmatic patients." Allergy **52**(4): 417-422.

Scott, James (trans.). *On the disinfecting properties of Labarraque's preparations of chlorine* (S. Highley, 1828) Accessed Apr 11, 2017.

Scherer, G. (2006). "Carboxyhemoglobin and thiocyanate as biomarkers of exposure to carbon monoxide and hydrogen cyanide in tobacco smoke." Exp Toxicol Pathol **58**(2-3): 101-124.

Schroder, E., J. A. Littlechild, A. A. Lebedev, N. Errington, A. A. Vagin and M. N. Isupov (2000). "Crystal structure of decameric 2-Cys peroxiredoxin from human erythrocytes at 1.7 A resolution." Structure **8**(6): 605-615.

Shi, X., N. N. Rao and A. Kornberg (2004). "Inorganic polyphosphate in Bacillus cereus: motility, biofilm formation, and sporulation." Proc Natl Acad Sci U S A **101**(49): 17061-17065.

Singh, V. K., J. Moskovitz, B. J. Wilkinson and R. K. Jayaswal (2001). "Molecular characterization of a chromosomal locus in Staphylococcus aureus that contributes to oxidative defence and is highly induced by the cell-wall-active antibiotic oxacillin." Microbiology **147**(Pt 11): 3037-3045.

Skaff, O., D. I. Pattison and M. J. Davies (2009). "Hypothiocyanous acid reactivity with low-molecular-mass and protein thiols: absolute rate constants and assessment of biological relevance." Biochem J **422**(1): 111-117.

Skaff, O., D. I. Pattison, P. E. Morgan, R. Bachana, V. K. Jain, K. I. Priyadarsini and M. J. Davies (2012). "Selenium-containing amino acids are targets for myeloperoxidase-derived hypothiocyanous acid: determination of absolute rate constants and implications for biological damage." Biochem J **441**(1): 305-316.

Small, D. A., W. Chang, F. Toghrol and W. E. Bentley (2007). "Toxicogenomic analysis of sodium hypochlorite antimicrobial mechanisms in Pseudomonas aeruginosa." Appl Microbiol Biotechnol **74**(1): 176-185.

Smock, R. G., M. E. Blackburn and L. M. Gierasch (2011). "Conserved, Disordered C Terminus of DnaK Enhances Cellular Survival upon Stress and DnaK in Vitro Chaperone Activity." Journal of Biological Chemistry **286**(36): 31821-31829.

Storz, G. and J. A. Imlay (1999). "Oxidative stress." Curr Opin Microbiol **2**(2): 188-194.

Stull, F., P. Koldewey, J. R. Humes, S. E. Radford and J. C. Bardwell (2016). "Substrate protein folds while it is bound to the ATP-independent chaperone Spy." Nat Struct Mol Biol **23**(1): 53-58.

Tamarit, J., E. Cabiscol and J. Ros (1998). "Identification of the major oxidatively damaged proteins in Escherichia coli cells exposed to oxidative stress." J Biol Chem **273**(5): 3027-3032.

Tao, K., N. Fujita and A. Ishihama (1993). "Involvement of the RNA polymerase alpha subunit C-terminal region in co-operative interaction and transcriptional activation with OxyR protein." Mol Microbiol **7**(6): 859-864.

Tapley, T. L., T. M. Franzmann, S. Chakraborty, U. Jakob and J. C. Bardwell (2010). "Protein refolding by pH-triggered chaperone binding and release." Proc Natl Acad Sci U S A **107**(3): 1071-1076.

Tapley, T. L., J. L. Korner, M. T. Barge, J. Hupfeld, J. A. Schauerte, A. Gafni, U. Jakob and J. C. Bardwell (2009). "Structural plasticity of an acid-activated chaperone allows promiscuous substrate binding." Proc Natl Acad Sci U S A **106**(14): 5557-5562.

Teixeira, F., H. Castro, T. Cruz, E. Tse, P. Koldewey, D. R. Southworth, A. M. Tomas and U. Jakob (2015). "Mitochondrial peroxiredoxin functions as crucial chaperone reservoir in Leishmania infantum." Proc Natl Acad Sci U S A **112**(7): E616-624.

Toledano, M. B., C. Kumar, N. Le Moan, D. Spector and F. Tacnet (2007). "The system biology of thiol redox system in Escherichia coli and yeast: differential functions in oxidative stress, iron metabolism and DNA synthesis." FEBS Lett **581**(19): 3598-3607.

Tomoyasu, T., A. Mogk, H. Langen, P. Goloubinoff and B. Bukau (2001). "Genetic dissection of the roles of chaperones and proteases in protein folding and degradation in the Escherichia coli cytosol." Mol Microbiol **40**(2): 397-413.

Tompa, P. and P. Csermely (2004). "The role of structural disorder in the function of RNA and protein chaperones." FASEB J **18**(11): 1169-1175.

Tsaneva, I. R. and B. Weiss (1990). "soxR, a locus governing a superoxide response regulon in Escherichia coli K-12." J Bacteriol **172**(8): 4197-4205.

Umezawa, Y., T. Shimada, A. Kori, K. Yamada and A. Ishihama (2008). "The uncharacterized transcription factor YdhM is the regulator of the nemA gene, encoding N-ethylmaleimide reductase." J Bacteriol **190**(17): 5890-5897.

van Dalen, C. J., M. W. Whitehouse, C. C. Winterbourn and A. J. Kettle (1997). "Thiocyanate and chloride as competing substrates for myeloperoxidase." Biochem J **327 (Pt 2)**: 487-492.

Vazquez-Torres, A. (2012). "Redox active thiol sensors of oxidative and nitrosative stress." Antioxid Redox Signal **17**(9): 1201-1214.

Vesey, C. J. and P. V. Cole (1985). "Blood cyanide and thiocyanate concentrations produced by long-term therapy with sodium nitroprusside." Br J Anaesth **57**(2): 148-155.

Vijayalakshmi, J., M. K. Mukhergee, J. Graumann, U. Jakob and M. A. Saper (2001). "The 2.2 A crystal structure of Hsp33: a heat shock protein with redox-regulated chaperone activity." Structure **9**(5): 367-375.

Wang, J. and A. Slungaard (2006). "Role of eosinophil peroxidase in host defense and disease pathology." Arch Biochem Biophys **445**(2): 256-260.

Wang, L., C. D. Fraley, J. Faridi, A. Kornberg and R. A. Roth (2003). "Inorganic polyphosphate stimulates mammalian TOR, a kinase involved in the proliferation of mammary cancer cells." Proc Natl Acad Sci U S A **100**(20): 11249-11254.

Wang, S., K. Deng, S. Zaremba, X. Deng, C. Lin, Q. Wang, M. L. Tortorello and W. Zhang (2009). "Transcriptomic response of Escherichia coli O157:H7 to oxidative stress." Appl Environ Microbiol **75**(19): 6110-6123.

Weiss, M., M. Bental and U. Pick (1991). "Hydrolysis of polyphosphates and permeability changes in response to osmotic shocks in cells of the halotolerant alga dunaliella." Plant Physiol **97**(3): 1241-1248.

Weiss, S. J. and A. F. LoBuglio (1982). "Phagocyte-generated oxygen metabolites and cellular injury." Lab Invest **47**(1): 5-18.

Weitzman, S. A. and L. I. Gordon (1990). "Inflammation and cancer: role of phagocyte-generated oxidants in carcinogenesis." Blood **76**(4): 655-663.

Williams, C. H., Jr. (1995). "Mechanism and structure of thioredoxin reductase from Escherichia coli." FASEB J **9**(13): 1267-1276.

Winter, J., M. Ilbert, P. C. Graf, D. Ozcelik and U. Jakob (2008). "Bleach activates a redox-regulated chaperone by oxidative protein unfolding." Cell **135**(4): 691-701.

Winter, J., M. Ilbert, P. C. F. Graf, D. Özcelik and U. Jakob (2008). "Bleach Activates a Redox-Regulated Chaperone by Oxidative Protein Unfolding." Cell **135**(4): 691-701.

Winter, J., K. Linke, A. Jatzek and U. Jakob (2005). "Severe oxidative stress causes inactivation of DnaK and activation of the redox-regulated chaperone Hsp33." Mol Cell **17**(3): 381-392.

Winterbourn, C. C. and S. O. Brennan (1997). "Characterization of the oxidation products of the reaction between reduced glutathione and hypochlorous acid." Biochem J **326 (Pt 1)**: 87-92.

Winterbourn, C. C. and A. J. Kettle (2000). "Biomarkers of myeloperoxidase-derived hypochlorous acid." Free Radic Biol Med **29**(5): 403-409.

Winterbourn, C. C., A. J. Kettle and M. B. Hampton (2016). "Reactive Oxygen Species and Neutrophil Function." Annu Rev Biochem **85**: 765-792.

Wong, C., S. Sridhara, J. C. Bardwell and U. Jakob (2000). "Heating greatly speeds Coomassie blue staining and destaining." Biotechniques **28**(3): 426-428, 430, 432.

Wood, Z. A., L. B. Poole and P. A. Karplus (2003). "Peroxiredoxin evolution and the regulation of hydrogen peroxide signaling." Science **300**(5619): 650-653.

Wu, D. and P. Yotnda (2011). "Production and detection of reactive oxygen species (ROS) in cancers." J Vis Exp(57).

Wu, J. and B. Weiss (1991). "Two divergently transcribed genes, soxR and soxS, control a superoxide response regulon of Escherichia coli." J Bacteriol **173**(9): 2864-2871.

Xia, T. H., J. H. Bushweller, P. Sodano, M. Billeter, O. Bjornberg, A. Holmgren and K. Wuthrich (1992). "NMR structure of oxidized Escherichia coli glutaredoxin: comparison with reduced E. coli glutaredoxin and functionally related proteins." Protein Sci **1**(3): 310-321.

Xu, D. and Y. Zhang (2011). "Improving the physical realism and structural accuracy of protein models by a two-step atomic-level energy minimization." Biophys J **101**(10): 2525-2534.

Young, T. S., I. Ahmad, J. A. Yin and P. G. Schultz (2010). "An enhanced system for unnatural amino acid mutagenesis in E. coli." J Mol Biol **395**(2): 361-374.
Zhang, A., S. Altuvia, A. Tiwari, L. Argaman, R. Hengge-Aronis and G. Storz (1998). "The OxyS regulatory RNA represses rpoS translation and binds the Hfq (HF-I) protein." EMBO J **17**(20): 6061-6068.

Zhang, M., S. Lin, X. Song, J. Liu, Y. Fu, X. Ge, X. Fu, Z. Chang and P. R. Chen (2011). "A genetically incorporated crosslinker reveals chaperone cooperation in acid resistance." Nat Chem Biol **7**(10): 671-677.

Zheng, M., F. Aslund and G. Storz (1998). "Activation of the OxyR transcription factor by reversible disulfide bond formation." Science **279**(5357): 1718-1721.

Zheng, M., B. Doan, T. D. Schneider and G. Storz (1999). "OxyR and SoxRS regulation of fur." J Bacteriol **181**(15): 4639-4643.

Zuurbier, K. W., A. R. Bakkenist, R. Wever and A. O. Muijsers (1990). "The chlorinating activity of human myeloperoxidase: high initial activity at neutral pH value and activation by electron donors." Biochim Biophys Acta **1037**(2): 140-146.